

Berichte

zur Polar-
und Meeresforschung

673
2014

Reports
on Polar and Marine Research



Airborne Measurements of Methane Fluxes in Alaskan and Canadian Tundra with the Research Aircraft "Polar 5"

Edited by
Katrin Kohnert, Andrei Serafimovich, Jörg Hartmann & Torsten Sachs

 **HELMHOLTZ**
| GEMEINSCHAFT

Alfred-Wegener-Institut
Helmholtz-Zentrum für Polar-
und Meeresforschung
D-27570 BREMERHAVEN
Bundesrepublik Deutschland

ISSN 1866-3192

Hinweis

Die Berichte zur Polar- und Meeresforschung werden vom Alfred-Wegener-Institut Helmholtz-Zentrum für Polar- und Meeresforschung in Bremerhaven* in unregelmäßiger Abfolge herausgegeben.

Sie enthalten Beschreibungen und Ergebnisse der vom Institut (AWI) oder mit seiner Unterstützung durchgeführten Forschungsarbeiten in den Polargebieten und in den Meeren.

Es werden veröffentlicht:

- Expeditionsberichte
(inkl. Stationslisten und Routenkarten)
- Expeditions- und Forschungsergebnisse
(inkl. Dissertationen)
- wissenschaftliche Berichte der
Forschungsstationen des AWI
- Berichte wissenschaftlicher Tagungen

Die Beiträge geben nicht notwendigerweise die Auffassung des Instituts wieder.

Notice

The Reports on Polar and Marine Research are issued by the Alfred-Wegener-Institut Helmholtz-Zentrum für Polar- und Meeresforschung in Bremerhaven*, Federal Republic of Germany. They are published in irregular intervals.

They contain descriptions and results of investigations in polar regions and in the seas either conducted by the Institute (AWI) or with its support.

The following items are published:

- expedition reports
(incl. station lists and route maps)
- expedition and research results
(incl. Ph.D. theses)
- scientific reports of research stations
operated by the AWI
- reports on scientific meetings

The papers contained in the Reports do not necessarily reflect the opinion of the Institute.

The „Berichte zur Polar- und Meeresforschung“
continue the former „Berichte zur Polarforschung“

* Anschrift / Address

Alfred-Wegener-Institut
Helmholtz-Zentrum für Polar-
und Meeresforschung
D-27570 Bremerhaven
Germany
www.awi.de

Editor:
Dr. Horst Bornemann

Assistant editor:
Birgit Chiaventone

Die "Berichte zur Polar- und Meeresforschung" (ISSN 1866-3192) werden ab 2008 als Open-Access-Publikation herausgegeben (URL: <http://epic.awi.de>).

Since 2008 the "Reports on Polar and Marine Research" (ISSN 1866-3192) are available as open-access publications (URL: <http://epic.awi.de>)

Airborne Measurements of Methane Fluxes in Alaskan and Canadian Tundra with the Research Aircraft “Polar 5”

Edited by

Katrin Kohnert, Andrei Serafimovich, Jörg Hartmann & Torsten Sachs

**Please cite or link this publication using the identifier
hdl:10013/epic.43357 or <http://hdl.handle.net/10013/epic.43357>**

ISSN 1866-3192

German Research Centre for Geosciences GFZ

Alfred Wegener Institute Helmholtz Center for Polar- and Marine Research

Corresponding authors addresses

Katrin Kohnert, Andrei Serafimovich, Torsten Sachs

Geoforschungszentrum GFZ

Telegrafenberg

14473 Potsdam

Germany

katrin.kohnert@gfz-potsdam.de

andrei.serafimovich@gfz-potsdam.de

torsten.sachs@gfz-potsdam.de

Jörg Hartmann

Alfred Wegener Institute Helmholtz Center for Polar- and Marine Research

Am Handelshafen 12

27570 Bremerhaven

Germany

jorg.hartmann@awi.de

Contents

Summary	2
Zusammenfassung.....	3
1 Scientific background for AIRMETH campaigns	4
1.1 Biogeochemical and micrometeorological background.....	4
1.2 Image giving remote sensing (satellite and hyperspectral imagery)	5
2 Objectives of the AIRMETH campaigns	6
3 Description of the study sites	7
3.1 Barrow, North Slope, Alaska	7
3.2 Inuvik, Mackenzie Delta, Canada	9
4 Methods	11
4.1 Instrumentation of <i>Polar 5</i>	11
4.2 Observation strategies and approaches	14
4.3 Pre- and in-flight procedures	14
4.4 Post-flight Procedures.....	16
4.5 Calibration.....	17
5 Cooperation.....	18
5.1 Internal and national collaboration and synergies	18
5.2 International collaboration	18
6 Flight Protocol for AIRMETH 2013.....	20
7 Preliminary observations and lessons learned.....	60
References.....	62
Acknowledgements	65
Appendix.....	66
Participating institutions	66
Participants	66
Flight hours	67
Overview of all flight legs.....	68

Summary

AIRMETH (Airborne measurements of methane fluxes) aims at quantifying methane fluxes from Arctic tundra with airborne eddy covariance measurements. Measurements are done with the research aircraft *Polar 5* owned by Alfred Wegener Institute (AWI), Helmholtz Center for Polar- and Marine Research. In 2013 this joint campaign of AWI and the German Research Centre for Geosciences (GFZ) took place for the third time. The study areas the North Slope of Alaska accessed from Barrow, Alaska and the Mackenzie Delta accessed from Inuvik, Canada. The measurement period was July 4 to July 27, 2013.

Since the underlying method of the campaign is the eddy covariance technique, *Polar 5* was inter alia equipped with a turbulence nose boom including a 5-hole probe, temperature and humidity sensors, as well as a Fast Greenhouse Gas Analyzer (FGGA, Los Gatos Inc.) mounted inside the cabin. The flight patterns mainly consisted of horizontal transects with vertical profiles to well above the top of the boundary layer at the start and end of each transect. Measurement height was between 30 m and 60 m above ground level at a speed of about 215 kmh⁻¹. During AIRMETH 2013 turbulent flux data were collected along flight legs totaling some 10,000 km during 75.8 science flight hours. Additionally, hyperspectral and laser scanner data of certain transects were collected. During AIRMETH 2013 the science equipment worked nearly without any problems.

Zusammenfassung

Das Ziel von AIRMETH (Airborne measurements of methane fluxes) ist es, Methanflüsse aus der arktischen Tundra mit Hilfe von flugzeuggestützten Eddy-Kovarianz-Messungen zu bestimmen. Die Messungen werden mit dem Forschungsflugzeug *Polar 5* des Alfred Wegener Instituts (AWI), Helmholtz-Zentrum für Polar- und Meeresforschung durchgeführt. Im Jahr 2013 fand diese gemeinsame Kampagne von AWI und Deutschem Geoforschungszentrum (GFZ) zum dritten Mal statt. Die Untersuchungsflächen waren die Tundrangebiete der North Slope von Alaska mit Barrow als Ausgangsflughafen und das Mackenzie Delta in Kanada mit Inuvik als Basis. Der Messzeitraum war vom 4. Juli bis 27. Juli 2013.

Da die der Kampagne zugrunde liegende Messtechnik die Eddy-Kovarianz-Methode ist, war die *Polar 5* mit einem Nasenmast mit Fünflochsonde, Temperatur- und Feuchtesensoren, sowie mit einem in der Kabine installiertem Treibhausgasanalysator (Fast Greenhouse Gas Analyzer, FGGA, Los Gatos Inc.) ausgestattet. Die Flugmuster bestanden aus horizontalen Transekten mit vertikalen Profilmessungen am Start- und Endpunkt der Transekte, die bis über die Grenzschicht gingen. Geflogen und gemessen wurde in etwa 30 bis 60 m über Grund bei einer Geschwindigkeit von rund 215 kmh^{-1} . Insgesamt konnten während AIRMETH 2013 bei 75.8 Forschungsflugstunden, mehr als 10,000 km an Daten für turbulente Flussmessungen gesammelt werden. Zusätzlich wurden Hyperspektral- und Laserscanner-Daten von ausgewählten Transekten aufgenommen. Während AIRMETH 2013 kam es kaum zu Problemen mit den wissenschaftlichen Instrumenten.

1 Scientific background for AIRMETH campaigns

1.1 Biogeochemical and micrometeorological background

Tundra regions are an important sink for carbon dioxide (CO₂) sequestering between 0 and 0.8 Pg C/yr and at the same time a source for methane (CH₄) emitting about 32–112 Tg CH₄/yr (McGuire et al., 2009). With warmer climate and thawing permafrost, these sink/source terms might change (Lemke et al., 2007), which is fostering speculations of feedback processes that might enhance global warming further. In this context, methane is of particular interest due to its global warming potential of 21 CO₂ equivalents over a 100-year period.

Environmental and climate research has been working on quantifying the fluxes of CH₄ and CO₂ in tundra regions for two decades now (e.g. Torn and Chapin, 1993; Schimel, 1995; Christensen et al., 1995). Chamber measurements have played an important role from the beginning (e.g. Weller et al., 1995; Kutzbach et al., 2007; Wille et al., 2008; Zona et al., 2009; Zhang et al., 2012; Sistla et al., 2013). They are, however, only representative for the area covered with the chamber. Starting in the mid-1990s, the application of the eddy-covariance technique on flux tower data allowed continuous measurements areas of several hundred square meters.

Both methods have the shortcoming that the spatial coverage is limited and therefore knowledge about spatial heterogeneity of CH₄ and CO₂ fluxes above tundra regions is limited. This is, however, important for modeling greenhouse gas emissions for the entire tundra region and for projecting their impact on global warming. Only very recently CH₄ analyzers became sufficiently robust to be installed on an aircraft. Together with a turbulence probe, airborne methane flux measurements are now possible and information about spatial heterogeneity of methane fluxes can be collected.

For this kind of airborne measurements it is essential to decide on an appropriate altitude that ensures the safety of the flight and enables the collection of interpretable data. For both flux and concentration measurements it is necessary that the in-situ measurements are performed in that part of the atmosphere in which exchange processes between the earth's surface and the atmosphere happen. That part is referred to as boundary layer (BL) and differs from the air above regarding meteorological parameters and chemical composition. Apart from the concentration of (greenhouse) gases that changes between within and above the BL, also the potential temperature and the specific humidity vary. With a convective boundary layer over wetlands in summer, typically the potential temperature increases above the BL, whereas the relative humidity drops. Since the potential temperature Θ is defined as that temperature that an air parcel has when it is brought isentropically to the standard pressure p_0 , it cannot be measured, but is calculated as follows:

$$\Theta = T \cdot \left(\frac{p_0}{p}\right)^{R_L/c_p} \quad (1)$$

with T being the temperature in K, p_0 the standard pressure (1013.25 hPa), p the measured pressure in hPa, R_L the gas constant for dry air (287.04 J/(kgK)), and c_p the specific heat capacity for dry air (1005 J/(kgK)).

With an airplane the height of the BL can be determined in-situ from vertical profile flights, when the potential temperature, which is constant within the well-mixed boundary layer, increases above the boundary layer while relative humidity and ideally also CH₄ concentration decrease during the ascent.

Since the development in the BL is driven by thermal forcing, the height of the BL varies over the course of the day (Stull, 2000). The stable BL of the night is broken up after sunrise with the heating of the surface and the air above. With time, the BL height increases and then decreases towards sunset. Consequently, not only the altitude of the flight, but also its time slot have to be chosen carefully.

1.2 Image giving remote sensing (satellite and hyperspectral imagery)

Through cooperation with various remote sensing groups and as it is one aim of AIRMETH to relate greenhouse gas fluxes to surface properties, remote sensing information thereof is required. During previous AIRMETH campaigns mainly satellite imagery was used for the analysis. Additional detailed information could be derived from photo and video cameras that were part of the equipment of *Polar 5*. In 2013, for the first time also a hyperspectral camera was on board the *Polar 5* with which high resolution information about land cover and surface structures could be obtained with more than 100 spectral bands.

Hyperspectral imagery

Hyperspectral imaging is an enhancement of multispectral imaging and has been used for airborne measurements since the beginning of the 1980s. The advantage of this technique is that it takes hundreds of spectral channels for detecting different surface properties. One hyperspectral image consists of information of these hundreds of spectral channels (Chang, 2003). With statistical methods the hyperspectral data are processed (Hidden Markov Model and spectral information measure).

Underlying technique for hyperspectral image generation

There are different techniques for generating hyperspectral images. In general, a spectrophotometer emits a light source that travels through a filter system where the light is split into different wavelength bands. Moreover, the spectrophotometer is equipped with a detector and a digitization hardware, in which the incoming information is stored (Siesler et al., 2002). The light source for e.g. the near infrared spectral range can be different like tungsten halogen or xenon gas plasma lamps as well as diodes that emit light or tunable lasers (Grahm and Geladi, 2007).

A hyperspectral image itself is a stack of several images that are taken at different wave lengths. Matrices of spectral samples are then “built up on a line by line basis to form a two dimensional image” (Varshney and Arora, 2004) and the third dimension is containing the spectral data for each sample. As each mineral has a specific reflectance and absorption characteristics, different minerals can be differentiated by hyperspectral imaging (Varshney and Arora, 2004). Even biological and chemical processes can be distinguished (Varshney and Arora, 2004).

2 Objectives of the AIRMETH campaigns

AIRMETH is a joint project between the Helmholtz Young Investigators Group TEAM (Trace Gas Exchange in the Earth – Atmosphere System on Multiple Scales) based at the German Research Centre for Geosciences (GFZ) in Potsdam and the Alfred Wegener Institute for Polar and Marine Research (AWI) in Bremerhaven.

With AIRMETH (Airborne measurements of methane fluxes) we contribute to overcoming the lack of knowledge about regional differences in CH₄ fluxes above Arctic tundra by using airborne flux measurements. We aim at describing the spatial variability of the fluxes by environmental parameters like temperature or land cover derived from satellite imagery and to upscale the results to a larger area. The campaigns began in 2011 when measurements were conducted in Germany and northern Europe. The aim of this pilot campaign was to test both instruments and approach and to get first usable data. Since 2012 the campaign takes place in the North American Arctic covering extensive permafrost landscapes on the North Slope of Alaska based out of Barrow as well as in and around the Mackenzie Delta, Canada, based out of Inuvik. The measurements are conducted in the summer. In 2013 the measurement period was July 4 to July 27.

In 2013, additional to methane, also carbon dioxide and water vapor concentrations were measured. Since both study areas are being intensively studied by different university groups and research institutes regarding various aspects of changes in the Arctic, cooperation with the respective groups were established.

As part of the 2013 campaign we collected an extensive set of hyperspectral data for the analysis of land cover features and sea ice conditions, as well as laser scanner measurements of surface topography focusing on coastal erosion.

3 Description of the study sites

The two study areas of the campaign are located north of the polar circle. During the first half (July 2 – July 16, 2013) of the campaign, part of the North Slope of Alaska was studied. The study area is highlighted in light blue color in Fig. 1. During that time the base was in Barrow, Alaska ($71^{\circ} 18' N$, $156^{\circ} 46' W$). The second half (July 17 – July 29) of AIRMETH 2013 took place in the Mackenzie Delta in Canada close to Inuvik ($68^{\circ} 19' N$, $133^{\circ} 37' W$). The area that was covered by the flight legs in this region, namely the Mackenzie Delta and the coastline towards the Alaskan border, is marked in pink in Fig. 1.



Fig. 1: Study areas in Alaska and Canada. The area in the North Slope of Alaska covered in the first half of AIRMETH 2013 is highlighted in light blue; the area marked in pink is the area overflown during the second half of the campaign. It is mainly covering the Mackenzie Delta in Canada and the coastline towards the Alaskan border, including Herschel Island.

3.1 Barrow, North Slope, Alaska

Barrow is located in the North Slope Borough of Alaska (time zone: UTC - 9, daylight saving time UTC - 8), bordered to the west and north by the Beaufort Sea (Fig. 2) and is to the south and east surrounded by polygonal tundra. The area in Alaska covered by measurements extends 425 km in West-East direction and 150 km North-South.

The North Slope of Alaska is, apart from some smaller settlements like Barrow or the oil production area stretching west from Prudhoe Bay, widely left to nature. Polygonal structures (Fig. 2c), sandy areas (Fig. 2b) and lakes (Fig. 2d) are mainly characterizing the area.

The vegetation predominantly consists of lichens and grass species, but also some vascular plants can be found. In detail, the tundra is mainly characterized by (Villarreal et al., 2012):

- **Lichens:** *Cetraria islandica*, *Cetraria cucullata*, *Dactylina arctica*

- **Grass species:** *Eriophorum angustifolium*, *Eriophorum russeolum*, *Eriophorum scheuchzeri*, *Hierochloe pauciflora*, *Luzula arctica*, *Poa arctica*, *Dupontia fisheri*, *Arctagrostis latifolia*, *Arctophila fulva*, *Carex aquatilis*
- **Vascular plants:** *Salix pulchra*, *Salix rotundifolia*, *Cassiope tetragona*, *Petasites frigidus*, *Ranunculus pallasii*, *Saxifrage cernua*

The area is also home to about 700,000 migrating caribou and millions of birds belonging to more than 125 species that live on the North Slope. More than 10,000 bowhead and more than 30,000 beluga whales travel in the coastal area (National Geographic, 2006).

Barrow has an average annual temperature of -12 °C and an average annual amount of precipitation of 104 mm (US climate data, 2013). Overall the climate can be described as the tundra climate (ET) (Köppen, 1936). However, since the area is characterized by permafrost, the water cannot percolate which turns the region into a wetland in summer. During July 2013 the average high temperature was 10.4 °C and the overall precipitation was 42.7 mm (KTVA, 2013). During the time of the AIRMETH 2013 in Barrow, i.e. the first half of July, the average air temperature was 6.3 °C (data from Accuweather, 2013).

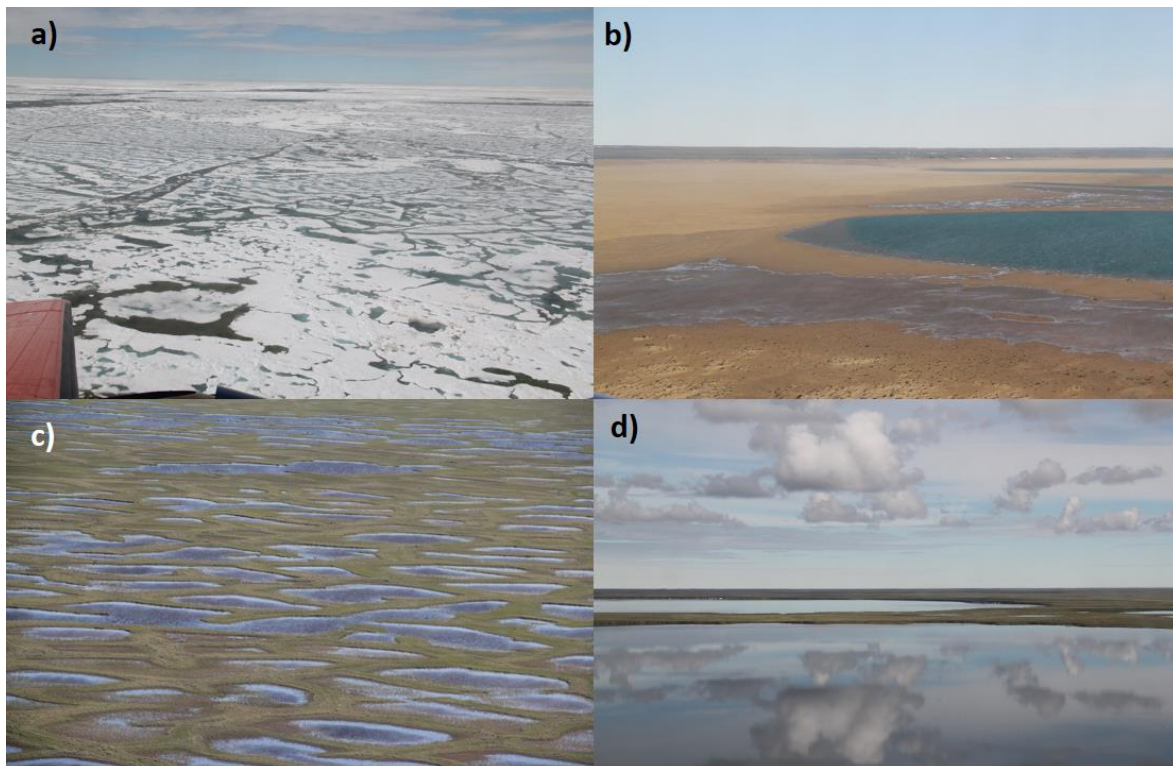


Fig. 2: Typical structures of the Alaskan North Slope. a) Ice cover on the Beaufort Sea close to Barrow; b) Sandy area at the shore of a lake; c) polygonal structures filled with water; d) smooth surface of one of the bigger lakes.

3.2 Inuvik, Mackenzie Delta, Canada

Inuvik is located at the central eastern edge of the Mackenzie Delta. In the Mackenzie Delta measurements covered a West-East extension of 320 km and a North-South extension of 240 km.

The study area belongs to the Mountain Daylight Time zone (UTC - 7; Daylight saving time UTC - 6). The region has a subarctic continental climate with an average temperature of -9.4 °C and average precipitation sum of 295 mm (Walch and Frater, 2004). The Mackenzie Delta covers an area of 13.000 km² (Burn and Kokelj, 2009) with a north-south extent of about 215 km and an east-west extent of about 75 km. It is the second largest Arctic delta of the world, second to the Lena Delta in Russia (Burn and Kokelj, 2009).

Due to its large north-south extension, the Mackenzie Delta covers a climatic gradient concomitant with a vegetation gradient from subarctic boreal forest in the south via low shrub tundra to low arctic tundra at its northern edge. The slow transition from forest to tundra vegetation happens at latitudes between 68°30'N and 69°30'N (Burn and Kokelj, 2009). The northern part of that transition zone is dominated by sedges and dwarf shrubs, mainly willow (*Salix* spp), alder (*Alnus crispa*) and ground birch (*Betula nana*) (Mackay, 1963). To the northern edge of the delta the low arctic tundra is mainly vegetated by sedges, grass, ericaceous shrubs, lichens and mosses.

The variability in the delta is not only caused by recent climate, but also by the glaciation history of the area, which resulted in huge differences in the permafrost thickness in the delta region (Burn and Kokelj, 2009). The uplands in the north of Richards Island (cf. waypoint C4 shown in Fig. 10) that were not glaciated during the Pleistocene and partly the upper delta are underlain by up to 500 m thick permafrost. In contrast, the permafrost of the uplands to the west and east of the delta only reaches depths of about 100 m. In the Mackenzie Delta itself, the ground is only frozen until depths lower than 100 m. Near Inuvik a permafrost thickness of 90 m is reported (Burn et al., 2009).

One characteristic of the permafrost region of the Mackenzie Delta is the existence of numerous pingos (Fig. 3b). Pingos are mostly conical structures in permafrost regions that have an ice core (Mackay, 1998) and are developed below the active layer (Gurney, 1998). A pingo develops under the existence of a pressure gradient which attracts groundwater towards the ice core (Gurney, 1998). The pingo grows due to the expansion that is happening when the semi-fluid material between bedrock and frozen surface is freezing (Porsild, 1938). In areas like the Mackenzie Delta, with continuous permafrost, unfrozen sediments can mainly be found beneath a deep lake that is not freezing during winter (Gurney, 1998).

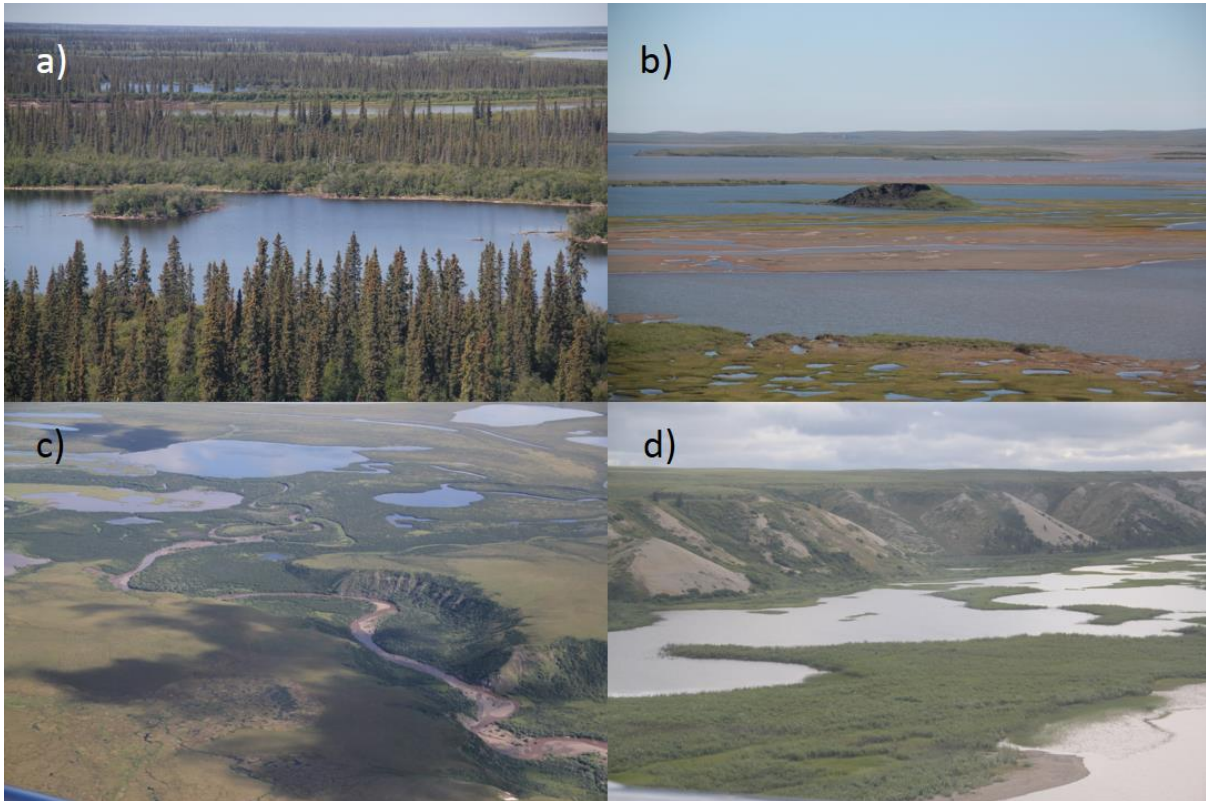


Fig. 3: Impressions from the Mackenzie Delta. a) Black spruce close to Inuvik; b) partly collapsed pingo; c) meandering river; d) an arm of the Mackenzie River with its higher shore. Pictures: Katrin Kohnert.

4 Methods

4.1 Instrumentation of *Polar 5*

4.1.1 General instrumentation

For the campaign the research aircraft *Polar 5* owned by AWI was equipped with the turbulence nose boom (Fig. 4) that had been used in previous AIRMETH campaigns as well as in other projects. Fig. 4 depicts (a) the measurement of the nose boom attached to *Polar 5* and (b) the inside of the nose boom with attached instruments.

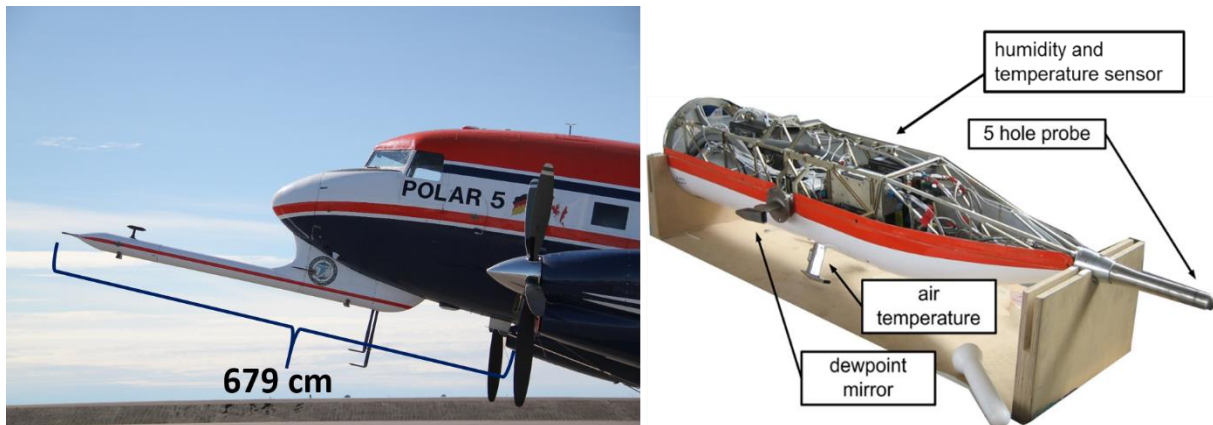


Fig. 4: a) *Polar 5* with the nose boom at Inuvik Airport (Picture: K. Kohnert); b) Insight in the nose boom and attached instruments (Picture modified from: <https://spaces.awi.de/confluence/display/AEROdevices/Meteorologischer+Nasenmast>).

At the tip of the turbulence nose boom a 5 hole probe is attached that measures the differential pressure for obtaining the 3D wind vector. Additionally, air temperature, air humidity and the dew point are measured at the nose boom.

Apart from the instruments mounted at the nose boom, numerous instruments were installed inside, at the top and at the bottom of the airplane. Table 1 gives an overview over these devices.

Table 1: Instrumentation of *Polar 5* during the AIRMETH campaign 2013

Instrument	Type/Brand	Relevant derived data	Location
Inertial Navigation System (INS)	Laseref V/ Honeywell	roll, pitch, yaw, heading, accelerations, latitude, longitude, wind speed, wind direction, ground speed	Cockpit
GPS 1	FlexPak 6/ Novatel	Geographic position, time	Antenna on roof
GPS 2-5	OEMV-3/ Novatel	Position of the aircraft	Antenna on roof
Greenhouse Gas Analyzer	GGA 24EP/ Los Gatos Research Inc.	Methane/carbon dioxide/ water vapor concentration	Cabin
Radiation	KT19, Heitronics	Surface temperature	Under-floor,

thermometer/Infrared radiation thermometer			roller shutter
Pyranometer	CMP22 SN110293 and SN110275 / Kipp and Zonen	Short wave radiation	Top and bottom of fuselage and lower side of the body
Pygeometer	CGR4 SN110385 and SN110384, Kipp and Zonen	Long wave radiation	Top and bottom of fuselage
Radar altimeter	KRA 405B/ Honeywell	Altitude above ground	Antennas on lower side of the body
Laser altimeter	LD90/ Riegl	Altitude above ground	Under-floor, roller shutter
Downward looking photo camera	Canon EOS 1D Mark III	Surface cover, geographic position	Lower side of the body
Downward looking video camera	Dallmeier	Surface cover, geographic position	Lower side of the body behind roller shutter
Upward looking video camera	Dallmeier	Sky coverage	Upper side of the body
Hyperspectral camera	EAGLE/ Aisa	Land cover	Lower side of the body
Laser scanner	VQ580 SNS9997784 /Riegl	Surface topography	
Total Temperature Sensor	102EXX SN70511		Nose boom
Humidity and Temperature Transmitter	HMT333 SN A4650017		

4.1.2 Hyperspectral camera

In addition to satellite images, information from hyperspectral images can be used for high resolution land cover information. The hyperspectral camera onboard the *Polar 5* was an Aisa EAGLE with a spectral range from 400 – 970 nm and a spectral resolution of 3.3 nm. The spectral binning options and the dependent parameters are shown in Table 2. During AIRMETH 2013 the hyperspectral camera was mainly operated with a spectral binning of 4 and a spatial binning of 2.

Since hyperspectral imaging is based on surface reflection, discontinuous shadows, as they are caused by clouds, render it challenging or even impossible to process and interpret the derived images. Therefore, the camera was only operated under blue sky conditions or in exceptions also under continuous cloud coverage. The flight height for hyperspectral scanning during AIRMETH was between 1,200 m and 1,800 m above ground level (agl).

With hyperspectral images it is possible to differentiate between different land cover types and characteristics of the surface. For instance, it can be differentiated between clean lakes and those with sediment. Also polygonal structures can be clearly detected (Fig. 5).

Table 2: Spectral binning options of the hyperspectral camera Aisa EAGLE and the respective values for the dependent parameters (AisaEAGLE, 2012)

Spectral binning options	1x	2x	4x	8x
Number of spectral bands	488	244	122	60
Spectral sampling/band (nm)	1.25	2.3	4.6	9.2
Frame rate, up to (frames/s)	30	59	100	160

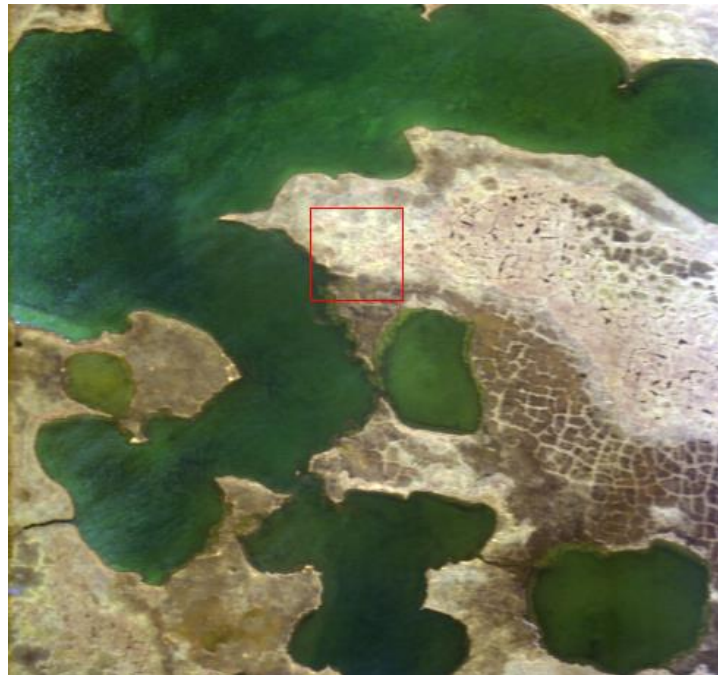


Fig. 5: Screenshot of an exemplary hyperspectral image taken during the flight on July 11 in the North Slope, Alaska. For this display the following wave lengths were chosen for the respective channels: Red: 698 nm, green: 596 nm, blue: 407 nm.

4.2 Observation strategies and approaches

When greenhouse gases are emitted from the ground, their concentration in the air above the surface is dependent on the boundary layer height. The BL height shows a diurnal cycle with a developing phase after sunrise leading to a maximum height about 2 hours after the sun reaches its highest point and a declining phase around sunset. Consequently, if the weather allowed, science flights started around noon to conduct measurements in a well-developed BL.

In order to derive greenhouse gas and energy fluxes from airborne measurements, it is essential to measure within the lowest part of the BL, preferably within its lowest ten percent, which is also referred to as surface layer. During AIRMETH 2013 the flight altitude on the low level transects for flux calculation was between 40 and 80 m agl.

A typical science flight included about 700 – 800 km of horizontal transects always including low level flights for flux calculation and, where suitable, transects in 600 – 1,400 m agl for laser scanner and/or hyperspectral camera operation. With additional vertical profiles at least until the top of the BL at the beginning and end of each transect, the average flight day lasted 4.7 hours with a true air speed of about 215 kmh^{-1} . If a flux tower measurement site was in the area, transects were arranged in a way that the tower was passed with the airplane. Overall, during AIRMETH 2013 flux data were collected over a distance of more than 10,000 km.

4.3 Pre- and in-flight procedures

Before takeoff, all equipment was set to Coordinated Universal Time (UTC). The valves at the inlet to the FGGA were only opened after takeoff in order to avoid the pollution of the device by raised dirt from the runway.

During the flight it was ensured that all science equipment was running correctly via real time data display on several monitors. Especially during the profile flights, the pressure in the measurement cell had to be regulated to 140 Torr. In order to determine how high the profiles had to be to get to the top of the boundary layer, the changes in potential temperature and relative humidity were observed. Fig. 6 shows the changes of potential temperature and methane concentration with the height. The BL is in this case visually determined to be at about 580 m, because the potential temperature starts to strongly increase, whereas methane concentration starts to decrease.

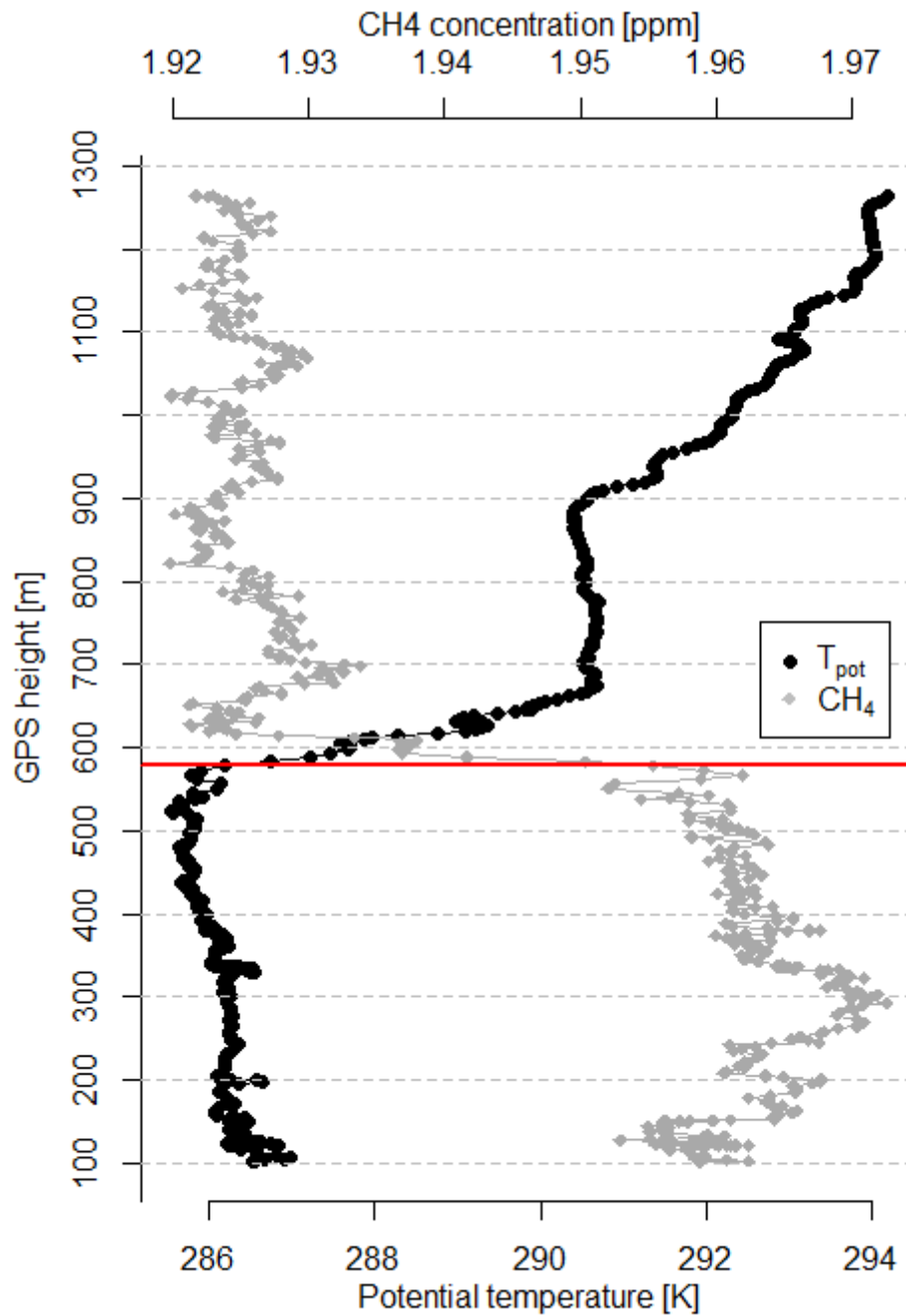


Fig. 6: Exemplary plot of the potential temperature (black) and the methane concentration (grey) against the height in order to determine the boundary layer. Here the height of the boundary layer is indicated by the horizontal red line.

For hyperspectral camera operation the settings of the camera had to be adapted to weather and surface conditions. Challenging was the search for appropriate settings for the camera above sea ice in preparation for the next MELTEX campaign, as the reflectivity of the ice is very high, whereas that of the water is quite low.

The laser scanner was used for mapping the terrain and for observing changes of the terrain. Since the laser scanner is not eye-safe below 50 m, it had to be ensured during flight that it is only switched on during high level legs.

On some rare occasions heating of the nose boom instruments was activated to avoid damage due to freezing water that might have collected during cloud passes. This heating influences some temperature recordings. Heating was not activated during low level flights for flux measurements.

4.4 Post-flight Procedures

After the flights, the flight track was cut in several sub-legs based on altitude, roll angle and heading (true track). This means that both altitude and heading of the airplane should be constant within one leg and the roll angle should only vary minimally. Fig. 7 illustrates the roll angle and the heading of an airplane.



Fig. 7: Illustration of the roll angle and the heading of an airplane. The picture shows Polar 5 at the airport in Inuvik. Picture: K. Kohnert.

Consequently, in the end, one science flight consists of several horizontal low level legs, several ascents and descents and on some days also additional horizontal legs in higher altitude or flight patterns for the calibration of instruments. Parts of the flight track where one of the three above mentioned parameters was too variable were excluded.

During and after the expedition the collected raw data were, if necessary, corrected and then also cut into legs according to the before defined legs.

4.5 Calibration

After the campaign the Los Gatos FGGA was checked for correctness and calibrated in the laboratory. It turned out that the wet mole fractions of methane and carbon dioxide as well as water vapor measured during AIRMETH 2013 had to be corrected, as the values measured by the FGGA were too high. Consequently, the values measured during the campaign had to be reduced afterwards with the correction factors determined based on the calibration (Table 3).

Table 3: Measured concentrations of methane, carbon dioxide and water vapor before calibration of the FGGA and concentration of the gases in the references gas and created by the dew point generator, respectively. The last row shows the correction coefficient calculated by the quotient of actual concentration in the gas and concentration measured before calibration.

	CH₄ wet	CO₂ wet	H₂O
Concentration before calibration ppm	2.07862	503.12	19807.7
Actual concentration ppm	2.04538	498.47	17718.37
Correction coefficient	0.98401	0.99076	0.8945

For methane and carbon dioxide the corrected dry mole fractions were computed based on the dilution effect with the formula

$$X_{dry} = X_{wet} / (1 - (X_{H_2O} / 10^6)) \quad (2)$$

5 Cooperation

Since 2012, AIRMETH has developed a number of internal (i.e. within AWI and GFZ), national, and international collaborations with individual research groups as well as large collaborative projects, which will be briefly introduced here.

5.1 Internal and national collaboration and synergies

AIRMETH contributes to several remote sensing research activities at AWI's Potsdam Unit. The Helmholtz Young Investigators Group COPER (Coastal permafrost erosion, organic carbon and nutrient release in the Arctic nearshore zone) led by Hugues Lantuit is supported by repeated high-resolution mapping of the entire Yukon Territory Beaufort Sea coastline between the Mackenzie Delta and the Alaskan border as well as on Herschel Island using an onboard Riegl VQ580 laser scanner. These data enable the COPER team to precisely determine the rate of coastal erosion and help to quantify the volume of organic material transferred into the near-shore coastal system.

Hyperspectral imaging of the tundra surface during higher-altitude flights along the North American Arctic Transect (NAAT) and elsewhere on the North Slope of Alaska using the AWI AISA Eagle camera supports ongoing and proposed investigations of vegetation and permafrost properties by Birgit Heim and Marcel Buchhorn (AWI, Potsdam) and feeds into the preparation of upcoming satellite missions such as EnMAP. Both laser scanning and hyperspectral remote sensing also contribute to work by Guido Grosse (AWI, Potsdam) within his NSF and ERC projects. Hyperspectral data are processed and analyzed in close collaboration between remote sensing groups at GFZ and AWI. In total, more than 800 km of hyperspectral and laser scan data were collected on the North Slope of Alaska alone.

Specific to AIRMETH 2013 were AISA Eagle tests above melting sea ice in order to optimize camera settings for the upcoming MELTEX campaign (Impact of melt ponds on energy and momentum fluxes between atmosphere and sea ice; Gerit Birnbaum, AWI, Bremerhaven)

Nationally, a newly developed collaboration between AWI (Birgit Heim), GFZ and the University of Erlangen (Matthias Braun) depends on the high-resolution AIRMETH hyperspectral data and DLR/University of Würzburg ground validation work for TerraSAR-X on Richards Island (Mackenzie Delta) benefits greatly from both hyperspectral and laser scan data acquired during AIRMETH, while AIRMETH gains access to much needed Delta-wide remote sensing products.

AIRMETH is also a major contribution to the Helmholtz Network Regional Climate Change (REKLIM, Topic 3) and will provide results to the AWI coordinated EU FP7 project PAGE 21 (Changing Permafrost in the Arctic and its Global Effects in the 21st Century).

5.2 International collaboration

Internationally, collaborations have been developed both with several multi-year large-scale projects in Alaska and with Canadian institutions operating in the Mackenzie Delta area.

In Alaska, AIRMETH cooperates with the NASA Carbon in Arctic Reservoirs Vulnerability Experiment (CARVE) by coordinating flights and sharing data and results. Since March 2012, CARVE has spent 465 science flight hours in monthly campaigns on NASA's C-23 Sherpa aircraft to measure concentrations of various trace gases over various Alaskan permafrost areas including the North Slope. While CARVE

relies on inverse modeling to derive trace gas fluxes from their concentration measurements, AIRMETH gets fluxes directly based on the combination of the fast 3D wind measurements at the turbulence nose boom and 20 Hz CH₄, CO₂, and H₂O measurements. The collaboration and simultaneous flights allow us to compare concentration patterns, vertical profiles, aircraft-measured fluxes, and concentration-derived modeled fluxes during multiple years.

The US Department of Energy funded Next Generation Ecosystem Experiments (NGEE) project conducts intensive ground-based measurements and modeling of permafrost processes and development on the Barrow Peninsula. While NGEE is interested in regional scale measurements for up-scaling their local results and validating model results, AIRMETH benefits from a wealth of information on the state of vegetation, permafrost, heat and carbon fluxes and other relevant environmental parameters.

In Canada, AIRMETH collaborates with Environment Canada via both the TerraSAR-X ground validation efforts and the COPER coastal erosion work as well as with the Geological Survey of Canada (Scott Dallimore), focusing on the geogenic methane emissions in the outer Mackenzie Delta.

New Canadian partners at the Université de Montréal (Oliver Sonnentag) operate a flux tower at Trail Valley, which currently constitutes the only ground reference site for carbon fluxes in the Mackenzie Delta area.

6 Flight Protocol for AIRMETH 2013

In this chapter the 16 science flights will be described separately. For each day, the flight route will be shown and some in-flight observations will be described. During AIRMETH 2013 the 16 science flights consisted of tracks with different aims that are listed and explained in the following:

Table 4: Description of different science flight and calibration pattern flown during AIRMETH 2013.

Name	Description
• Flux measurements	Flight at altitude of about 50 m agl, constant heading and roll angle
• Boundary layer profiles (BL profiles)	At the beginning and end of each transect, at least until the top of the BL, usually, however, until 600 – 1,800 m.
• Hyperspectral camera operation	Flight in 600 – 1,800 m agl, constant heading and roll angle.
• Laser scanner operation	Flight in 600 – 1,800 m agl, constant heading and roll angle.
• Hyperspectral area mapping	Flight in about 1,200 m (4,000 ft) (Barrow)/ 1,800 m (6,000 ft) (Inuvik) agl, flight lines close to each other in order to get the hyperspectral information of an area instead of only a transect.
• Coastal scan	Laser scanner operation along the part of the northern Canadian coast and Herschel Island for coastal erosion studies.
• Calibration hyperspectral camera/laser scanner	Aim: calibration of the boresight angle. “Boresight is the physical mounting angles between an [inertial mounting unit] IMU and a digital camera that theoretically describe the misalignment angles between the IMU and the digital camera frames of reference” (Mostafa, 2001). It is important to know the relative orientation of the camera frame in relation to the mounting unit. For airborne calibration of the boresight angle the airplane flies above control points on the ground that are clearly defined. Three transects are flown that are crossing in 1 point under an angle of 60°, flight altitude 1,200 m.
• Calibration of the radiation sensors/Radiation Square	Aim: detection of potential difference in the angle between the platform where the upward-looking pyranometer is installed and the inertial platform of the airplane. Prerequisite: blue sky and no clouds above the air plane, square, 1 minute per direction, constant speed; One direction towards the sun, one with the sun from behind; Flight above potential clouds.
• Calibration of alpha	One line, 5 minutes increase of indicated air speed (IAS) from the minimum flown during the campaign (approx. 100 knots) to the maximum (approx.. 160 knots); 5 minutes decrease of IAS from 160

knots to 100 knots. Prerequisites are: no vertical movement of neither the air, nor the airplane. Quasi stationary coverage of the IAS spectrum that was relevant during the campaign. Here this calibration was done above sea ice.

- Calibration of beta Square; each direction for one minute at constant speed, after one square is completed repetition at different speed (100/120/140/90 knots). Assumption: wind is spatially and temporarily constant during the calibration. Therefore it would be useful to fly quickly and use small squares. However, those quick and narrow curves are followed up by impreciseness in the measurement of direction.
-

The waypoints were the following:

Barrow, North Slope, Alaska:

- AK1: 71° 18.851'N / 156° 34.226'W Barrow
- AK2: 70° 22.700'N / 157° 21.100'W Atqasuk
- AK3: 70° 13.136'N / 153° 10.298'W Inigok
- AK4: 70° 24.000'N / 153° 10.298'W Teshekpuk
- AK5: 70° 33.450'N / 157° 12.500'W Atquasuk-north
- AK6: 70° 9.000'N / 156° 41.250'W
- AK7: 70° 0.190'N / 153° 1.560'W Inigok-south
- AK8: 71° 10.000'N / 156° 00.000'W UIC east
- AK9: 70° 7.700'N / 156° 00.000'W
- AK10: 70° 9.686'N / 148° 28.008'W Deadhorse
- AK11: 70° 36.800'N / 159° 49.800'W Wainright-north
- AK12: 70° 25.600'N / 159° 49.180'W Wainright-central
- AK13: 70° 13.000'N / 159° 49.800'W Wainright-south
- UIC: 71° 2.100'N / 157° 16.700'W



Fig. 8: Overview over the waypoints and transects flown during AIRMETH 2013 in the area around Barrow. Yellow lines show transects with flux measurements, orange transects for hyperspectral camera and laser scanner operation. Blue lines show lines only overflown during boundary layer profiles. Not shown are legs for calibration and the hyperspectral grid.

Hyperspectral grid near Barrow:

HS-1:	71° 19.100'N / 156° 39.250'W
HS-2:	71° 14.600'N / 156° 39.810'W
HS-3:	71° 19.100'N / 156° 38.320'W
HS-4:	71° 14.600'N / 156° 38.870'W
HS-5:	71° 19.100'N / 156° 37.390'W
HS-6:	71° 14.600'N / 156° 37.930'W
HS-7:	71° 19.100'N / 156° 36.450'W
HS-8:	71° 14.600'N / 156° 36.990'W
HS-9:	71° 19.100'N / 156° 35.500'W
HS-10:	71° 14.600'N / 156° 36.050'W



Fig. 9: Location of waypoints for hyperspectral grid near Barrow

Inuvik, Mackenzie Delta, Canada:

- | | |
|-------------------------------------------------------|-----------------------------------|
| C1: 68° 24.000'N / 134° 31.000'W | C12: 68° 44.850'N / 136° 55.400'W |
| C2: 69° 19.500'N / 135° 30.500'W | C13: 68° 24.000'N / 134° 53.000'W |
| C3: 68° 54.000'N / 135° 30.000'W | C14: 67° 30.000'N / 134° 53.000'W |
| C4: 69° 33.000'N / 134° 21.000'W (Richards Island) | C15: 67° 30.000'N / 134° 31.000'W |
| C5: 69° 27.500'N / 134° 39.500'W (Mallik) | C16: 67° 30.000'N / 134° 2.000'W |
| C6: 68° 38.000'N / 133° 23.000'W | C17: 69° 25.000'N / 134° 12.300'W |
| C8: 68° 24.000'N / 134° 02.000'W | C18: 68° 33.000'N / 135° 36.000'W |
| C9: 68° 48.500'N / 136° 22.500'W | C19: 68° 24.000'N / 134° 18.000'W |
| C10: 69° 38.800'N / 141° 00.000'W (Demarcation Point) | C20: 68° 23.000'N / 135° 16.000'W |
| C11: 69° 26.500'N / 139° 31.500'W | |

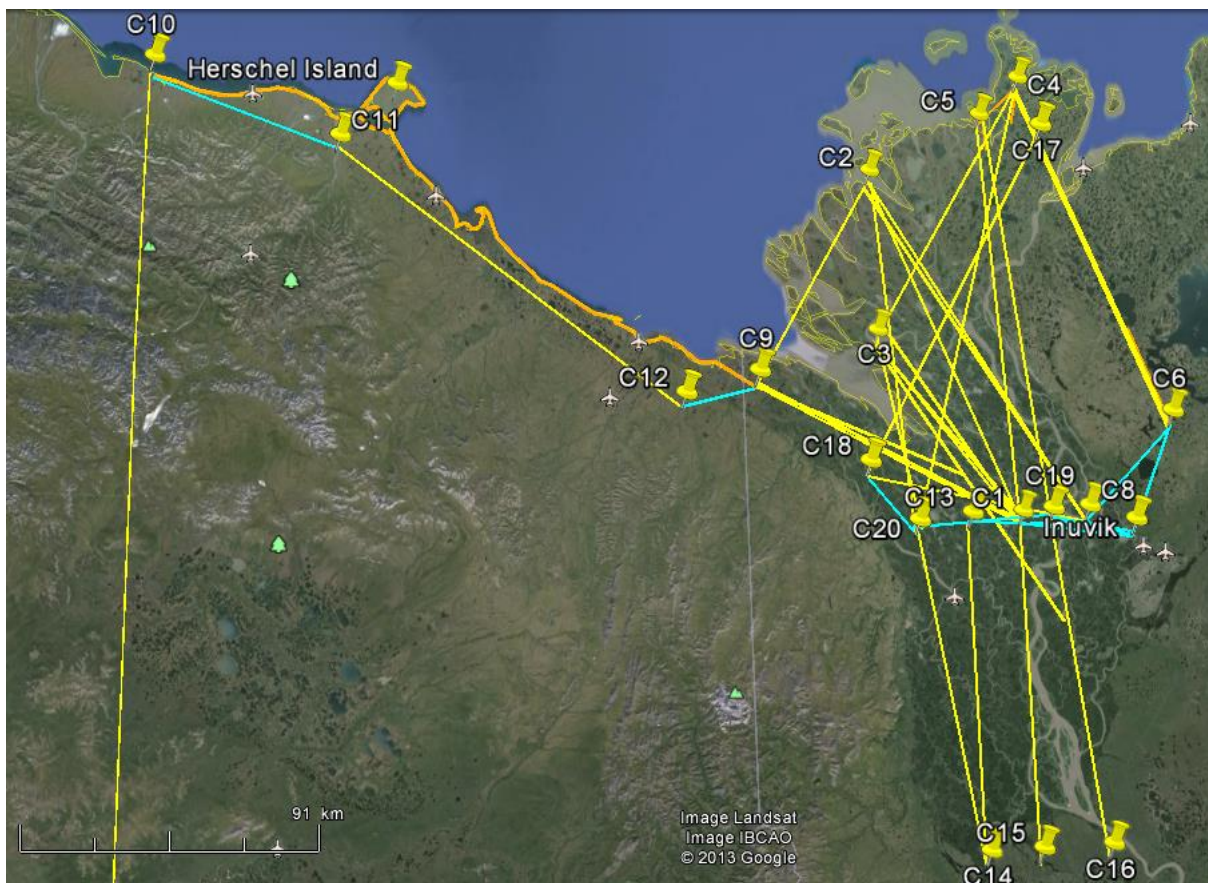


Fig. 10: Overview over the waypoints and transects flown during AIRMETH 2013 in the area around Inuvik. Yellow lines show transects with flux measurements, orange transects for hyperspectral camera and laser scanner operation. Blue lines show lines only overflown during boundary layer profiles. The yellow line southwards from C10 is the Canadian-Alaskan border. Not shown are lines for the hyperspectral grid and for calibration flights.

Hyperspectral grid Inuvik, 6,000 ft:

HS1	68° 24.400'N / 133° 49.500'W
HS2	68° 30.000'N / 133° 49.300'W
HS3	68° 30.000'N / 133° 50.600'W
HS4	68° 24.400'N / 133° 50.800'W
HS5	68° 24.400'N / 133° 52.100'W
HS6	68° 30.000'N / 133° 51.900'W
HS7	68° 30.000'N / 133° 53.200'W
HS8	68° 24.400'N / 133° 53.400'W
HS9	68° 24.400'N / 133° 54.700'W
HS10	68° 30.000'N / 133° 54.500'W



Fig. 11: Location of waypoints for hyperspectral grid near Inuvik

Hyperspectral camera calibration above Inuvik airport



Fig. 12: Location of waypoints for the calibration of the hyperspectral camera above the airport in Inuvik.

HSC-P1	68° 17.88717 N / 133° 41.33583 W
HSC-P2	68° 18.27467 N / 133° 26.87683 W
HSC-P3	68° 18.97067 N / 133° 27.73683 W
HSC-P4	68° 17.50133 N / 133° 29.44717 W
HSC-P5	68° 17.5605 N / 133° 27.29283 W
HSC-P6	68° 18.84567 N / 133° 29.94933 W

Timetable of AIRMETH 2013

Table 5: Overview over the program and activities during AIRMETH 2013. Dates printed in bold letters are days of science flights and are linked to the more detailed description of that day.

Date	Description
July 4	1 st flight: Barrow-Atqasuk-Inigok
July 05	No flight due to fog
July 6	2 nd flight: Barrow-Atqasuk-Inigok, alpha and beta calibration
July 7	3 rd flight, Barrow - Atqasuk - Inigok - Teshekpuk, partly coordinated with CARVE
July 8	4 th flight, Barrow – Atqasuk, flight was interrupted due to technical problems
July 09	No flight due to fog
July 10	5 th flight, Barrow – Atqasuk – Inigok south – Teshekpuk
July 11	6 th flight, Barrow – Inigok - Deadhorse
July 12	7 th flight, Barrow – Atqasuk – Wainwright, hyperspectral area near Barrow
July 13	8 th flight, Barrow – Atqasuk south - Wainwright south – Wainwright – Teshekpuk - Inigok south
July 14	9 th flight, Barrow – Atqasuk – Wainwright – Wainwright south
July 15	Packing <i>Polar 5</i> for the ferry flight to Inuvik; tour for locals through <i>Polar 5</i>
July 16	Ferry flight from Barrow to Inuvik
July 17	Rest day, data analysis
July 18	No flight due to rain
July 19	10 th flight, Inuvik – Mallik – Richards Island - Seeps
July 20	11 th flight, Inuvik – Richards Island – Seeps – Western Delta
July 21	12 th flight, southern delta, hyperspectral area, radiation square in 2,400 m
July 22	13 th flight, coastal scan towards the Alaskan border including Herschel Island, hyperspectral camera calibration
July 23	14 th flight, Inuvik – Richards Island – across the delta
July 24	No flight due to rain
July 25	15 th flight, 2 long transects through the entire delta
July 26	16 th flight, Richards Island, northern part of the delta
July 27	No flight due to technical problems on <i>Polar 5</i> , interviews with a Canadian film crew
July 28	Packing <i>Polar 5</i> for departure
July 29	End of the campaign, flight to Calgary/Edmonton

July 4

Location: Barrow

Takeoff: 12:14 local time, 20:14 UTC

Landing: 15:48 local time, 23:48 UTC

Weather: sunny, convective clouds at the horizon, wind from easterly directions

Route: Barrow - AK1 – AK2 – AK3 – AK2 – AK1- Barrow (see Fig. 13)

Flux measurements, hyperspectral camera operation from half way between AK3 and AK2 to AK2

Observations:

During the first science flight of the campaign the highest concentration of methane (CH_4) was measured on both the first and last leg between a huge lake close to Barrow and Barrow (Fig. 15). The wind was at that day coming from eastern directions, so that the source of the high concentration must have been located south-east of Barrow. Whether there is any connection of the high concentrations with plumes from major brush fires near Ivotuk during that time has to be analyzed. On July 4, no distinct boundary layer could be determined *in-situ* with profiles of potential temperature, relative humidity and methane concentration.

During that flight the altitude was mainly kept low at about 30 m agl (Fig. 14). The pilots mostly contoured the terrain with the plane.

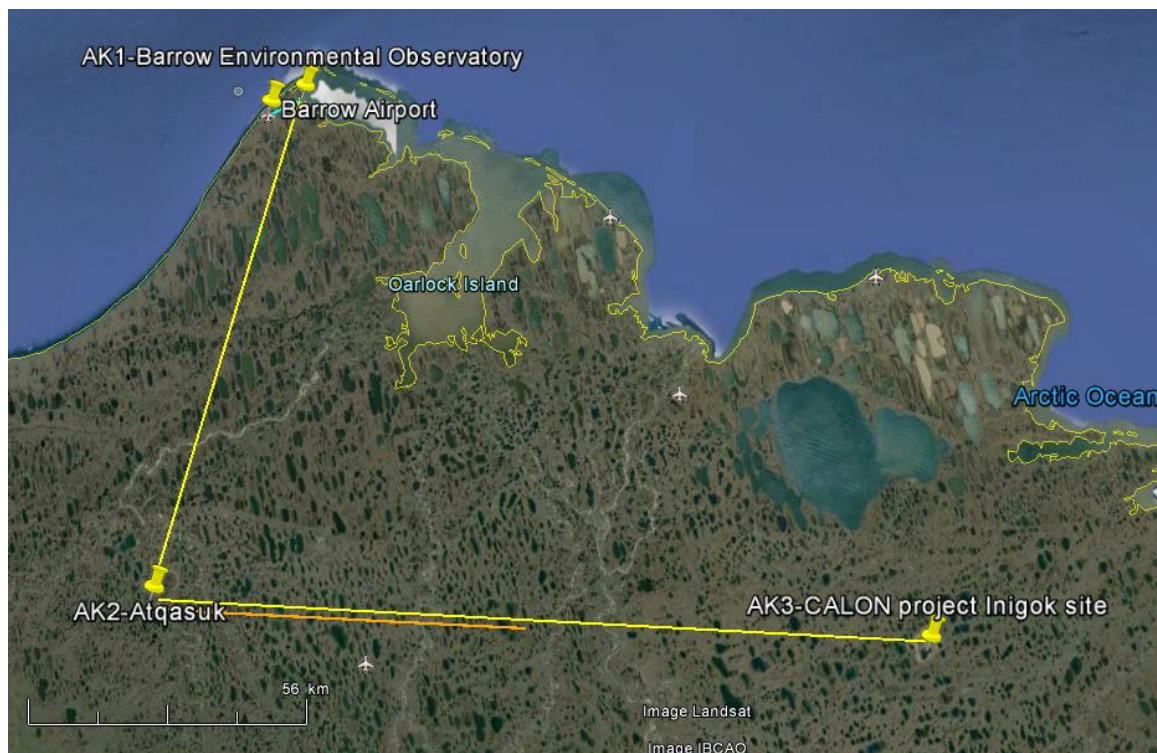


Fig. 13: Flight pattern on July 4, 2013. Yellow lines show transects with flux measurements, orange transects for hyperspectral camera and laser scanner operation.

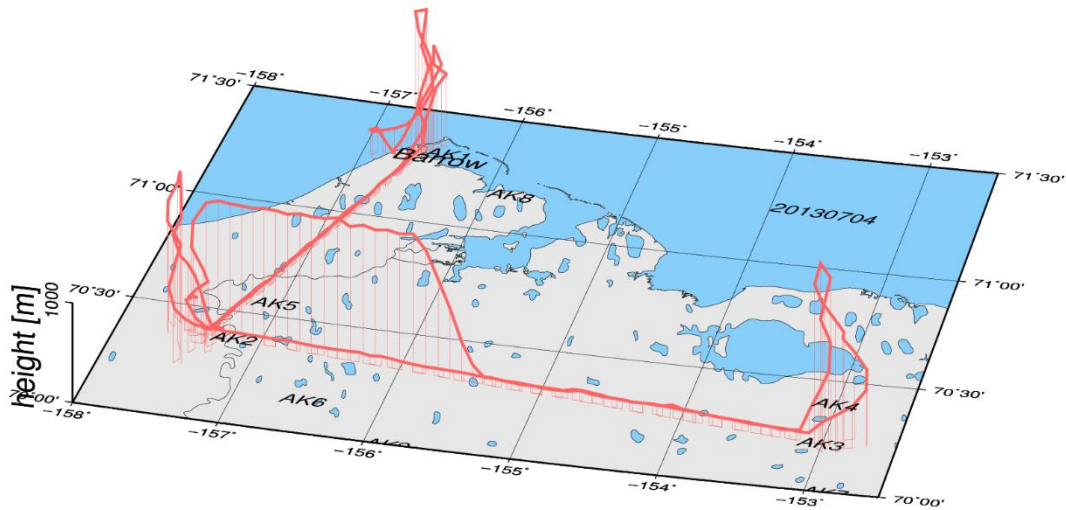


Fig. 14: 3D illustration of the flight track. Shown are low level and high level legs as well as the vertical profile flights.

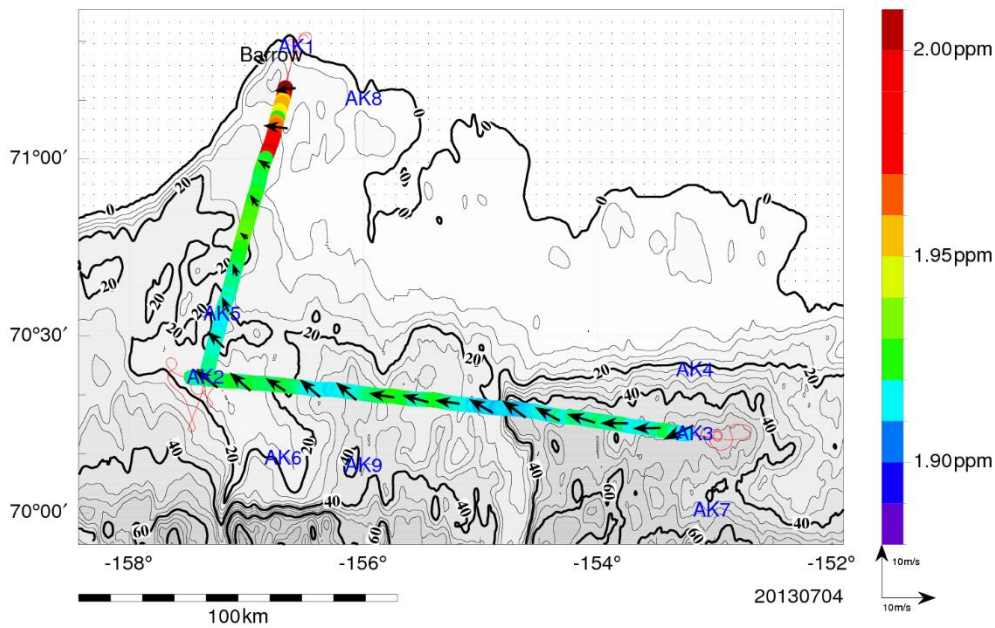


Fig. 15: Methane concentration along the flight transect with respective wind direction. Since the way there and the way back followed the same track, only the data for way there is plotted to get an overview of the situation. Here the runs CP50704h02 and CP50704h04 are shown.

July 6

Location: Barrow

Takeoff: 10:17 local time, 18:17 UTC

Landing: 14:53 local time, 22:53 UTC

Weather: sunny, convective clouds at the horizon, wind from south-western direction

Route: Barrow - AK1 – AK2 – AK3 – Beta Calibration - AK2 – AK1 – Alpha Calibration above ocean – Barrow (see Fig. 16)

During that day only flux measurements at low flight altitude were conducted (Fig. 17).

Observations:

On July 6, the highest methane concentrations were measured close to AK1 and AK3. The boundary layer varied between 400 m at AK2 and 600 m at AK3. The beta calibration was performed close to AK2 at 1,800 m altitude in order to be above cloud level. For that calibration flight about 20 to 25 minutes have to be scheduled. On the last leg from AK2 to AK1 there was a sudden change in wind direction going along with an increase in methane concentration (Fig. 18). The alpha calibration was done at about 45 m above the sea ice in order to have a lower vertical wind speed. For that calibration about 10 to 15 minutes have to be accounted. During that calibration flight melt ponds on the sea ice were observed which were needed for testing hyperspectral camera settings as preparation for the next MELTEX campaign. These hyperspectral camera pictures were recorded on July 12.



Fig. 16: Flight pattern on July 6, 2013. Yellow lines show transects with flux measurements. Blue lines show transects only overflown during boundary layer profiles.

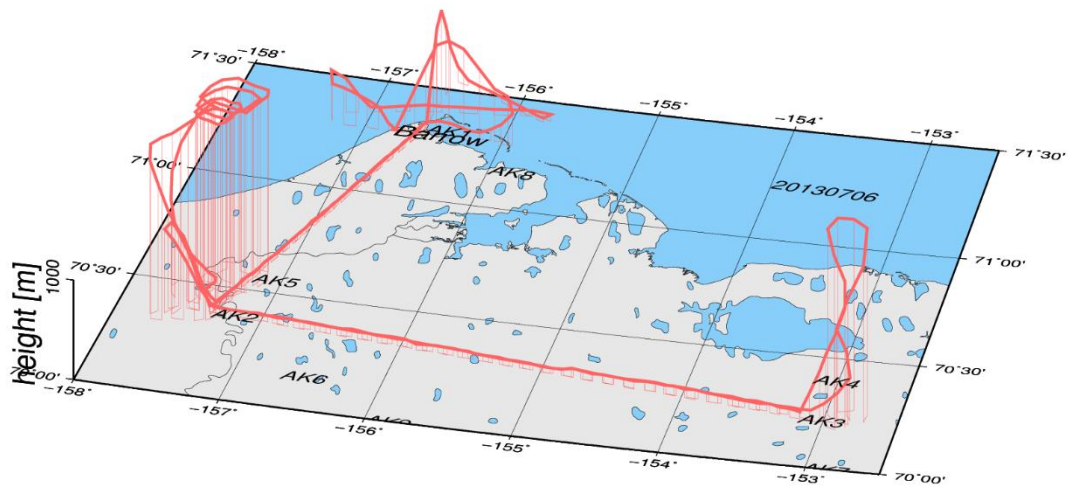


Fig. 17: 3D illustration of the flight track. Shown are low level and high level legs as well as the vertical profile flights.

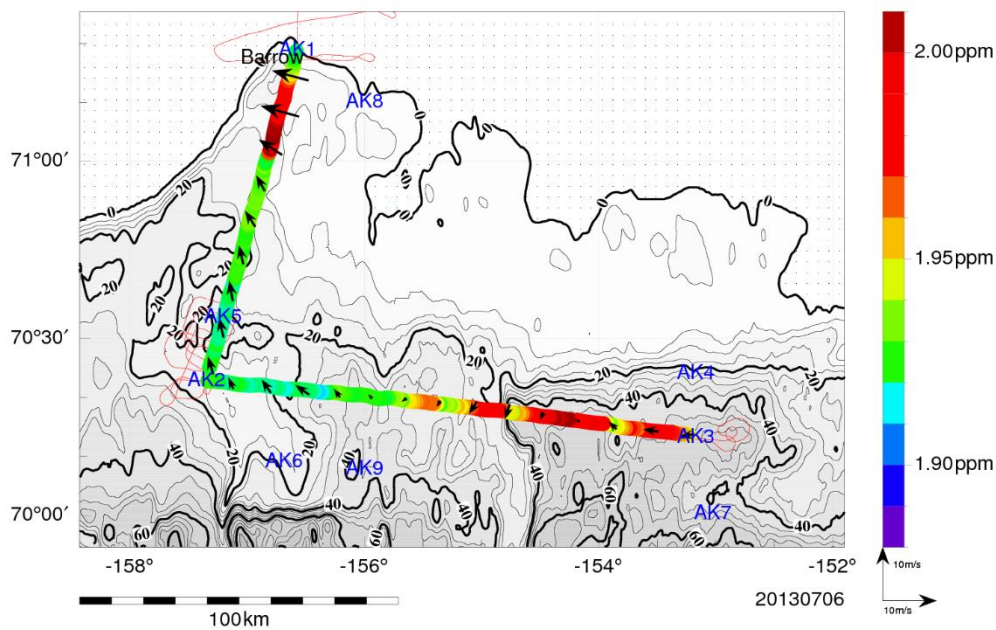


Fig. 18: Methane concentration along the flight transect with respective wind direction. Since the way there and the way back followed the same track only the data for way there is plotted to get an overview of the situation. Here the runs CP50706h03 and CP50706h04 are shown.

July 7

Location: Barrow

Takeoff: 13:31 local time, 21:31 UTC

Landing: 18:44 local time, 02:44 (+1) UTC

Weather: very windy

Route: Barrow - AK 1 – AK 2 – AK 3 – AK 4 – AK 5 – AK 2 – AK 3 – AK 4 – AK 5 – AK 1 – Barrow (see Fig. 19)

During that day only flux measurements at low flight altitude were conducted (Fig. 20).

Observations:

During that flight it was quite windy so that the height above ground was rather variable. After the first leg the flight altitude was increased to 45 – 60 m agl. During the second profile flight of that day at AK2, the plane went through light rain. Apart from the profiles at AK1 with much lower boundary layer heights, the boundary layer was determined to be between 400 and 500 m during that day. During that flight no concentration above 2.00 ppm was measured (Fig. 21).

Remarks:

On July 7, NASA's campaign "CARVE" campaign (Carbon in Arctic Reservoirs Vulnerability Experiment) led by Charles Miller was conducting airborne measurements with the C-23 Sherpa owned by NASA in the area between Barrow and Atqasuk. CARVE is a joint project of the University of California Irvine, Cires University Colorado, JPL, NASA, CALTECH, Harvard University, and San Diego State University.

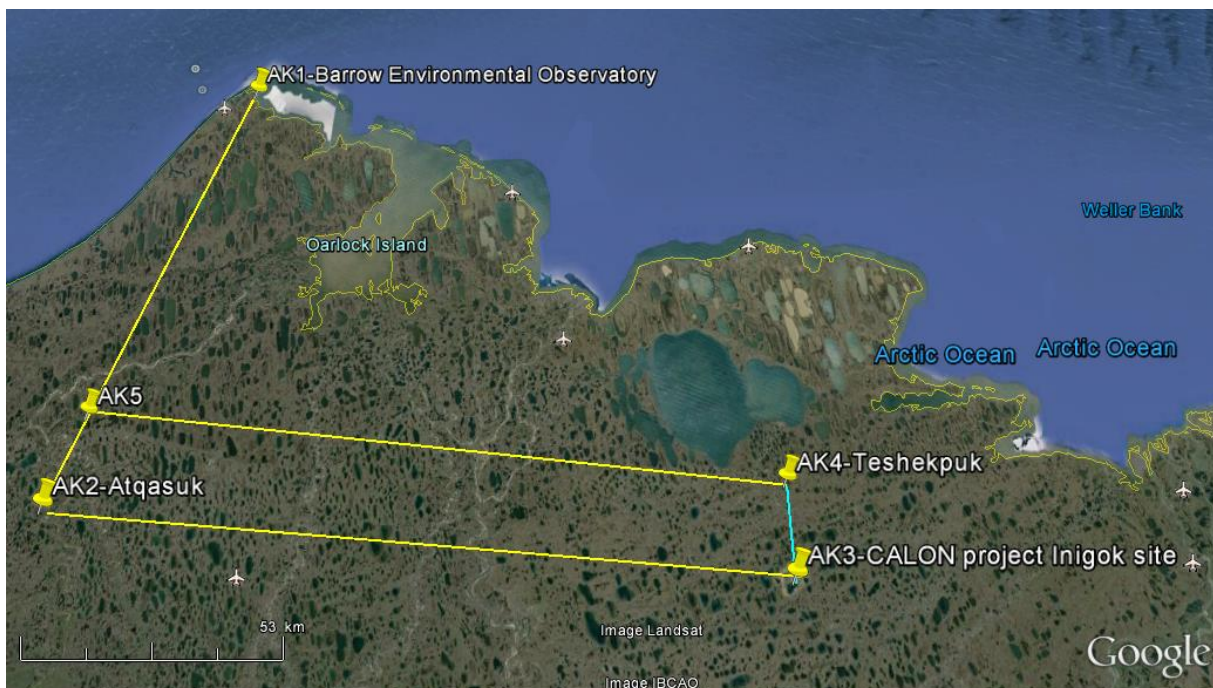


Fig. 19: Flight pattern on July 7, 2013. Yellow lines show transects with flux measurements. Blue lines show transects that were only overflown during boundary layer profiles.

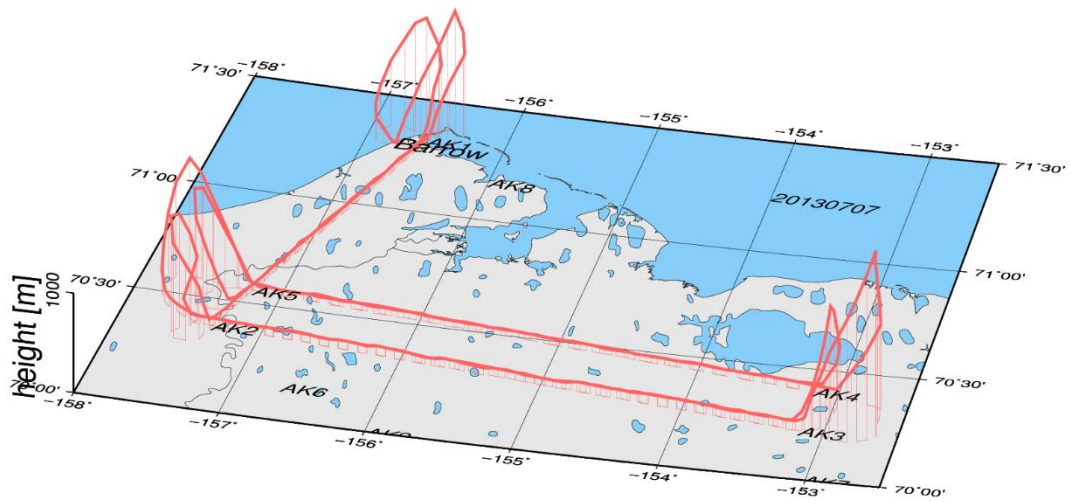


Fig. 20: 3D illustration of the flight track. Shown are low level and high level legs as well as the vertical profile flights.

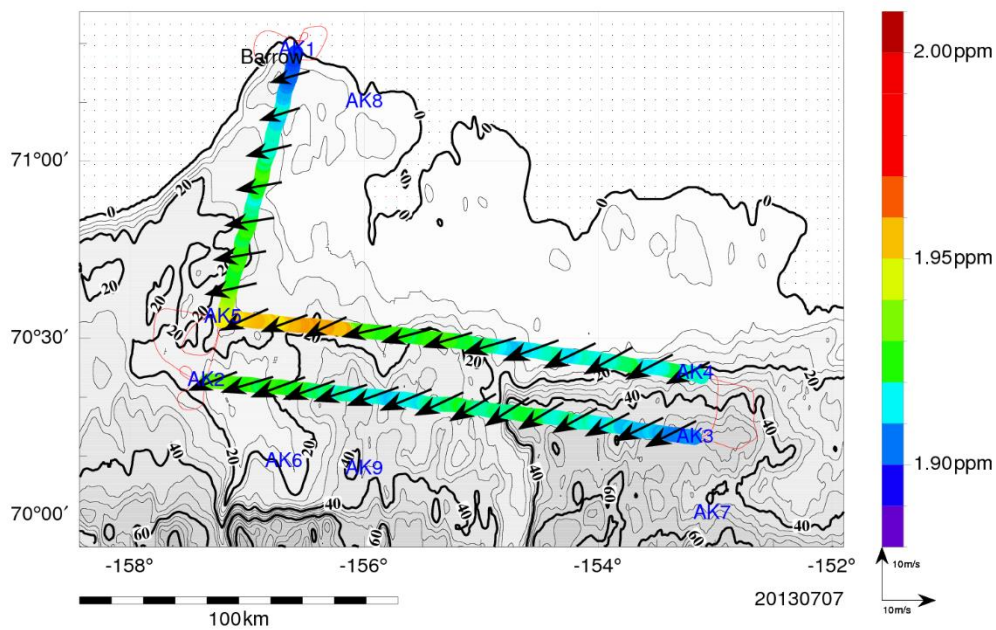


Fig. 21: Methane concentration along the flight transect with respective wind direction. Since the way there and the way back followed the same track only the data for way there is plotted to get an overview of the situation. Here the runs CP50707h03, CP50707h04 and CP50707h06 are shown.

July 8

Location: Barrow

Takeoff: 11:46 local time, 19:46 UTC; Interruption of planned flight pattern. 22:07 UTC

Landing: 14:24 local time, 22:24 UTC

Weather: sunny, wind from northeast

Route: Barrow – AK1 – AK2 – AK1 – AK5 – a bit towards AK4 – heading back to Barrow (see Fig. 22)

Observations: Overall the CH₄ concentrations were lower on July 8 than on the previous days (Fig. 24). The second leg from AK2 to AK1 was flown with a saw-tooth pattern, meaning the plane flew several profiles upwards until the boundary layer was determined and then again downwards to low level (Fig. 23). A technical problem with the aircraft forced us to shorten the pattern and return to Barrow shortly after commencing leg AK5-AK4. The leg from that point towards Barrow airport (shown in purple in Fig. 22) was flown at mainly low level.



Fig. 22: Flight pattern on July 8, 2013. Yellow lines show transects with flux measurement that were flown as planned. White lines show the additional legs that had been planned for that day, but were not flown. The light pink line shows the route that was flown instead of the original plan after the interruption of the regular flight.

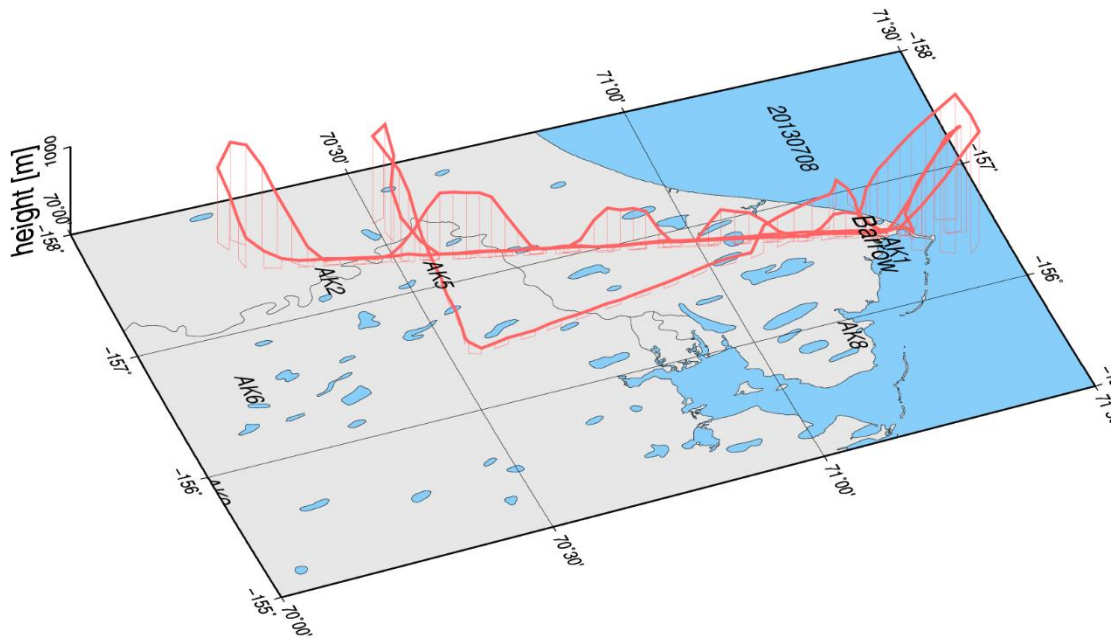


Fig. 23: 3D illustration of the flight track. Shown are low level and high level legs as well as the vertical profile flights.

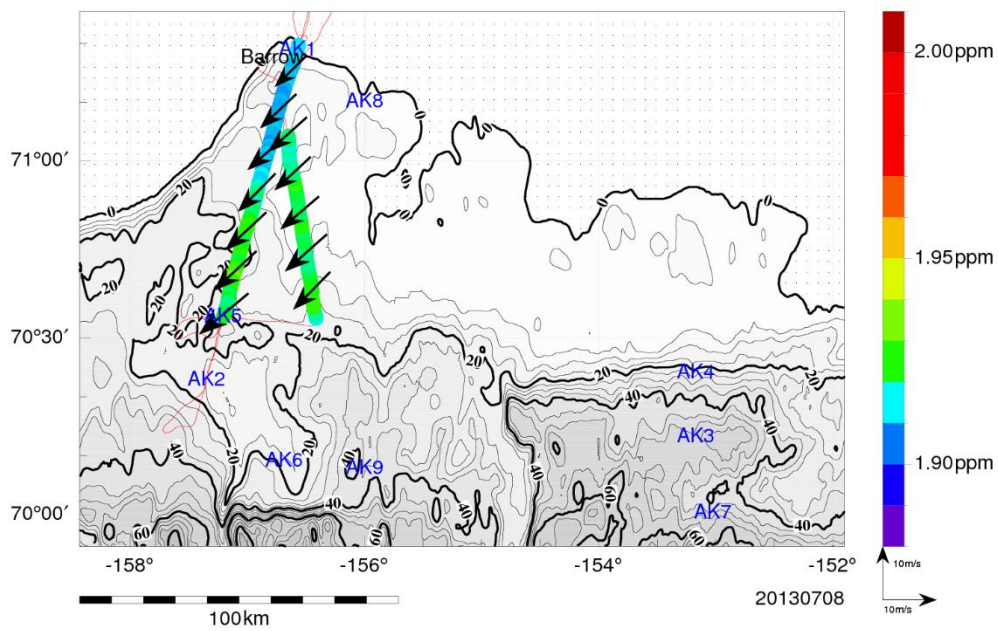


Fig. 24: Methane concentration along the flight transect with respective wind direction. Since the way there and the way back followed the same track only the data for way there is plotted to get an overview of the situation. Here the runs CP50708h06 and CP50708h08 are shown.

July 10

Location: Barrow

Takeoff: 13:04 local time, 21:04 UTC

Landing: 17:16 local time, 01:16 (+1) UTC

Weather: sunny, wind from east/north-east

Route: Barrow – AK1 – AK5 – AK4 – AK7 – AK9 – AK8 – AK6 – AK2 – AK1 – AK8 – AK1 – Barrow (see Fig. 25)

Flux measurements and hyperspectral camera operation between AK1 and AK5 and between AK8 and AK1 (Fig. 26).

Observations:

On July 10 the CH₄ concentrations measured during the flight were mainly between 1.95 and 2.0 ppm and did not exceed 2.0 ppm (Fig. 27).

Remarks:

Between AK8 and AK1 the coast line was laser-scanned at 600 m agl in support of coastal erosion studies.



Fig. 25: Flight pattern on July 10, 2013. Yellow lines show transects with flux measurements, orange transects for hyperspectral camera and laser scanner operation. Blue lines show legs only overflown during boundary layer profiles.

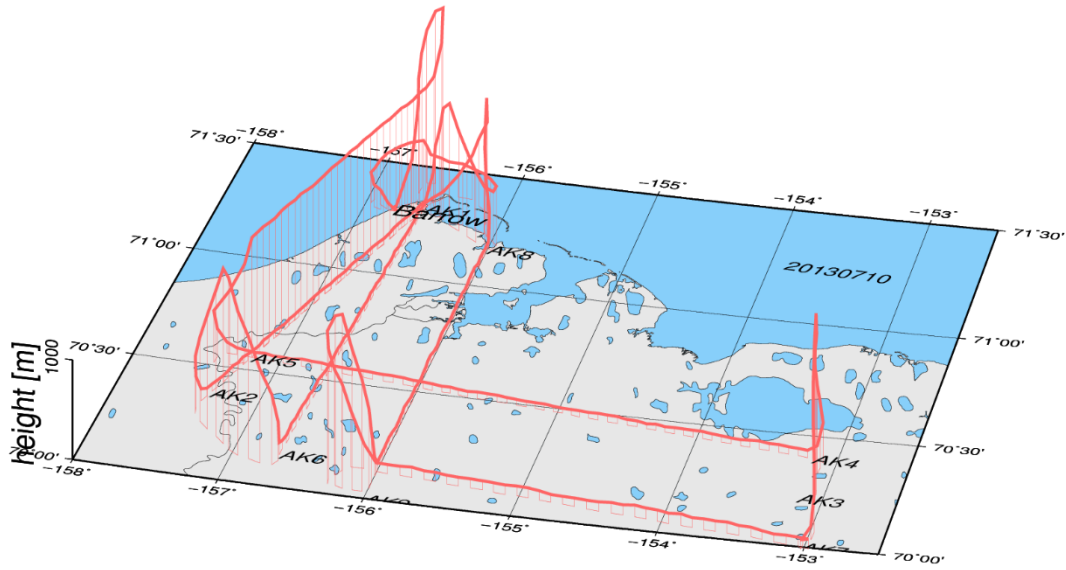


Fig. 26: 3D illustration of the flight track. Shown are low level and high level legs as well as the vertical profile flights.

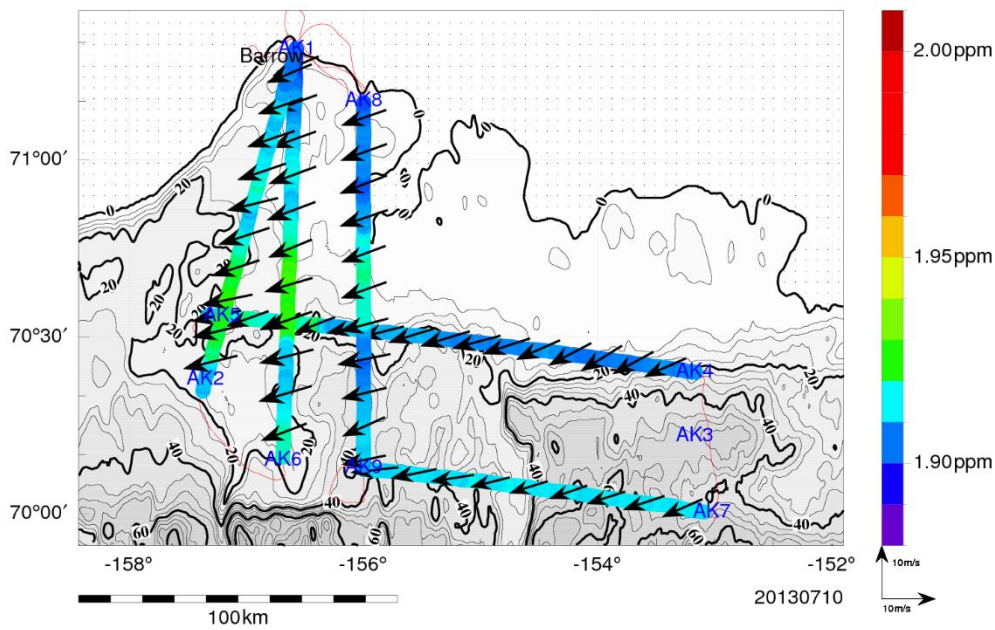


Fig. 27: Methane concentration along the flight transect with respective wind direction. Since the way there and the way back followed the same track only the data for way there is plotted to get an overview of the situation. Here the runs CP50710h01, CP50710h02, CP50710h03, CP50710h04, and CP50710h05 are shown.

July 11

Location: Barrow

Takeoff: 11:01 local time, 19:01 UTC

Landing: 16:15 local time, 00:15 (+1) UTC

Weather: blue sky, sunny and a bit misty

Route: Barrow – AK1 – HS1 – AK3 – AK10 – AK3 – UIC – HS1 – Hyperspectral Area – Barrow (see Fig. 28)

Flux measurements, hyperspectral camera operation between AK10 and AK3, hyperspectral area grid at HS1 in 1,200 m altitude (Fig. 29).

Observations:

The level of methane concentrations on the leg from HS1 to AK3 was low, which might be due to flying parallel and close to the coast. At the oil fields close to Deadhorse CH₄ concentration increased abruptly for a short time above 2.0 ppm (Fig. 30). However, this was only found on the first way towards east. On the way back the concentrations were lower above the same area. The hyperspectral area near Barrow was overflowed at 1,200 m altitude.



Fig. 28: Flight pattern on July 11, 2013. Yellow lines show transects with flux measurements, orange transects for hyperspectral camera and laser scanner operation. Blue lines show legs only overflowed during boundary layer profiles.

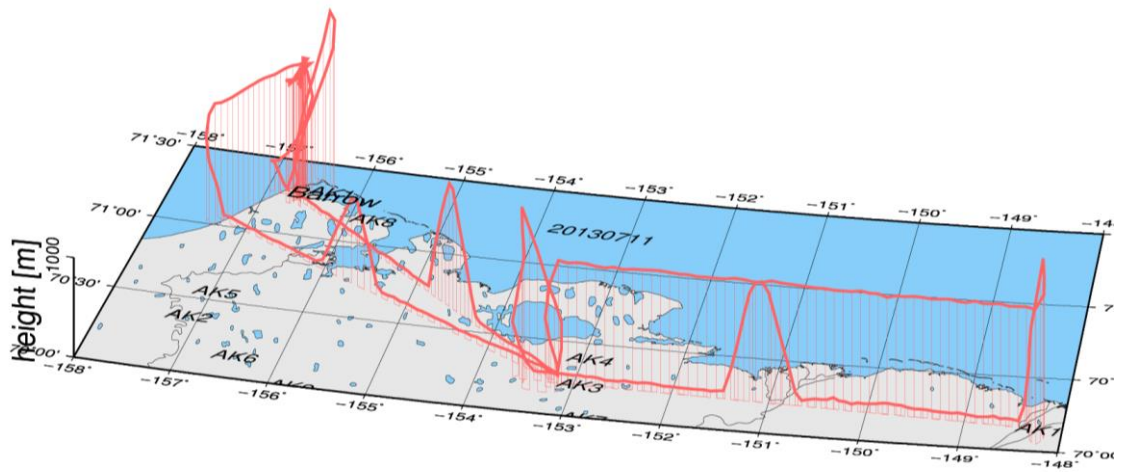


Fig. 29: 3D illustration of the flight track. Shown are low level and high level legs as well as the vertical profile flights.

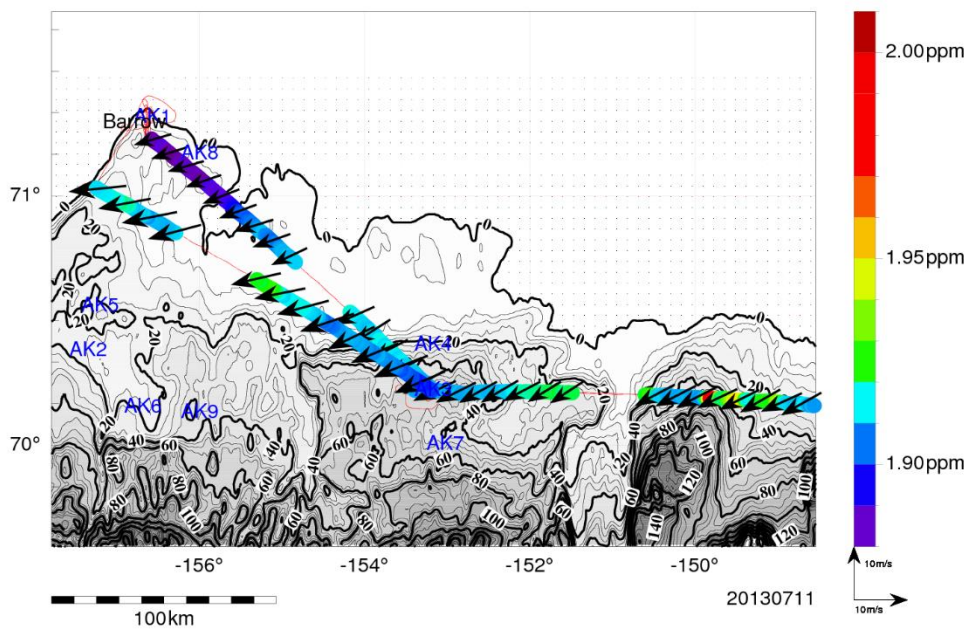


Fig. 30: Methane concentration along the flight transect with respective wind direction. Since the way there and the way back followed the same track only the data for way there is plotted to get an overview of the situation. Here the runs CP50711h01, CP50711h02, CP50711h03, CP50711h04, CP50711h05, and CP50711h06 are shown. Gaps in the lines are due to vertical profile flights in the middle of the respective legs.

July 12

Location: Barrow

Takeoff: 11:12 local time, 19:12 UTC

Landing: 16:06 local time, 00:06 (+1) UTC

Weather: sunny, blue sky, very few clouds on the horizon

Route: Barrow - AK1 – AK2 – AK12 – AK2 – AK12 – AK11 – AK5 – AK11 – AK5 – AK1 Hyperspectral camera testing over sea ice + calibration of the radiation sensors– Barrow (see Fig. 31)

Flux measurements, hyperspectral camera operation between AK1 and AK2, AK2 and AK12 and AK11 – AK5 and Hyperspectral camera test over sea ice (Fig. 32).

Observations:

During that flight the first leg was flown at 1,200 m. On that transect between AK1 and AK2 strong and abrupt variations in water vapor concentration occurred. The concentrations varied between 2,200 ppm and 4,000 ppm. During the profile to 1,800 m at AK2, the water vapor concentration even dropped to 1,000 ppm; the boundary layer was determined to be at 450 m. During the low water vapor concentrations, maybe the methane background level could be seen. A square above the sea was flown for the calibration of the radiation sensors.



Fig. 31: Flight pattern on July 12, 2013. Yellow lines show transects with flux measurements, orange transects for hyperspectral camera and laser scanner operation. Blue lines show legs only overflown during boundary layer profiles. The picture is excluding the location of the waypoints for the hyperspectral grid near Barrow (Fig. 9).

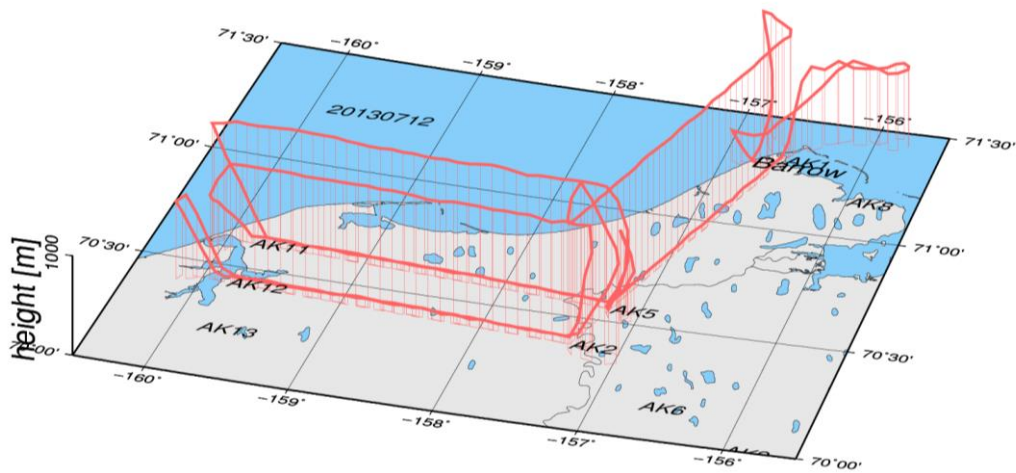


Fig. 32: 3D illustration of the flight track. Shown are low level and high level legs as well as the vertical profile flights.

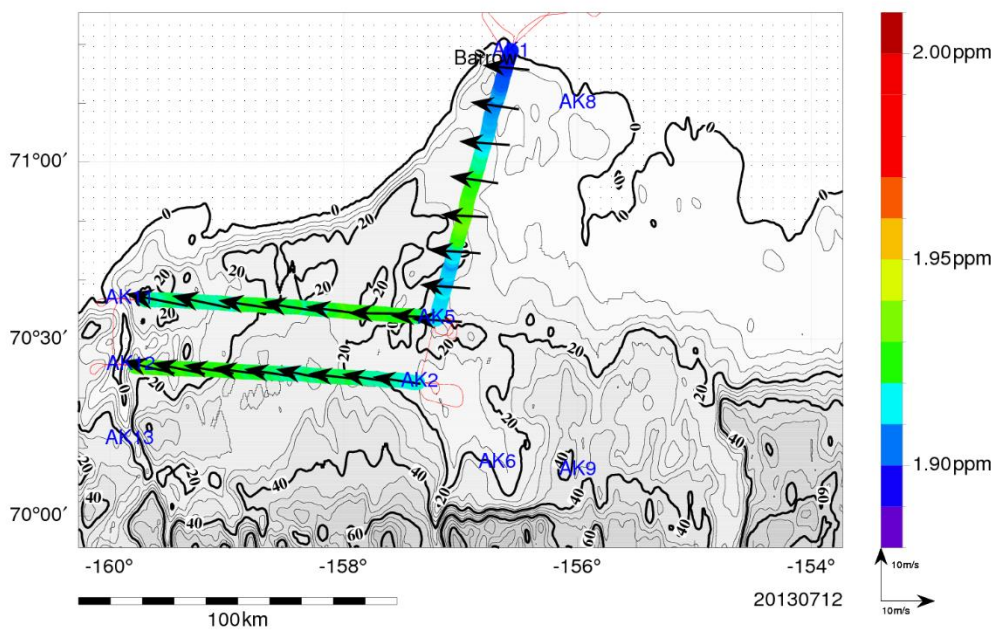


Fig. 33: Methane concentration along the flight transect with respective wind direction. Since the way there and the way back followed the same track only the data for way there is plotted to get an overview of the situation. Here the runs CP50712h02, CP50712h04, and CP50712h05 are shown.

July 13

Location: Barrow

Takeoff: 11:11 local time, 19:11 UTC

Landing: 15:58 local time, 23:58 UTC

Weather: wind from east, sunny

Route: Barrow – AK1 – AK6 – AK13 – AK11 – AK4 – AK5 – AK7 – AK6 – AK1 – Barrow (see Fig. 34)

Flux measurements, hyperspectral camera operation between AK1 and AK6 (Fig. 35).

Observations:

Like on July 12, strong variations in water vapor concentration occurred on the first north-south transect between AK1 and AK6 in an altitude of 1,200 m. The leg between AK6 and AK13 showed that the terrain and surface cover in this area is different to the other regions, as the terrain is more flat and less intersected by rivers. Since the wind came from east, the source for the measured CH₄ concentrations can be far upwind. Eventually, the methane concentration to the west can be higher as the emitted methane can be accumulated over the path. The highest CH₄ concentrations were found towards the west end of the southern leg (Fig. 36).



Fig. 34: Flight pattern on July 13, 2013. Yellow lines show transects with flux measurements, orange transects for hyperspectral camera and laser scanner operation. Blue lines show lines only overflowed during boundary layer profiles.

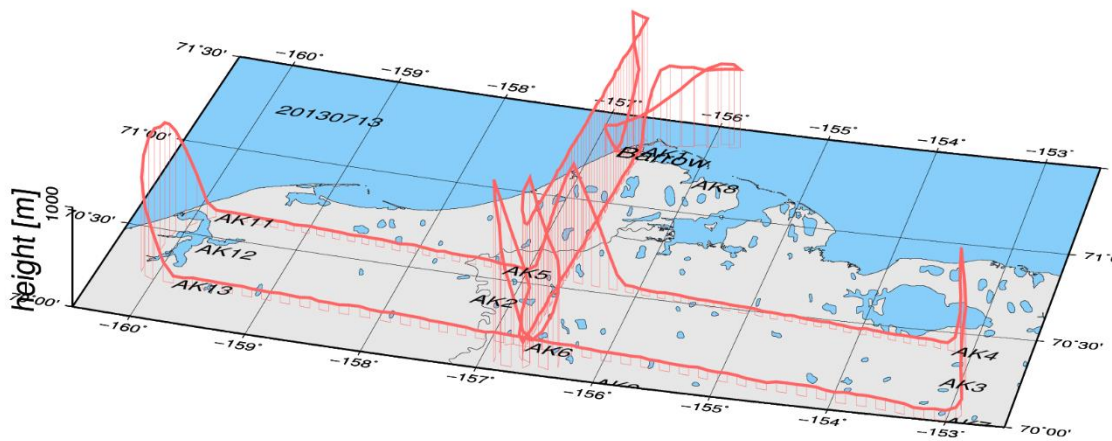


Fig. 35: 3D illustration of the flight track. Shown are low level and high level legs as well as the vertical profile flights.

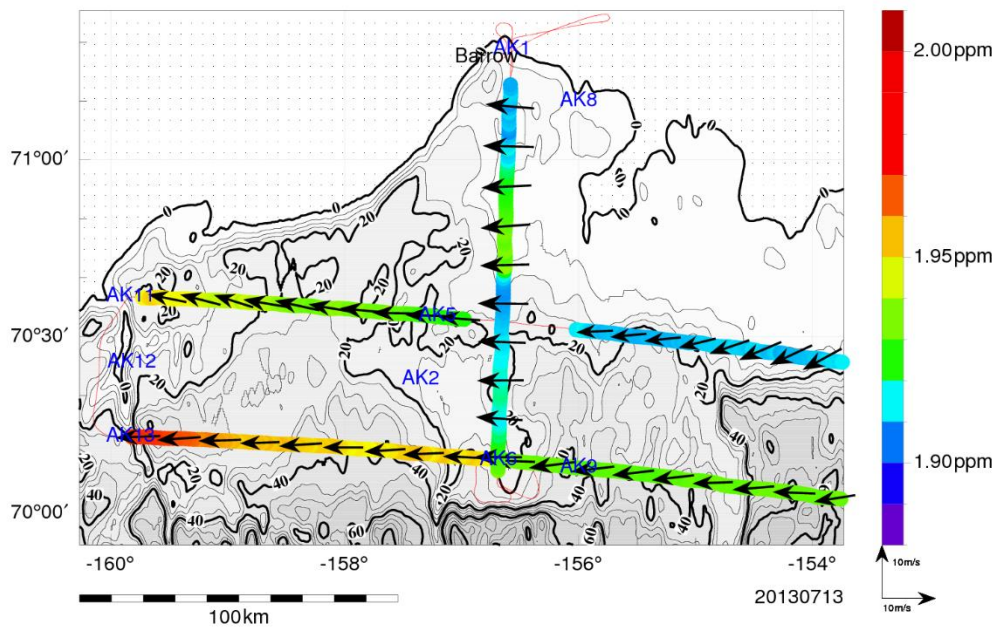


Fig. 36: Methane concentration along the flight transect with respective wind direction. Since the way there and the way back followed the same track only the data for way there is plotted to get an overview of the situation. Here the runs CP50713h01, CP50713h02, CP50713h03, CP50713h04, and CP50713h05 are shown. The gap in the lines is due to a vertical profile flight.

July 14

Location: Barrow

Takeoff: 12:11 local time, 20:11 UTC

Landing: 15:58 local time, 23:58 UTC

Weather: misty, wind from south east, very windy

Route: Barrow – AK8 – AK9 – AK6 – AK13 – AK12 – AK2 – AK6 – AK13 – AK12 – AK2 – AK1 – Barrow
(see Fig. 37)

During that day only flux measurements at low flight altitude were conducted (Fig. 38).

Observations:

On the east-west transects the CH₄ concentration was higher than on the north-south transects (Fig. 39). CH₄ concentration appeared to increase towards west, whereas the CO₂ concentration decreased. Between AK12 and AK2 high surface temperatures up to 29 °C were measured. On the east-west transects, the CH₄ concentration level was higher than on July 12. This might be related to the fact that it was sunny and warm on July 13 accompanied by increasing surface temperatures.



Fig. 37: Flight pattern on July 14, 2013. Yellow lines show transects with flux. Blue lines show transects only overflown during boundary layer profiles.

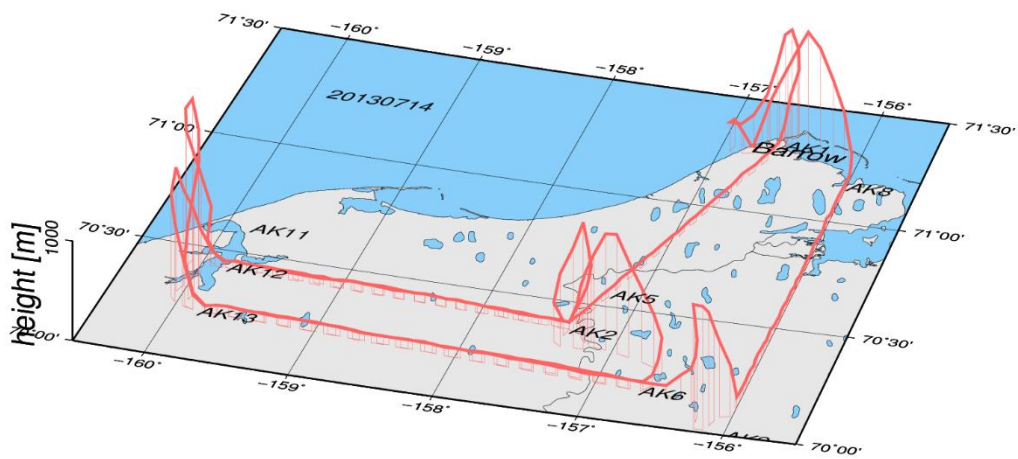


Fig. 38: 3D illustration of the flight track. Shown are low level and high level legs as well as the vertical profile flights.

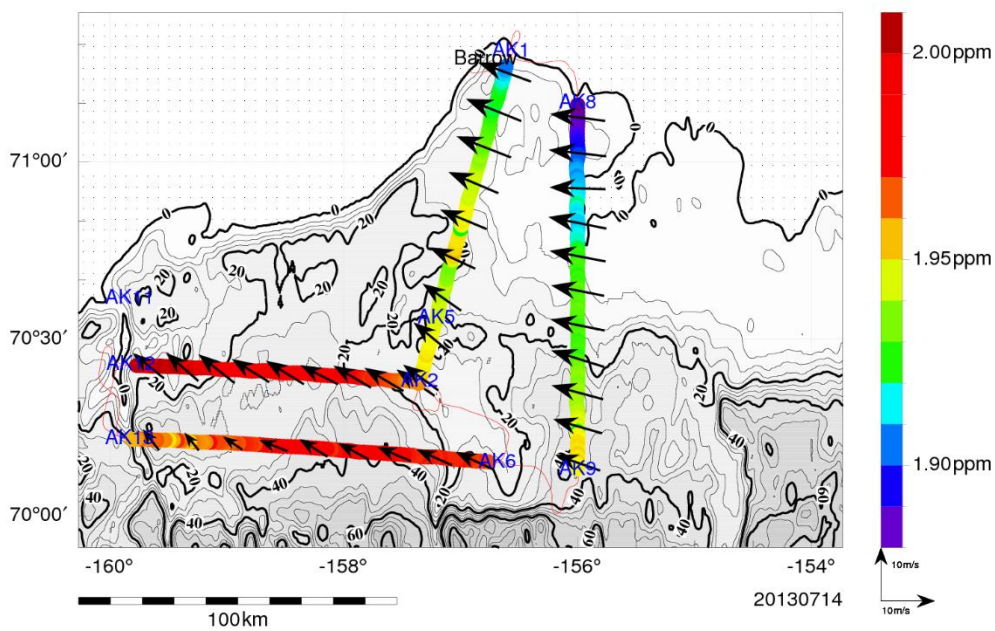


Fig. 39: Methane concentration along the flight transect with respective wind direction. Since the way there and the way back followed the same track only the data for way there is plotted to get an overview of the situation. Here the runs CP50714h01, CP50714h03, CP50714h04, and CP50714h06 are shown.

July 19

Location: Inuvik

Takeoff: 12:25 local time, 18:25 UTC

Landing: 16:39 local time, 22:39 UTC

Weather: sunny, blue sky

Route: Inuvik – C1 – C2 – C1 – C5 – C4 – C3 – C4 – C5 – C1 – Inuvik (see Fig. 40)

Flux measurements, hyperspectral camera operation between C5 and C4 above Mallik site (Fig. 41)

Observations:

The CH₄ concentration level in the Mackenzie Delta was lower than in the area around Barrow and did not exceed 2.0 ppm (Fig. 42). The water vapor concentration, however, seemed higher. The terrain in the Mackenzie Delta and its surrounding shows differences, since it is bordered to the west and east by hills. Especially between C1 and C5 a lot of terrain changes occur. Moreover the land cover changes from south to north as the tree line is crossed.

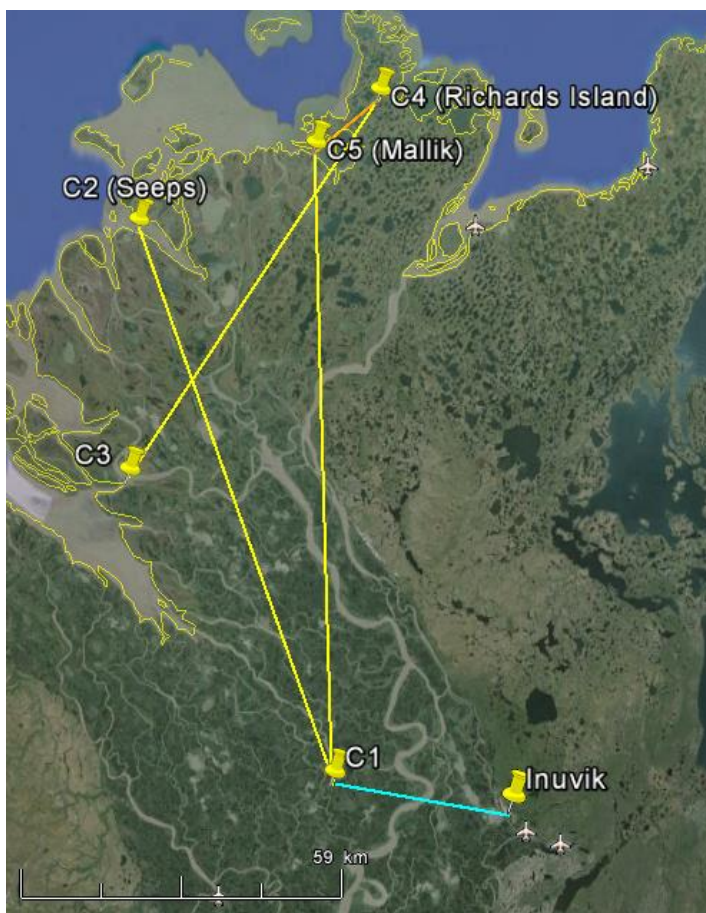


Fig. 40: Flight pattern on July 19, 2013. Yellow lines show transects with flux measurements, orange transects for hyperspectral camera and laser scanner operation. Blue lines show lines only overflowed during boundary layer profiles.

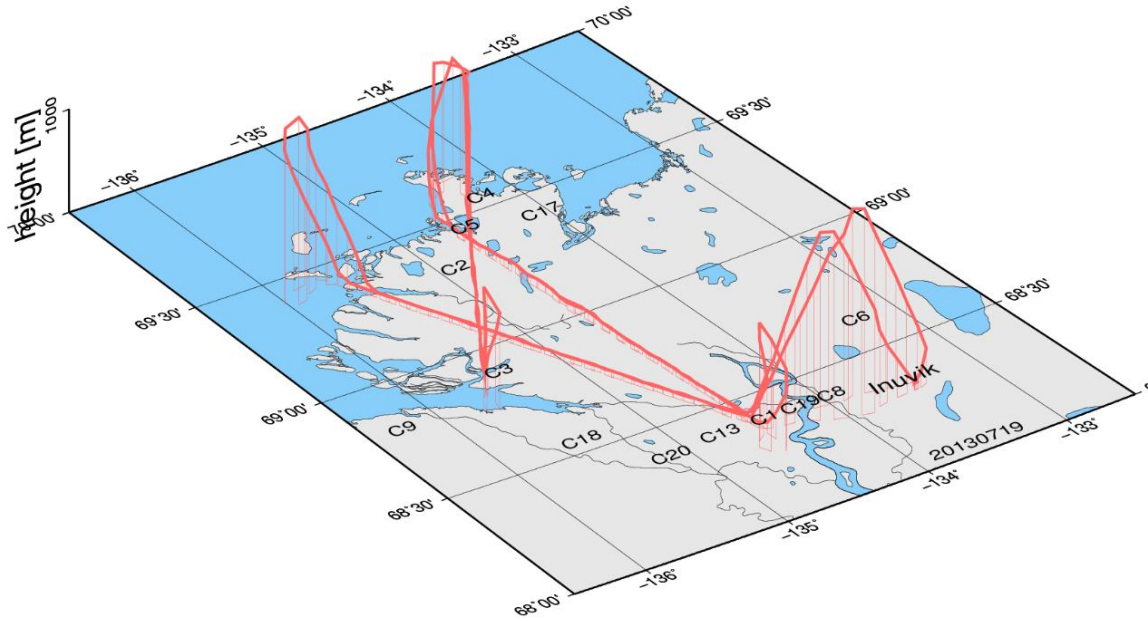


Fig. 41: 3D illustration of the flight track. Shown are low level and high level legs as well as the vertical profile flights.

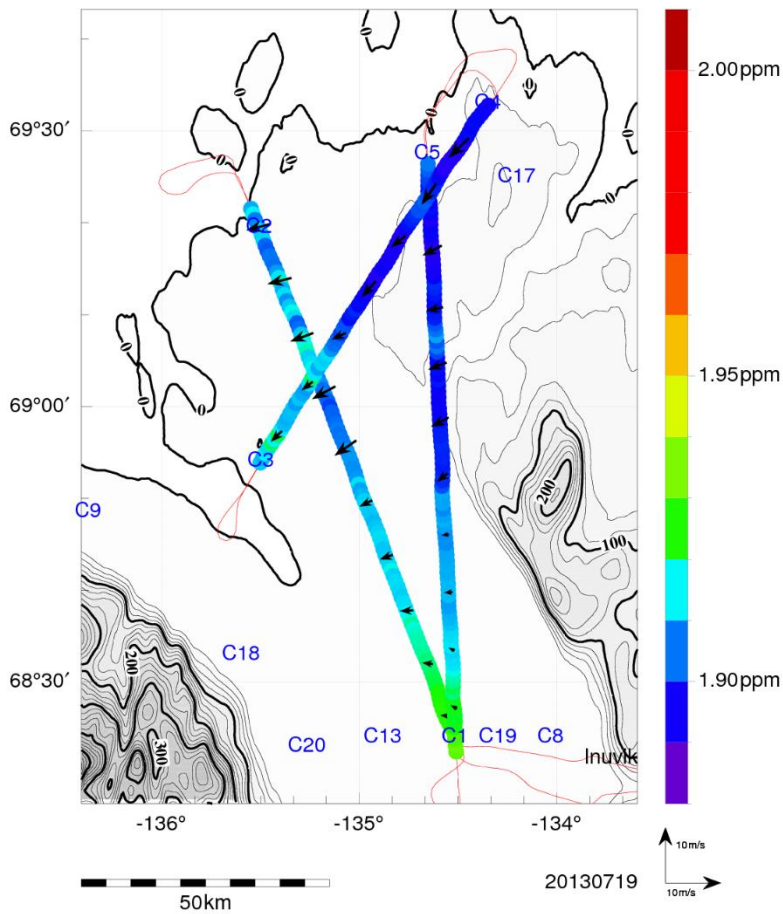


Fig. 42: Methane concentration along the flight transect with respective wind direction. Since the way there and the way back followed the same track only the data for way there is plotted to get an overview of the situation. Here the runs CP50719h02, CP50719h03, and CP50719h05 are shown.

July 20

Location: Inuvik

Takeoff: 12:13 local time, 18:13 UTC

Landing: 17:25 local time, 23:25 UTC

Weather: dry, minor clouds, wind from north-east

Route: Inuvik – C6 – C4 – C6 – C8 – C2 – C8 – C1 – C3 – C1 – C9 – C1 – Inuvik (see Fig. 43)

Only flux measurements at low flight altitude (Fig. 44)

Observations:

The terrain between C6 and C4 is very hilly and therefore has to be treated carefully when calculating fluxes. This leg was mainly chosen because there is a flux tower operated by partners at the Université de Montréal located close to C6 in Trail Valley. Between C4 and C2 the permafrost thickness is reduced to only 60 m. In the area around C2, methane seeps emitting thermogenic methane from shallow gas deposits align along geological fault zones. However, the CH₄ concentration measured on that day did not vary much and mainly reached values between 1.9 and 1.95 ppm (Fig. 45).

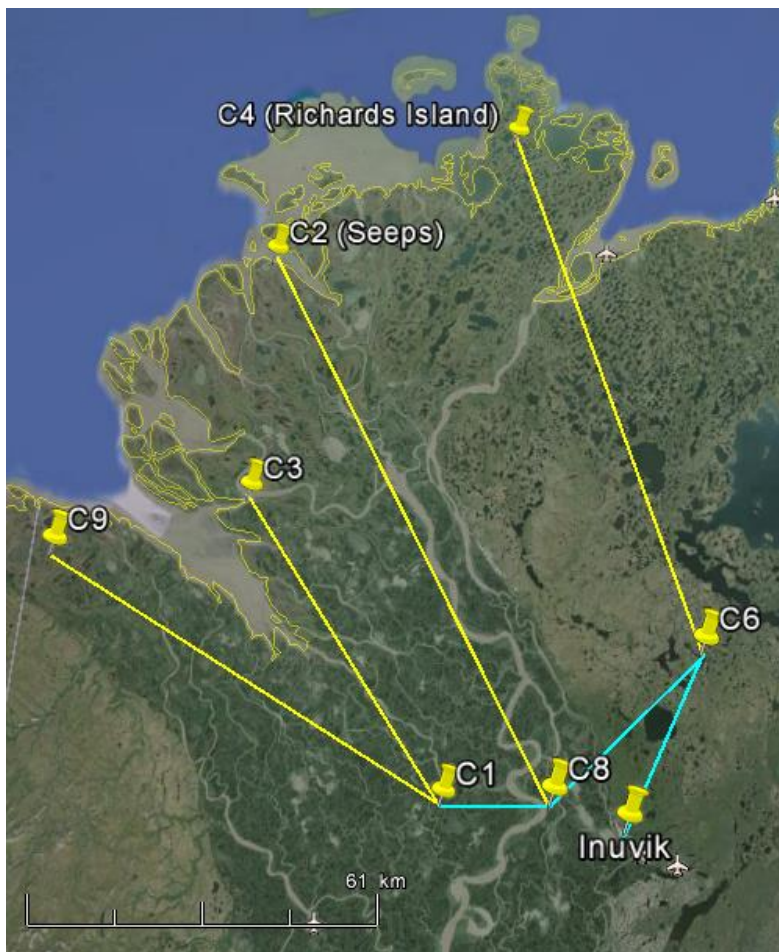


Fig. 43: Flight pattern on July 20, 2013. Yellow lines show transects with flux measurements. Blue lines show lines only overflown during boundary layer profiles.

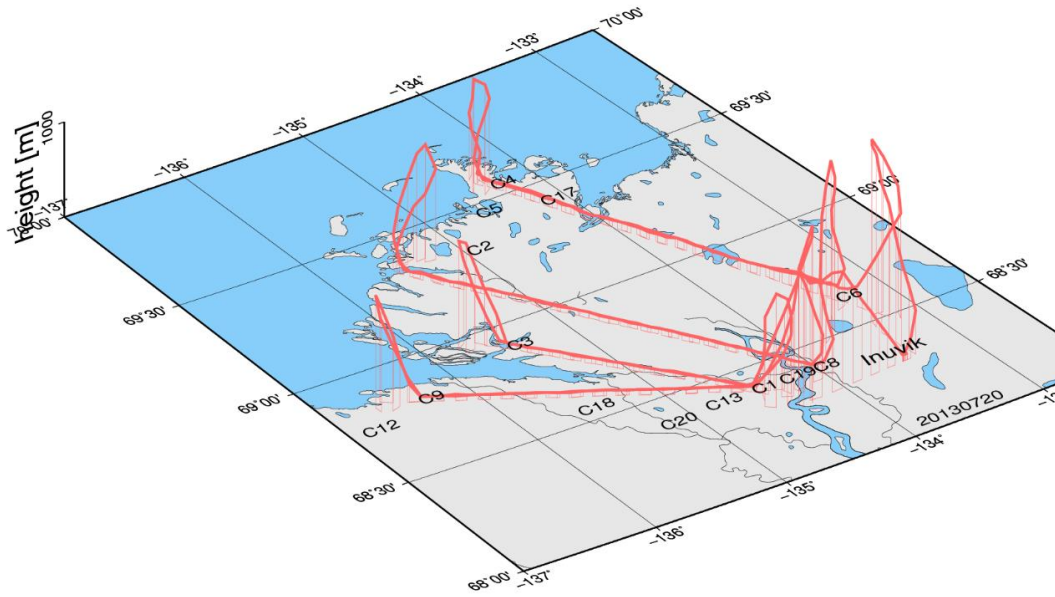


Fig. 44: 3D illustration of the flight track. Shown are low level and high level legs as well as the vertical profile flights.

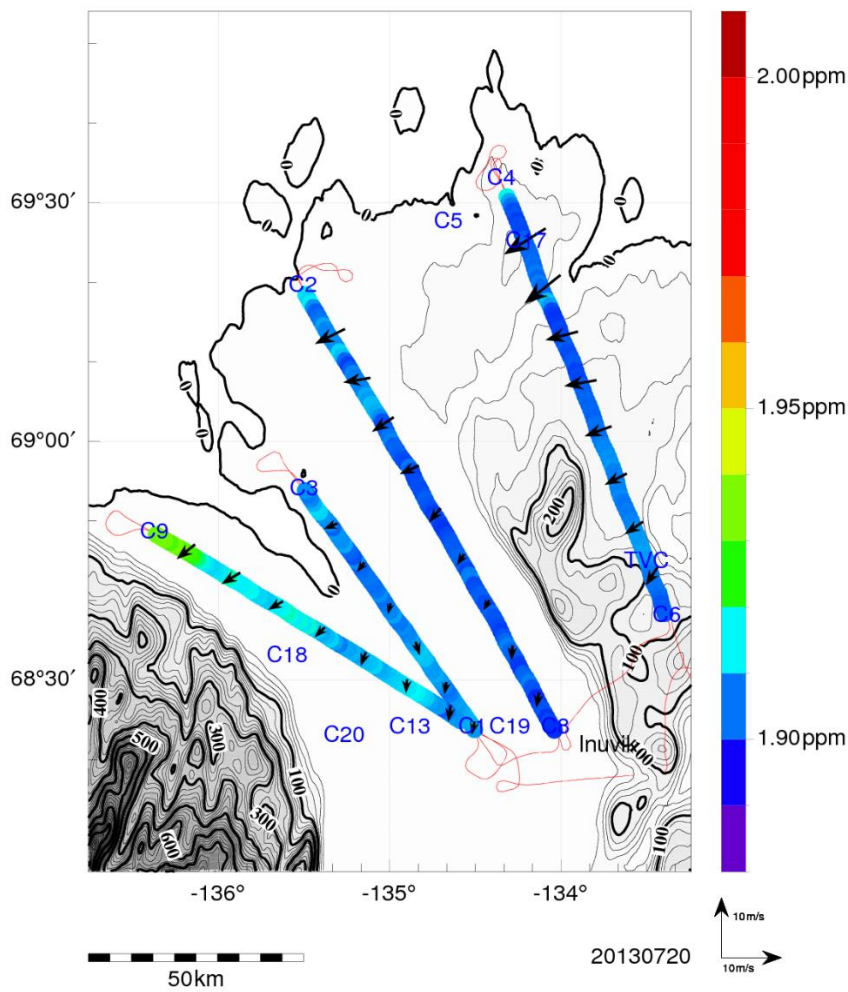


Fig. 45: Methane concentration along the flight transect with respective wind direction. Since the way there and the way back followed the same track only the data for way there is plotted to get an overview of the situation. Here the runs CP50720h02, CP50720h04, CP50720h05, and CP50720h07 are shown.

July 21

Location: Inuvik

Takeoff: 12:20 local time, 18:20 UTC

Landing: 15:53 local time, 21:53 UTC

Weather: slightly misty

Route: Inuvik – Hyperspectral lines – C1 – C15 – C1 – C13 – C14 – C13 – Radiation Square – Inuvik (see Fig. 46 and Fig. 47)

Observations:

The flight on July 21 was the first flight during which the part of the delta south of Inuvik was investigated. The CH₄ concentrations did not exceed 2.0 ppm and the highest concentrations were found in the southern parts of the legs (Fig. 48). This part is covered by a lot of black spruce that are heated by the sun. This, together with the strong variability in surface temperatures (25 °C and 17 °C) between the forested parts and the water surfaces caused strong near-surface turbulence. The flight altitude was increased to a destination altitude of 75 m agl and the aircraft speed was increased slightly.

For the radiation square the flight altitude was increased to about 2,400 m. In that altitude the pressure in the measurement cell of the Los Gatos FGGA could not be regulated to 140 Torr, anymore, but leveled off at 137.67 Torr. Therefore, it seems questionable whether it makes sense to operate the Los Gatos FGGA also during ferry flights at even higher altitudes. This issue has to be investigated.

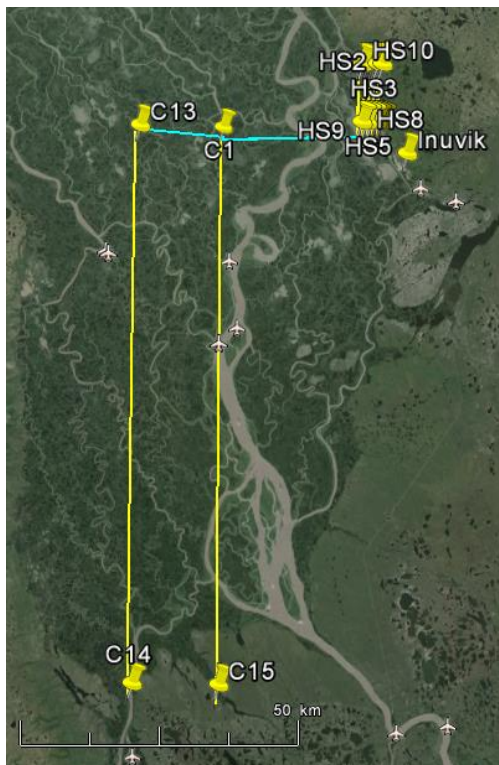


Fig. 46: Flight pattern on July 21, 2013. Yellow lines show transects with flux measurements. Blue lines show lines only overflown during boundary layer profiles.

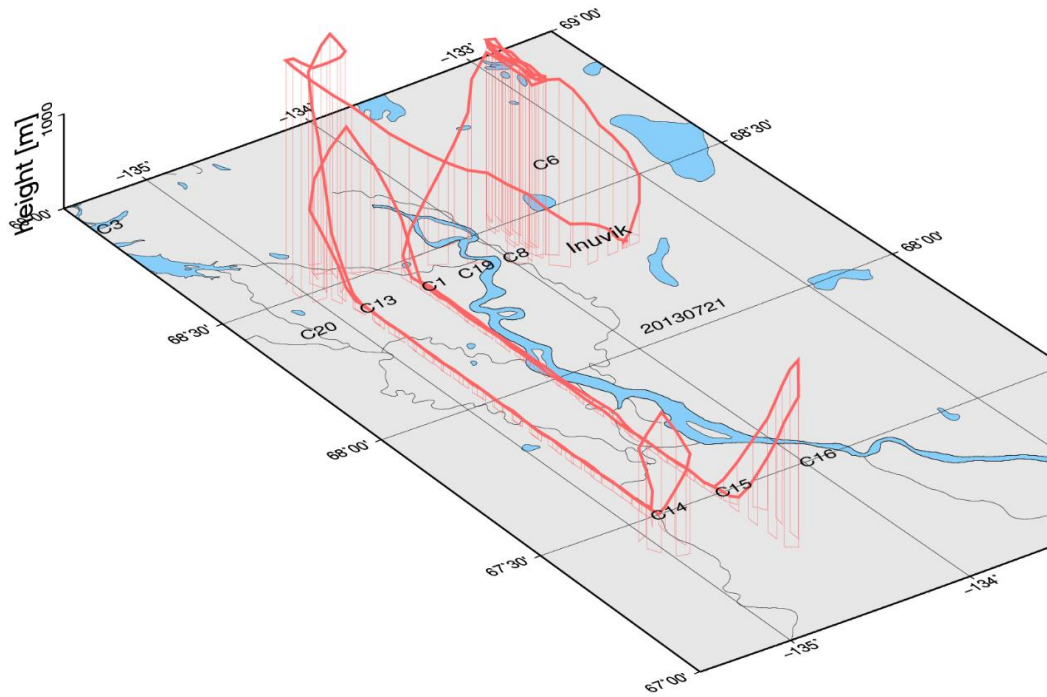


Fig. 47: 3D illustration of the flight track. Shown are low level and high level legs as well as the vertical profile flights.

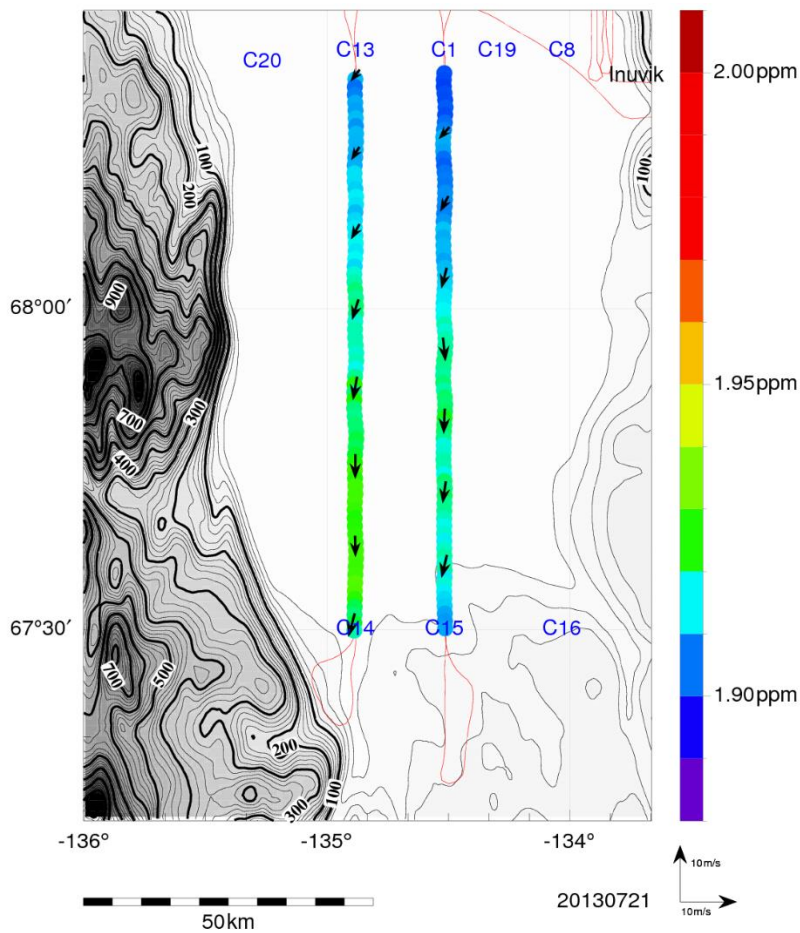


Fig. 48: Methane concentration along the flight transect with respective wind direction. Since the way there and the way back followed the same track only the data for way there is plotted to get an overview of the situation. Here the runs CP50721h01 and CP50721h03 are shown.

July 22

Location: Inuvik

Takeoff: 12:17 local time, 18:17 UTC

Landing: 17:24 local time, 23:24 UTC

Weather: wind from north-west

Route: Inuvik – C1 – C9 – Coastal scan at 760 m including Herschel Island starting in the south going clockwise – C10 – C11 – C12 – C9 – C1 – C3 – C1 – Hyperspectral camera calibration – Inuvik (see Fig. 49)

Flux measurements, laser scanner and hyperspectral camera operation along the coastline of the mainland and Herschel Island (Fig. 50)

Observations and remarks:

After the first leg from C1 to C9, the flight altitude was increased to 760 m and *Polar 5* followed the coastline of the mainland was laser-scanned in support of coastal erosion studies by the Helmholtz Young Investigators Group COPER based at AWI. The flight track followed the coastline to Herschel Island, surrounded the Island from the south clockwise and continued to the Alaskan-Canadian border.

Between C11 and C12 CH₄ concentrations exceeded 2.00 ppm (Fig. 51). On the leg between C9 and C1 high differences in surface temperature between 17 °C and 32 °C were measured. The high temperatures seemed to be accompanied by higher methane concentrations.

Under clear sky conditions, the calibration pattern for both the hyperspectral camera and the laser scanner was done above the airport in Inuvik at an altitude of 1,200 m. Since the flight altitude is quite low, it can only be performed above Inuvik airport during times with little air traffic. As backup, coordinates for the calibration above the less frequented airport in Aklavik had been prepared.

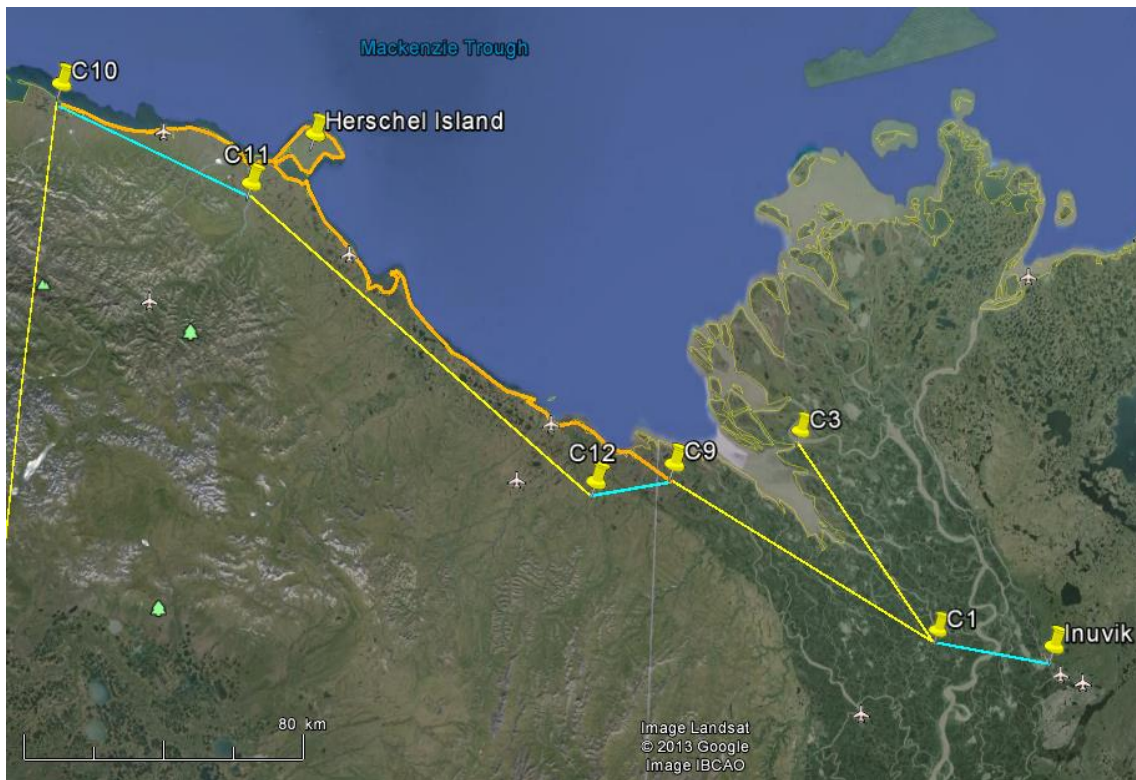


Fig. 49: Flight pattern on July 22, 2013. Yellow lines show transects with flux measurements, orange transects for hyperspectral camera and laser scanner operation. Blue lines show lines only overflowed during boundary layer profiles.

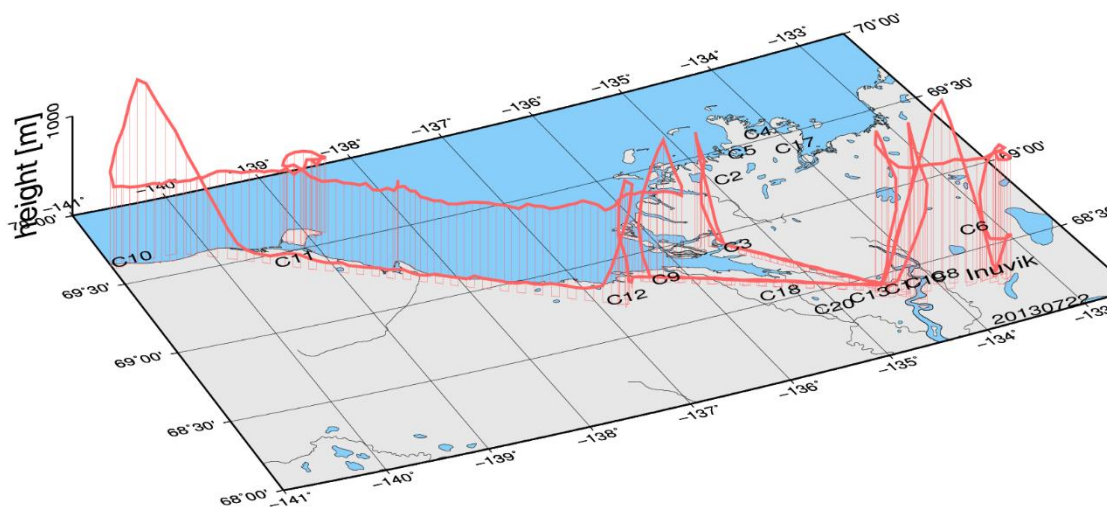


Fig. 50: 3D illustration of the flight track. Shown are low level and high level legs as well as the vertical profile flights.

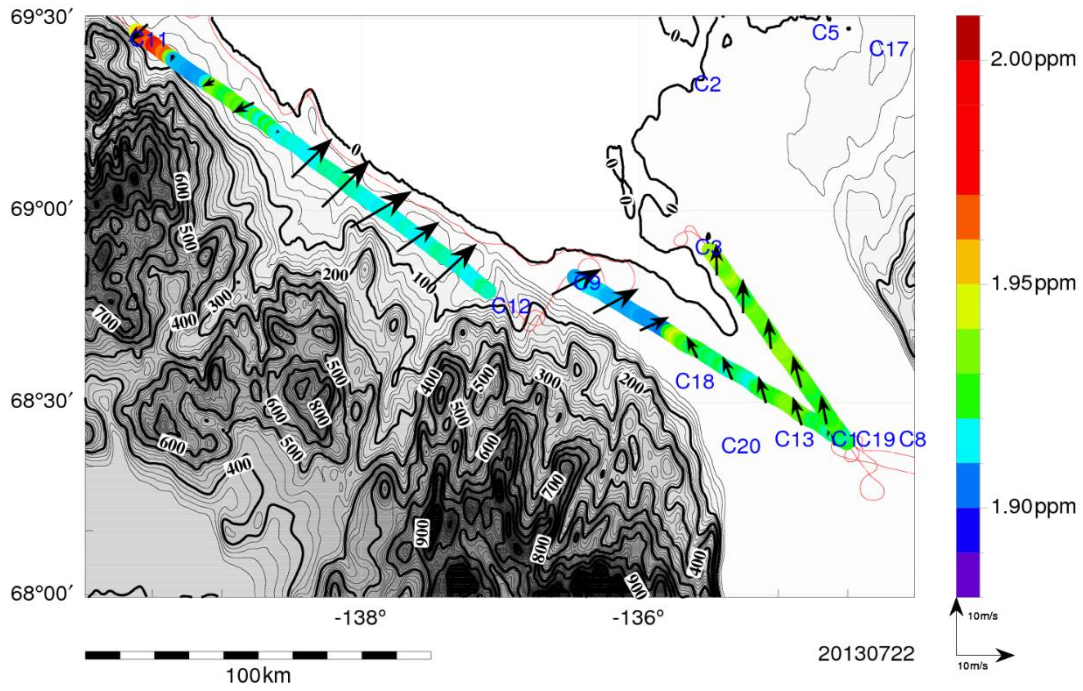


Fig. 51: Methane concentration along the flight transect with respective wind direction. Since the way there and the way back followed the same track only the data for way there is plotted to get an overview of the situation. Here the runs CP50722h02, CP50722h03, and CP50722h04 are shown.

July 23

Location: Inuvik

Takeoff: 12:04 local time, 18:04 UTC

Landing: 15:59 local time, 21:59 UTC

Weather: cloudy

Route: Inuvik – C6 – C4 – C3 – C4 – C17 – C18 – C17 – C6 – Inuvik (see Fig. 52)

Flux measurements, hyperspectral camera operation from C6 towards flux tower and at Richards Island (Fig. 53)

Observations:

Since it was cloudy on that day, there was hardly any turbulence. During that flight the flux tower in Trail Valley was passed at 1,200 m agl on the first way and at low level on the second leg. On July 23 the highest CH₄ concentrations were measured above the northern part of the delta (Fig. 54).



Fig. 52: Flight pattern on July 23, 2013. Yellow lines show transects with flux measurements, orange transects for hyperspectral camera and laser scanner operation. Blue lines show lines only overflown during boundary layer profiles.

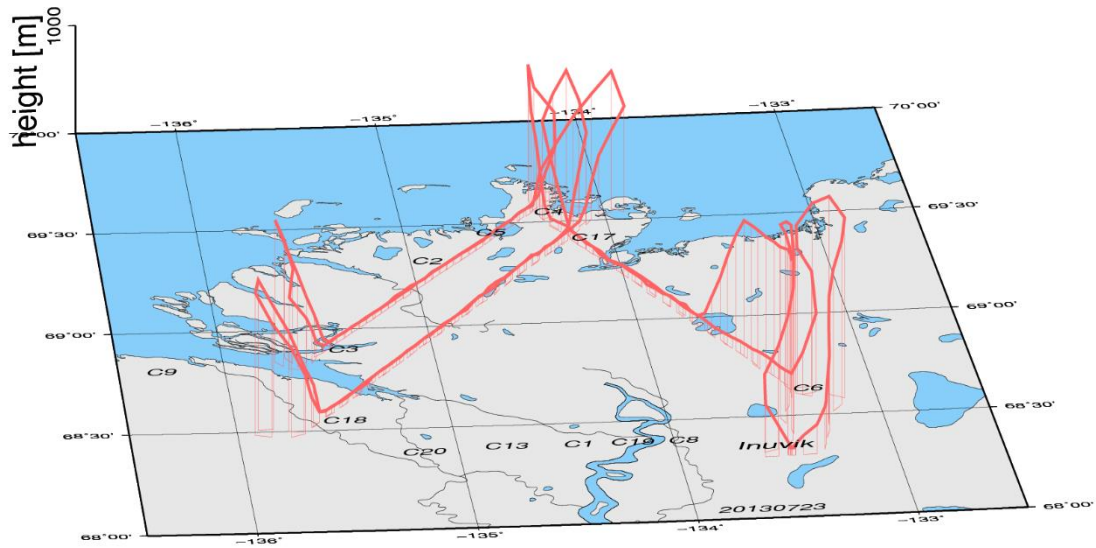


Fig. 53: 3D illustration of the flight track. Shown are low level and high level legs as well as the vertical profile flights.

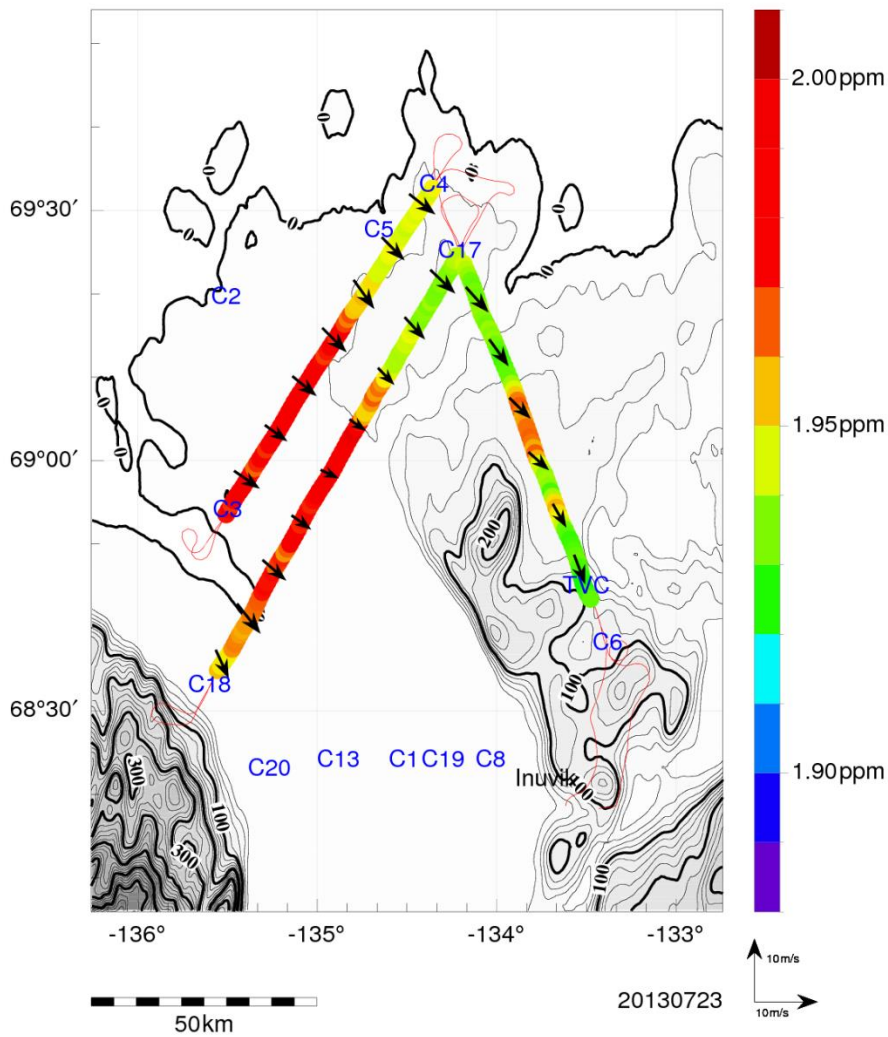


Fig. 54: Methane concentration along the flight transect with respective wind direction. Since the way there and the way back followed the same track only the data for way there is plotted to get an overview of the situation. Here the runs CP50723h03, CP50723h05, and CP50723h06 are shown.

July 25

Location: Inuvik

Takeoff: 12:22 local time, 18:22 UTC

Landing: 16:19 local time, 23:19 UTC

Weather: cloudy, rained the day before, light rain at takeoff, wind from south

Route: Inuvik – C19 – C5 – C19 – C16 – C19 – C20 – C14 – C20 – C3 – C20 – Inuvik (see Fig. 55)

Only flux measurements at low altitudes (Fig. 56)

Observations:

On July 25 it rained a bit during takeoff. During the flight itself light rain showers occurred between C19 and C5, which made it necessary to go slightly off-track to avoid a shower. During the profile flight at C5, the heating for the nose boom was turned on, in order to avoid freezing of potential rain water inside which might damage the instruments. The heating was left on for 20 minutes.

The leg from C19 and C16 was extraordinary for the whole campaign, as east of it the land was only covered with forest without any water bodies. On that leg the surface temperature of the Mackenzie River exceeded the temperature of the surrounding surfaces by about 5 °C.

The flight from C14 to C20 was again turbulent, as differences in surface temperature occurred. The differences in surface temperatures decreased on the section from C20 to C3, as both land and water surfaces were about 17 °C warm. During the entire flight CH₄ concentrations varied mainly below 1.95 ppm (Fig. 57).

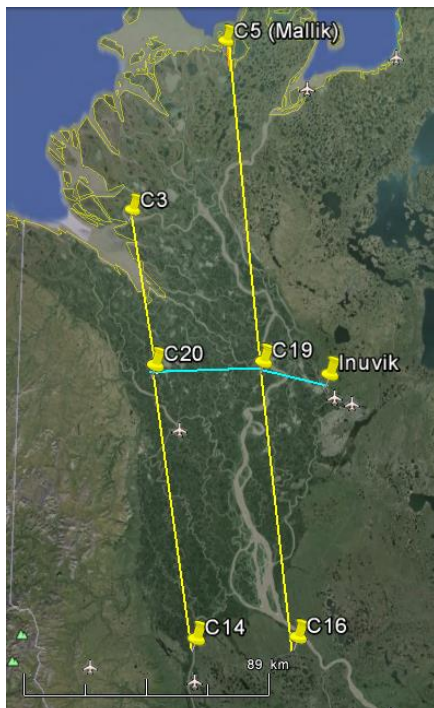


Fig. 55: Flight pattern on July 25, 2013. Yellow lines show transects with flux measurements, orange transects for hyperspectral camera and laser scanner operation. Blue lines show lines only overflowed during boundary layer profiles.

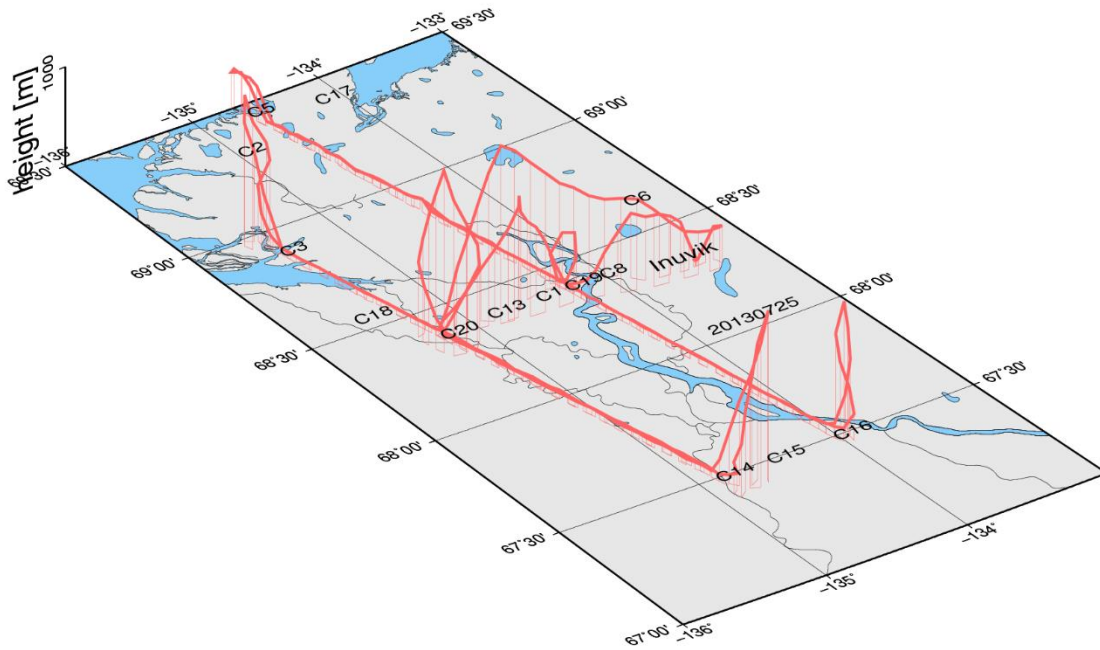


Fig. 56: 3D illustration of the flight track. Shown are low level and high level legs as well as the vertical profile flights.

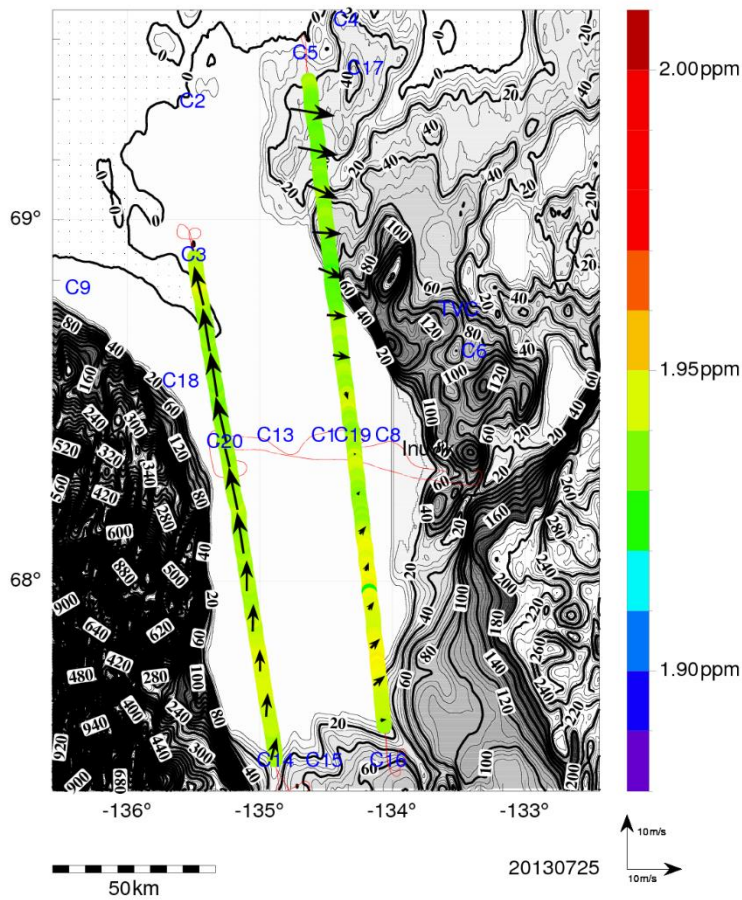


Fig. 57: Methane concentration along the flight transect with respective wind direction. Since the way there and the way back followed the same track only the data for way there is plotted to get an overview of the situation. Here the runs CP50725h02, CP50725h03, CP50725h06, and CP50725h07 are shown.

July 26

Location: Inuvik

Takeoff: 12:00 local time, 18:00 UTC

Landing: 16:46 local time, 22:46 UTC

Weather: almost continuous cloud coverage at the beginning, during the flight sometimes clearing off; it had rained in the night before

Route: Inuvik – C8 – C2 – C9 – C2 – C20 – C4 – C20 – C18 – C8 – Inuvik (Fig. 58)

Flux measurements, laser scanner (and hyperspectral camera) operation at Richards Island (Fig. 59)

Observations:

On the last science flight of AIRMETH 2013, the weather was very variable. At takeoff, the sky was entirely cloud covered. The sky cleared off, however, on the leg from C8 to C2, when only some cumulus clouds were visible at the horizon and some cirrostratus covered the sky above the leg. Between C2 and C20, single low level cumulus clouds and blue sky alternated. The CH₄ concentrations mainly varied between 1.95 and 2.0 ppm (Fig. 60).



Fig. 58: Flight pattern on July 26, 2013. Yellow lines show transects with flux measurements, orange transects for hyperspectral camera and laser scanner operation. Blue lines show lines only overflown during boundary layer profiles.

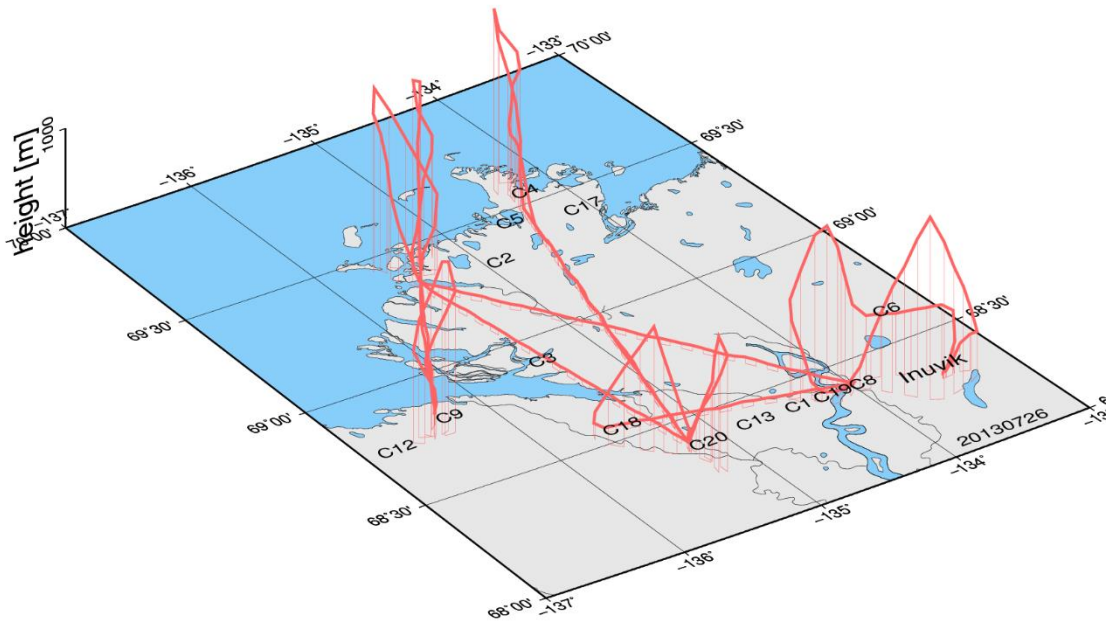


Fig. 59: 3D illustration of the flight track. Shown are low level and high level legs as well as the vertical profile flights.

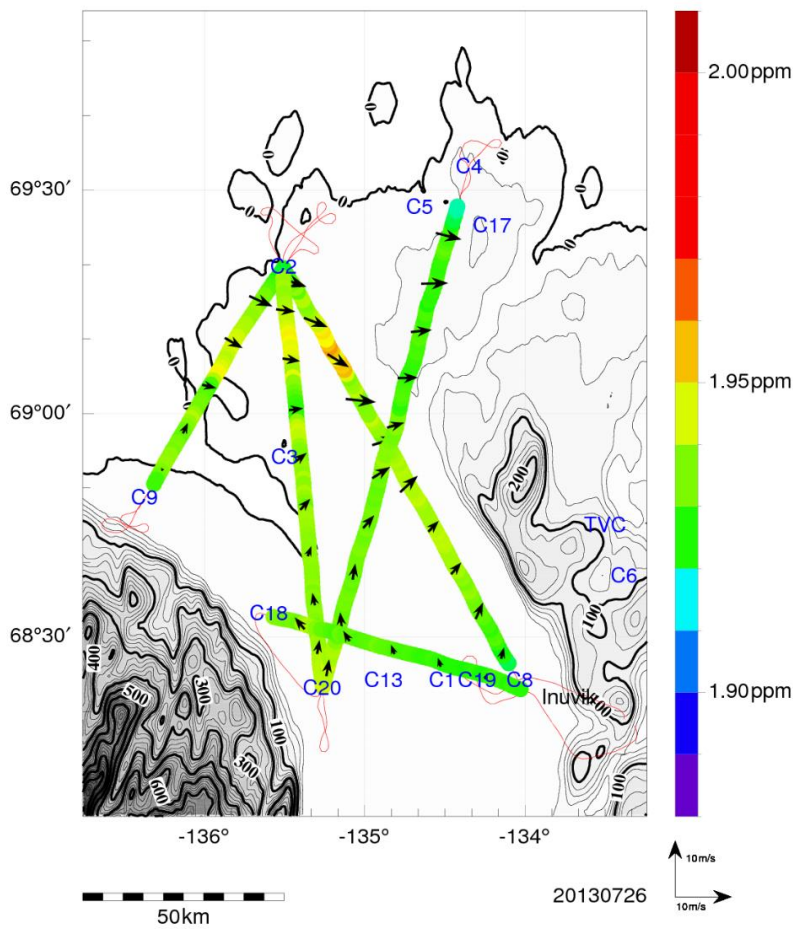


Fig. 60: Methane concentration along the flight transect with respective wind direction. Since the way there and the way back followed the same track only the data for way there is plotted to get an overview of the situation. Here the runs CP50726h01, CP50726h02, CP50726h04, CP50726h05, CP50726h06, and CP50726h07 are shown.

7 Preliminary observations and lessons learned

Final results will only be published after thorough data quality control and analysis. This section shall only give an overview of the observations that were made during the campaign, mainly not directly related to methane fluxes.

Meteorological and chemical observations

Since the boundary layer height is highly variable in both investigated regions due to different influences of the sea and the land, it is indispensable to include vertical profiles to the boundary layer top at least at the beginning and end of a transect. When flying long transects, it can make sense to include a profile in the middle of the leg. Especially towards the coast, the boundary layer height decreases strongly. For future campaigns it might be helpful to have pre-flight information about the boundary layer height at several parts of the planned route in order to decide on whether it is reasonable to fly and if so at which altitude.

Air temperature is strongly decreasing towards Barrow/the northern coast of the Alaskan North Slope. The effect of these differences in temperature on the methane concentration and the methane fluxes has to be analyzed and dealt with appropriately.

Air temperature seems more stable across several transects in the Mackenzie Delta than in the area close to Barrow.

In 2013, the overall methane concentration seems to have been lower and less variable in the Mackenzie Delta compared to the study area in Alaska. However, in 2012 the exact opposite was observed, demonstrating the need for multi-annual measurements.

The Los Gatos FGGA

Depending on the ambient temperature, the Los Gatos FGGA needs 30 to 40 minutes to warm up to working temperature of about 40°C. Consequently, usually the first transect was used for high level flights for hyperspectral camera and laser scanner operation to give the FGGA time to reach the required temperature. After AIRMETH 2013 the warming process was analyzed in the laboratory and showed that 40°C were reached after about 30 min (Fig. 61) and the gas temperature leveled in at 44°C after about 110 min.

The clock in the Los Gatos FGGA usually lost 5 to 6 seconds per day compared to the data acquisition system. Therefore, before each flight the time stamp of the FGGA had to be synchronized with the one of the data acquisition system.

Moreover, at an altitude of 2,400 m the pressure in the measurement chamber of the FGGA could not be regulated to 140 Torr anymore, since the two valves used for regulating the pressure were opened entirely and the pressure leveled off at 137.67 Torr. Before future campaigns this circumstance has to be investigated and it has to be checked whether there is a solution for this problem. If not, it might not make sense to use the FGGA in ferry flight altitudes that are higher than 3000 m.

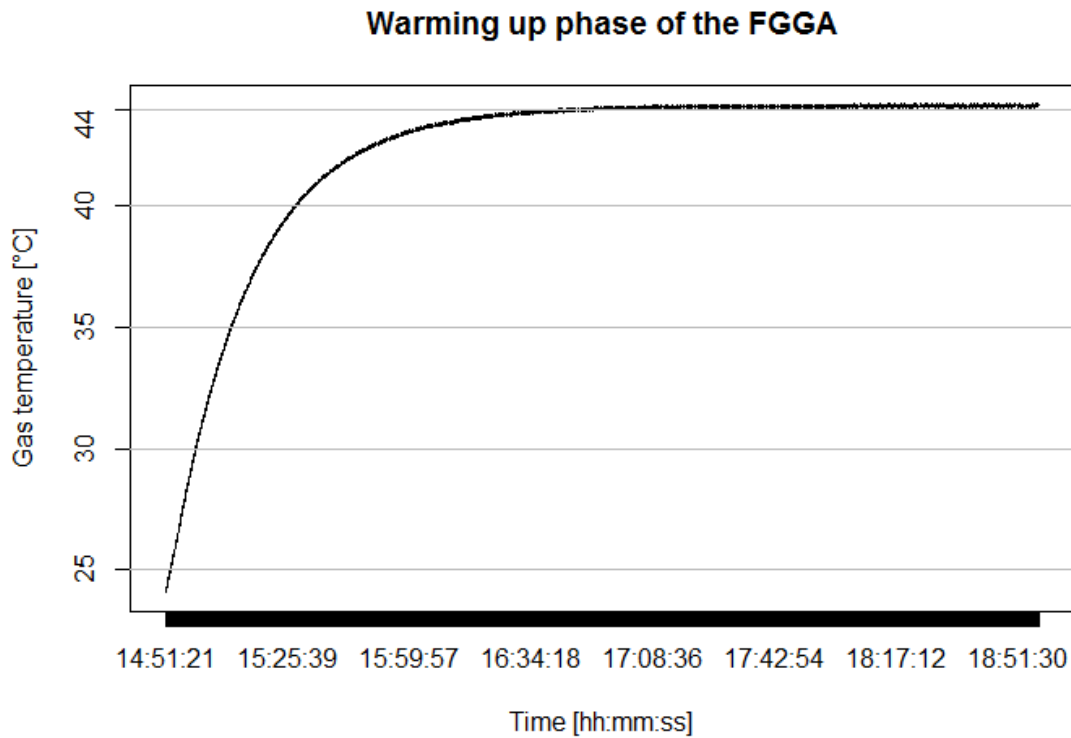


Fig. 61: Warming up of the Los Gatos FGGA as measured in the laboratory after AIRMETH 2013.

Hyperspectral camera settings

Finding appropriate settings for the hyperspectral camera was challenging especially above the ocean where sea ice, sea ice with melt ponds and water were recorded. In order to detect melt ponds it is important that the exposure is relatively short, as otherwise the high reflectivity of the sea ice causes oversaturation of the spectrum. Since the use of the hyperspectral camera above sea ice during AIRMETH was only for testing potential settings for the next MELTEX campaign, the optimum setting still has to be found. Here we tested both 4 and 8 times spectral binning combined with respectively 2 times spatial binning. The exposure was varied between 10 and 22 ms, and the framerate was varied from 30 to 60 frames per second. For the final test it was found that low exposures of 10 and 14.4 combined with a frame rate of 60 frames per second resulted in seemingly acceptable results in the pictures. Those pictures were, however, oversaturated and the settings need further improvement.

Above land surfaces, lakes and rivers different settings for the hyperspectral camera had to be chosen. In the end, mainly the following setting was used: 4 times spectral and 2 times spatial binning, 37 frames per second and 23 ms exposure. After the campaign remote sensing groups confirmed the good quality of the pictures.

References

Accuweather (2013):

<http://www.accuweather.com/en/us/barrowak/99723/month/331720?%20monyr=7/01/2013>; accessed online in August 2013.

AisaEAGLE, (2012): available at: <http://www.specim.fi/index.php/products/airborne/aisaeagle>; accessed online in August 2013.

Bange, J.; Beyrich, F.; Engelbart, D.A.M. (2002): Airborne measurements of turbulent fluxes during LITFASS-98: Comparison with ground measurements and remote sensing in a case study. *Theoretical and Applied Climatology* 73:35-51.

Burn, C.R.; Kokelj, S.V. (2009): The environment and permafrost of the Mackenzie Delta Area. *Permafrost and Periglacial Processes* 20:83-105.

Chang, C.-I. (2003): *Hyperspectral imaging techniques for spectral detection and classification*, Kluwer Academic/Plenum Publishers, New York, pp. 370, ISBN 10: 0306474832.

Christensen, T.R.; Jonasson, S.; Callaghan, T.V. (1995): Spatial variation in high-latitude methane flux along a transect across Siberian and European tundra environments. *Journal of Geophysical Research* 100(D10):21,035-21,045.

Desjardins, R.L.; Hart, R.L.; MacPherson, J.I.; Schuepp, P.H.; Verma, S.B. (1992): Aircraft- and tower-based fluxes of carbon dioxide, latent, and sensible heat. *Journal of Geophysical Research* 97(D17):477-485.

Grahn, H.F.; Geladi, P. (2007): *Techniques and applications of hyperspectral image analysis*. John Wiley and Sons Ltd, The Atrium, Southern Gate, Chichester, West Sussex, pp. 390, ISBN 10: 047001086X.

Gurney, S.D. (1998): Aspects of the genesis and geomorphology of pingos: perennial permafrost mounds. *Progress in Physical Geography* 22(3):307-324.

KTVA (2013): <http://www.ktva.com/weather/weather-blog/July-2013-Climate-Numbers-For-Alaska-218047831.html>; accessed online in August 2013.

Köppen, W. (1936): *Das geographische System der Klimate*. In: *Handbuch der Klimatologie in fünf Bänden*, [Köppen, W., Geiger, R. (eds.)], Verlag von Gebrüder Borntraeger, Berlin, pp. 43.

Kutzbach, L.; Wille, C.; Pfeiffer, E.-M. (2007): The exchange of carbon dioxide between wet arctic tundra and the atmosphere at the Lena River Delta, Northern Siberia. *Biogeosciences* 4:869-890.

Lemke, P.; Ren, J.; Alley, R.B.; Allison, I.; Carrasco, J.; Flato, G.; Fujii, Y.; Kaser, G.; Mote, P.; Thomas, R.H.; Zhang, T. (2007): *Observations: Changes in Snow, Ice and Frozen Ground*. In: *Climate Change 2007: The Physical Science Basis. Contribution of Working Group I to the Fourth Assessment Report of the Intergovernmental Panel on Climate Change* [Solomon, S.; Qin, D.; Manning, M.; Chen, Z.; Marquis, M.; Averyt, K.B.; Tignor, M.; Miller, H.L. (eds.)]. Cambridge University Press, Cambridge, United Kingdom and New York, NY, USA.

Mackay, J.R. (1963): *The Mackenzie delta area, N.W.T.*, Geographical Branch, Department of Mines and Technical Surveys, Memoir 8, Ottawa, pp. 202.

- Mackay, J.R. (1998): Pingo growth and collapse, Tuktoyaktuk Peninsula Area, Western Arctic Coast, Canada: a long-term field study. *Géographie physique et Quaternaire* 52(3):271-323.
- Mauder, M.; Desjardins, R.L.; MacPherson, I. (2007): Scale analysis of airborne flux measurements over heterogeneous terrain in a boreal ecosystem. *Journal of Geophysical Research* 112:D13112.
- McGuire, A.D.; Anderson, L.G.; Christensen, T.R.; Dallimore, S.; Guo, L.; Hayes, D.J.; Heimann, M.; Lorenson, T.D.; Macdonald, R.W.; Roulet, N. (2009): Sensitivity of the carbon cycle in the Arctic to climate change. *Ecological Monographs* 79(4):523-555.
- Metzger, S.; Junkermann, W.; Mauder, M.; Butterbach-Bahl, K.; Trancón y Widemann, B.; Neidl, F.; Schäfer, K.; Wieneke, S.; Zheng, X.H.; Schmid, H.P., Foken, T. (2013): Spatially explicit regionalization of airborne flux measurements using environmental response functions. *Biogeosciences* 10:2193-2217.
- Mostafa, M.M.R. (2001): Boreasight calibration of integrated inertial/camera systems. *Proceed. Int. Symposium on Kinematic Systems in Geodesy, Geomatics and Navigation – KIS 2001, Banff, Canada, June 5-8.* Available at: http://www.ucalgary.ca/engo_webdocs/SpecialPublications/KIS%2001/PDF/0707.PDF; accessed online in August 2013.
- National Geographic (2006): <http://ngm.nationalgeographic.com/ngm/0605/feature1/map.html>; accessed online in August 2013.
- Porsild, A.E. (1938): Earth mounds in unglaciated Arctic, north western America. *Geographical Review* 28:46-58.
- Ritchie, J.C. (1984): *Past and Present Vegetation of the Far Northwest of Canada.* University of Toronto Press: Toronto. ISBN 10: 0802025234.
- Schimel, J.P. (1995): Plant transport and methane production as controls on methane flux from arctic wet meadow tundra. *Biogeochemistry* 28:183-200.
- Siesler, H.W.; Ozaki, Y.; Kawata, S.; Heise, H.M. (2002): *Near-Infrared Spectroscopy. Principles, Instruments, Applications.* Weinheim, Wiley-VCH, pp. 361.
- Sistla, S.A.; Moore, J.C.; Simpson, R.T.; Gough, L.; Shaver, G.R.; Schimel, J.P. (2013): Long-term warming restructures Arctic tundra without changing net soil carbon storage. *Nature*, doi:10.1038/nature12129.
- Stull, R.B. (2000): *Meteorology for Scientists and Engineers.* Brooks/Cole, Pacific Grove, pp. 502.
- Torn, M.S.; Chapin, F.S. (1993): Environmental and biotic controls over methane flux from arctic tundra. *Chemosphere* 26(1-4):357-368.
- US climate data (2013): <http://www.usclimatedata.com/climate.php?location=USA0025>; accessed online in August 2013.
- Varshney, P.K.; Arora, M.K. (2004): *Advanced image processing techniques for remotely sensed hyperspectral data.* Heidelberg, New York, Springer, pp. 323. ISBN 10: 3540216685.
- Villarreal, S.; Hollister, R.D.; Johnson, D.R.; Lara, M.J.; Webber, P.J.; Tweedie, C.E. (2012): Tundra vegetation change near Barrow, Alaska (1972-2010). *Environmental Research Letters* 7 015508.

- Walch, D.; Frater, H. (Hrsg.), 2004. Wetter und Klima. Das Spiel der Elemente – Atmosphärische Prozesse verstehen und deuten. Heidelberg, New York. Springer, pp.264. ISBN 10: 354000839X
- Weller, G.; Chapin, F.S.; Everett, K.R.; Hobbie, J.E.; Kane, D.; Oechel, W.C.; Ping, C.L.; Reeburgh, W.S.; Walker, D.; Walsh, J. (1995): The Arctic Flux Stud: A regional view of trace gas release. Journal of Biogeography. Journal of Biogeography 22(2/3):365-374.
- Wille, C.; Kutzbach, L.; Sachs, T.; Wagner, D.; Pfeiffer, E.-M. (2008): Methane emission from Siberian arctic polygonal tundra: eddy covariance measurements and modeling. Global Change Biology 14:1395-1408.
- Zhang, Y.; Sachs, T.; Li, C.; Boike, J. (2012): Upscaling methane fluxes from closed chambers to eddy covariance based on permafrost biogeochemistry. Global Change Biology 18:1428-1440.
- Zona, D.; Oechel, W.C.; Kochendorfer, J.; Paw U, K.T.; Salyuk, A.N.; Olivas, P.C.; Oberbauer, S.F.; Lipson, D.A. (2009): Methane fluxes during the initiation of a large-scale water table manipulation experiment in the Alaskan Arctic tundra. Global Biogeochemical Cycles 23:GB2013.

Pictures:

<https://spaces.awi.de/confluence/display/AEROdevices/Meteorologischer+Nasenmast>

Acknowledgements

We thank the engineers Julia Binder from AWI Bremerhaven and Heiner Baumgarten from FIELAX for their technical support before and during the campaign. Furthermore we thank the staff from AWI Bremerhaven and FIELAX who prepared *Polar 5* for AIRMETH 2013.

We thank the Kenn Borek pilots Dean Emberley and Kirk Allen and the airplane mechanics Neil MacAuley and Brian Rose for flying and maintaining *Polar 5*.

The campaign was mainly funded by AWI Logistics.

The work was conducted in the Helmholtz Young Investigators Group TEAM (Trace Gas Exchange in the Earth –Atmosphere System on Multiple Scales) that is funded by the Helmholtz-Association through the President’s Initiative and Networking Fund, and by GFZ.

Appendix

Participating institutions

GFZ	German Research Centre for Geosciences, Telegrafenberg, 14473 Potsdam, Germany
AWI	Alfred Wegener Institute Helmholtz Center for Polar- and Marine Research, Am Handelshafen 12, Bremerhaven, Germany

Participants

Table-A 1: Names, affiliations and profession of the participants of AIRMETH 2013.

Name	First Name	Institute	Profession
Sachs	Torsten	GFZ	Scientist, PI
Hartmann	Jörg	AWI	Scientist, Co-PI
Serafimovich	Andrei	GFZ	Scientist
Kohnert	Katrin	GFZ	PhD-Student
Binder	Julia	AWI	Engineer
Baumgarten	Heiner	FIELAX	Engineer
Emberley	Dean	Kenn Borek	Pilot
Allen	Kirk	Kenn Borek	Pilot
MacAuley	Neil	Kenn Borek	Mechanic
Rose	Brian	Kenn Borek	Mechanic

Flight hours

Table-A 2: Date, start and end time of the measurements in UTC as well as the duration of the measurement. The air time would be about 10 minutes longer than the measurement time. In the column "end measurement time" the (+1) shows that a change of date occurred in UTC time.

Date	Start measurement time [UTC]	End measurement time [UTC]	Measurement duration
July 4	20:14	23:48	3 h 34 min
July 6	18:17	22:53	4 h 36 min
July 7	21:31	02:44 (+1)	5 h 13 min
July 8	19:46	22:24	2 h 38 min
July 10	21:04	01:16 (+1)	4 h 12 min
July 11	19:01	00:15 (+1)	5 h 14 min
July 12	19:12	00:06 (+1)	4 h 54 min
July 13	19:11	23:58	4 h 47 min
July 14	20:11	00:23	4 h 12 min
July 19	18:25	22:39	4 h 14 min
July 20	18:13	23:25	5 h 12 min
July 21	18:20	21:53	3 h 33 min
July 22	18:17	23:24	5 h 07 min
July 23	18:04	21:59	3 h 55 min
July 25	18:22	23:19	4 h 57 min
July 26	18:00	22:46	4 h 46 min
Total	-		70 h 48 min

Overview of all flight legs

Table-A 3: Summary for each flight leg described by start time, end time, starting and ending longitude (lon), and starting and ending latitude (lat). The column “Run” displays the name of the file with “CP5” being campaign specific characters followed by the month (mm) and day of month (dd), a symbol for the type of the run (t = vertical profile/temp, h = horizontal low level flight, L plateau/horizontal leg in higher altitude, R = leg for the calibration of the radiation sensors, n = leg for calibration of alpha or beta. The letter is followed by the number of that type of leg on that day. The columns “Starttime” and “Endtime” are the time in seconds after midnight in UTC of that day, the coordinates are given in degrees. Black lines in the table mark the end of one flight day.

Run	Start time	End time	Start lon	End lon	Start lat	End lat
CP50704t01	72854	72904	-156.48	-156.53	71.34	71.35
CP50704t02	72921	73311	-156.54	-156.66	71.35	71.22
CP50704h01	73339	74974	-156.67	-157.35	71.20	70.38
CP50704t03	74979	75419	-157.35	-157.50	70.37	70.30
CP50704t04	75421	75849	-157.50	-157.49	70.30	70.38
CP50704h02	75851	78819	-157.49	-153.22	70.38	70.22
CP50704t05	78859	79252	-153.16	-153.00	70.22	70.23
CP50704t06	79254	79894	-153.00	-153.14	70.23	70.22
CP50704h03	79901	81189	-153.16	-155.44	70.22	70.32
CP50704t07	81191	81441	-155.44	-155.86	70.32	70.33
CP50704L01	81447	82296	-155.87	-157.35	70.33	70.38
CP50704t08	82301	82859	-157.36	-157.39	70.38	70.38
CP50704h04	83306	85257	-157.35	-156.59	70.38	71.31
CP50704t09	85261	85635	-156.59	-156.57	71.31	71.28
CP50704t10	85637	85681	-156.57	-156.64	71.28	71.30
CP50706t01	65826	65945	-156.63	-156.44	71.29	71.29
CP50706t02	65947	66394	-156.44	-156.20	71.29	71.30
CP50706h01	66721	68561	-156.65	-157.35	71.23	70.38
CP50706t03	68566	68775	-157.36	-157.59	70.38	70.33
CP50706t04	68777	69030	-157.60	-157.33	70.33	70.38
CP50706h02	69056	71884	-157.29	-153.15	70.38	70.21
CP50706t05	71886	72308	-153.15	-152.96	70.21	70.26
CP50706t06	72310	72884	-152.95	-153.18	70.26	70.22
CP50706h03	72901	75667	-153.21	-157.36	70.23	70.38
CP50706t07	75669	76054	-157.36	-157.69	70.38	70.31
CP50706n01	76251	76735	-157.52	-157.49	70.42	70.43
CP50706n05	76271	76329	-157.51	-157.47	70.43	70.46
CP50706n06	76416	76474	-157.37	-157.30	70.48	70.47
CP50706n07	76541	76599	-157.27	-157.31	70.44	70.42
CP50706n08	76676	76734	-157.41	-157.48	70.42	70.43
CP50706n02	76737	77289	-157.49	-157.48	70.43	70.46
CP50706n09	76821	76879	-157.51	-157.46	70.48	70.51
CP50706n10	76969	77027	-157.34	-157.26	70.52	70.51
CP50706n11	77091	77149	-157.24	-157.28	70.48	70.45
CP50706n12	77231	77289	-157.39	-157.48	70.44	70.46

Run	Start time	End time	Start lon	End lon	Start lat	End lat
CP50706n03	77291	77859	-157.49	-157.44	70.46	70.49
CP50706n13	77381	77439	-157.51	-157.46	70.52	70.56
CP50706n14	77516	77574	-157.33	-157.23	70.58	70.57
CP50706n15	77671	77729	-157.17	-157.21	70.52	70.49
CP50706n16	77811	77869	-157.34	-157.46	70.47	70.49
CP50706n04	77861	78434	-157.44	-157.46	70.49	70.51
CP50706n17	77958	78016	-157.53	-157.48	70.55	70.60
CP50706n18	78086	78144	-157.33	-157.19	70.61	70.60
CP50706n19	78240	78298	-157.11	-157.16	70.54	70.50
CP50706n20	78371	78429	-157.30	-157.45	70.49	70.51
CP50706t08	78441	79093	-157.48	-157.33	70.51	70.41
CP50706h04	79099	80864	-157.33	-156.58	70.41	71.32
CP50706t09	80863	81064	-156.58	-156.57	71.32	71.43
CP50706t10	81066	81284	-156.56	-156.42	71.43	71.53
CP50706n21	81261	81679	-156.46	-155.78	71.53	71.41
CP50706n22	81821	82079	-155.88	-156.40	71.43	71.40
CP50706n23	82076	82389	-156.39	-157.04	71.40	71.36
CP50707t01	77450	77716	-156.67	-156.37	71.29	71.32
CP50707t02	77718	77972	-156.37	-156.55	71.32	71.33
CP50707h01	77997	79809	-156.56	-157.35	71.32	70.37
CP50707t03	79812	80092	-157.35	-157.59	70.37	70.34
CP50707t04	80098	80381	-157.59	-157.49	70.34	70.38
CP50707h02	80397	83655	-157.47	-153.16	70.38	70.22
CP50707t05	83657	84080	-153.15	-152.64	70.22	70.23
CP50707t06	84082	84423	-152.64	-153.01	70.23	70.38
CP50707h03	84471	86859	-153.10	-157.21	70.39	70.55
CP50707t07	86861	87106	-157.22	-157.64	70.56	70.58
CP50707t08	87112	87494	-157.65	-157.61	70.58	70.42
CP50707h04	87701	90708	-157.37	-153.17	70.38	70.22
CP50707t09	90710	90935	-153.16	-152.99	70.22	70.29
CP50707t10	90938	91180	-152.99	-153.12	70.29	70.40
CP50707h05	91242	93519	-153.23	-157.21	70.40	70.56
CP50707t11	93515	93751	-157.20	-157.54	70.56	70.49
CP50707t12	93754	93981	-157.54	-157.30	70.49	70.47
CP50707h06	94156	95692	-157.22	-156.58	70.55	71.31
CP50707t13	95695	95934	-156.58	-156.61	71.32	71.34
CP50707t14	95936	96231	-156.62	-156.91	71.35	71.29
CP50708t01	71123	71574	-156.71	-156.30	71.28	71.41
CP50708t02	71576	71883	-156.30	-156.56	71.41	71.32
CP50708h01	72051	73573	-156.65	-157.35	71.23	70.38
CP50708t03	73577	73840	-157.35	-157.66	70.37	70.26
CP50708t04	73842	74210	-157.67	-157.39	70.26	70.33
CP50708h02	74301	74584	-157.36	-157.26	70.38	70.50
CP50708t05	74586	74777	-157.26	-157.19	70.50	70.58
CP50708p01	74779	74954	-157.19	-157.13	70.58	70.65
CP50708t06	74956	75147	-157.13	-157.06	70.65	70.74

Run	Start time	End time	Start lon	End lon	Start lat	End lat
CP50708h03	75144	75289	-157.06	-157.02	70.73	70.79
CP50708t07	75286	75405	-157.02	-156.97	70.79	70.84
CP50708p02	75407	75557	-156.97	-156.91	70.85	70.91
CP50708t08	75559	75671	-156.91	-156.88	70.91	70.96
CP50708h04	75673	75775	-156.88	-156.84	70.96	71.00
CP50708t09	75777	75864	-156.84	-156.82	71.00	71.04
CP50708p03	75866	75965	-156.82	-156.77	71.04	71.08
CP50708t10	75967	76125	-156.77	-156.69	71.08	71.16
CP50708h05	76127	76183	-156.69	-156.67	71.16	71.19
CP50708t11	76185	76272	-156.67	-156.65	71.19	71.23
CP50708p04	76274	76361	-156.65	-156.61	71.23	71.26
CP50708t12	76363	76468	-156.61	-156.57	71.26	71.31
CP50708t13	76470	76745	-156.57	-156.47	71.31	71.42
CP50708t14	76747	77082	-156.47	-156.56	71.42	71.34
CP50708h06	77084	78439	-156.56	-157.21	71.33	70.56
CP50708t15	78441	78670	-157.21	-157.50	70.56	70.51
CP50708t16	78672	78970	-157.51	-157.34	70.51	70.56
CP50708h07	78970	79592	-157.34	-156.48	70.56	70.53
CP50708h08	79667	80629	-156.41	-156.66	70.55	71.08
CP50708t17	80631	80699	-156.66	-156.68	71.08	71.12
CP50710t01	75856	76250	-156.71	-156.54	71.28	71.42
CP50710L01	76384	77814	-156.55	-157.21	71.34	70.56
CP50710t03	77821	78089	-157.21	-157.35	70.55	70.56
CP50710h01	78091	81149	-157.34	-153.16	70.56	70.40
CP50710t04	81151	81515	-153.16	-153.05	70.40	70.24
CP50710t05	81517	81830	-153.05	-152.98	70.23	70.03
CP50710h02	82036	83817	-153.08	-156.01	70.00	70.13
CP50710t06	83819	84197	-156.02	-156.19	70.13	70.04
CP50710t07	84199	84494	-156.18	-156.00	70.04	70.12
CP50710h03	84506	86651	-156.00	-156.00	70.13	71.17
CP50710t08	86656	86901	-156.00	-156.11	71.17	71.29
CP50710t09	86903	87168	-156.11	-156.49	71.29	71.37
CP50710h04	87261	89495	-156.57	-156.69	71.32	70.15
CP50710t10	89497	89837	-156.69	-157.06	70.15	70.15
CP50710t11	89839	90180	-157.07	-157.37	70.15	70.34
CP50710h05	90182	92310	-157.37	-156.57	70.35	71.32
CP50710t12	92312	92555	-156.57	-156.36	71.32	71.26
CP50710t13	93439	93679	-156.79	-156.91	71.30	71.29
CP50711t01	68465	68810	-156.68	-156.34	71.29	71.35
CP50711t02	68812	69269	-156.34	-156.67	71.35	71.25
CP50711h01	69336	71040	-156.60	-154.83	71.23	70.73
CP50711t03	71042	71332	-154.83	-154.57	70.73	70.65
CP50711t04	71334	71699	-154.56	-154.20	70.65	70.54
CP50711h02	71701	72676	-154.19	-153.17	70.54	70.22
CP50711t05	72678	73027	-153.17	-153.49	70.22	70.16
CP50711t06	73029	73386	-153.49	-153.41	70.16	70.22

Run	Start time	End time	Start lon	End lon	Start lat	End lat
CP50711h03	73388	74824	-153.40	-151.48	70.22	70.21
CP50711t07	74826	75054	-151.47	-151.17	70.21	70.21
CP50711t08	75156	75409	-151.03	-150.69	70.21	70.20
CP50711h04	75461	77182	-150.62	-148.44	70.20	70.16
CP50711t09	77184	77573	-148.44	-148.18	70.16	70.08
CP50711L01	77826	80376	-148.44	-153.14	70.16	70.22
CP50711t10	80401	80633	-153.19	-153.16	70.22	70.21
CP50711h05	80646	82169	-153.18	-155.33	70.22	70.67
CP50711t11	82171	82354	-155.33	-155.61	70.67	70.72
CP50711t12	82356	82629	-155.61	-156.09	70.72	70.81
CP50711h06	82741	83389	-156.27	-157.28	70.85	71.04
CP50711t13	83391	83613	-157.28	-157.37	71.04	71.00
CP50711L02	84651	84829	-156.65	-156.67	71.33	71.24
CP50711L03	84991	85149	-156.67	-156.64	71.23	71.32
CP50711L04	85301	85434	-156.64	-156.65	71.33	71.25
CP50711L05	85571	85716	-156.66	-156.62	71.24	71.32
CP50711L06	85836	85999	-156.63	-156.63	71.33	71.24
CP50711L07	86201	86325	-156.63	-156.61	71.24	71.32
CP50711L08	86456	86694	-156.59	-156.60	71.34	71.20
CP50711L09	86834	86971	-156.62	-156.61	71.24	71.32
CP50711t14	86965	87433	-156.61	-156.82	71.32	71.28
CP50712t01	69129	69339	-156.68	-156.79	71.29	71.39
CP50712L01	69631	71489	-156.55	-157.35	71.34	70.38
CP50712t02	71658	72005	-157.20	-157.32	70.32	70.38
CP50712h01	72051	73422	-157.41	-159.83	70.38	70.43
CP50712t03	73424	73606	-159.83	-160.11	70.43	70.40
CP50712t04	73608	73881	-160.11	-159.85	70.40	70.43
CP50712h02	73926	75790	-159.80	-157.35	70.42	70.38
CP50712t05	75792	76038	-157.35	-157.21	70.38	70.38
CP50712L02	76141	77503	-157.40	-159.82	70.38	70.43
CP50712t06	77505	77883	-159.83	-159.83	70.43	70.61
CP50712h03	77895	79907	-159.81	-157.21	70.61	70.56
CP50712t07	79909	80121	-157.20	-157.11	70.56	70.51
CP50712t08	80123	80336	-157.11	-157.21	70.51	70.56
CP50712h04	80401	81691	-157.34	-159.72	70.56	70.61
CP50712t09	81693	81931	-159.72	-160.10	70.61	70.59
CP50712p04	82101	83711	-159.84	-157.20	70.61	70.56
CP50712t10	83713	84034	-157.20	-157.21	70.56	70.56
CP50712h05	84021	85519	-157.21	-156.57	70.55	71.32
CP50712t11	85521	85690	-156.56	-156.43	71.32	71.39
CP50712R01	85976	86042	-155.93	-155.87	71.44	71.47
CP50712R02	86086	86145	-155.82	-155.76	71.47	71.46
CP50712R03	86196	86246	-155.77	-155.83	71.44	71.42
CP50712R04	86294	86363	-155.90	-156.00	71.42	71.44
CP50712t12	86447	86810	-156.18	-156.80	71.44	71.27
CP50713t01	69095	69282	-156.66	-156.70	71.29	71.38

Run	Start time	End time	Start lon	End lon	Start lat	End lat
CP50713L01	69421	71594	-156.57	-156.69	71.34	70.15
CP50713t02	71777	72161	-156.59	-156.61	70.07	70.15
CP50713h01	72163	74036	-156.61	-159.84	70.15	70.22
CP50713t03	74038	74361	-159.84	-160.12	70.22	70.33
CP50713t04	74363	74791	-160.12	-159.80	70.34	70.61
CP50713h02	74831	76839	-159.74	-156.96	70.61	70.55
CP50713t05	76838	77118	-156.96	-156.58	70.55	70.54
CP50713t06	77120	77421	-156.58	-156.11	70.54	70.52
CP50713h03	77475	79542	-156.03	-153.19	70.52	70.40
CP50713t07	79556	79833	-153.17	-153.03	70.40	70.28
CP50713t08	79835	80285	-153.02	-152.93	70.28	70.01
CP50713h04	80521	82459	-153.35	-156.68	70.02	70.15
CP50713t09	82461	82785	-156.69	-156.87	70.15	70.04
CP50713t10	82787	83122	-156.87	-156.69	70.04	70.12
CP50713h05	83124	85114	-156.69	-156.58	70.12	71.22
CP50713t11	85288	85465	-156.58	-156.37	71.32	71.36
CP50713t12	85871	86263	-155.90	-156.74	71.41	71.27
CP50714t01	72663	72895	-156.68	-156.35	71.29	71.28
CP50714t02	72897	73274	-156.35	-156.00	71.28	71.17
CP50714h01	73287	75400	-156.00	-156.00	71.16	70.13
CP50714t03	75401	75668	-156.00	-156.14	70.13	70.02
CP50714t04	75733	76051	-156.21	-156.53	70.01	70.14
CP50714h02	76096	77964	-156.61	-159.83	70.15	70.22
CP50714t05	77949	78179	-159.81	-160.05	70.22	70.28
CP50714t06	78181	78433	-160.05	-159.85	70.28	70.43
CP50714h03	78481	80186	-159.78	-157.35	70.43	70.38
CP50714t07	80188	80463	-157.35	-157.00	70.38	70.31
CP50714t08	80465	80817	-157.00	-156.64	70.30	70.16
CP50714h04	80884	82669	-156.75	-159.84	70.15	70.22
CP50714t09	82671	83001	-159.84	-160.02	70.22	70.36
CP50714t10	83003	83367	-160.02	-159.86	70.36	70.43
CP50714h05	83401	85034	-159.81	-157.36	70.42	70.38
CP50714t11	85041	85282	-157.35	-157.19	70.38	70.30
CP50714t12	85284	85509	-157.19	-157.37	70.30	70.36
CP50714h06	85526	87199	-157.36	-156.61	70.37	71.28
CP50714t13	87261	87506	-156.59	-156.54	71.31	71.32
CP50714t14	87508	87801	-156.54	-156.93	71.32	71.27
CP50719t01	66355	66665	-133.39	-133.78	68.32	68.36
CP50719t02	66668	67126	-133.79	-134.54	68.36	68.42
CP50719h01	67171	68919	-134.56	-135.51	68.44	69.32
CP50719t03	68921	69367	-135.51	-135.98	69.33	69.39
CP50719t04	69369	69732	-135.98	-135.58	69.39	69.39
CP50719h02	69781	71739	-135.55	-134.51	69.36	68.40
CP50719t05	71742	72008	-134.51	-134.64	68.40	68.29
CP50719t06	72010	72319	-134.64	-134.51	68.29	68.38
CP50719h03	72302	74381	-134.51	-134.66	68.37	69.45

Run	Start time	End time	Start lon	End lon	Start lat	End lat
CP50719t07	74383	74686	-134.66	-134.50	69.45	69.59
CP50719t08	75041	75317	-134.52	-134.77	69.46	69.32
CP50719h04	75326	76191	-134.78	-135.50	69.31	68.90
CP50719t09	76193	76420	-135.50	-135.71	68.90	68.79
CP50719t10	76422	76714	-135.71	-135.52	68.79	68.88
CP50719h05	76736	78249	-135.51	-134.34	68.89	69.55
CP50719t11	78251	78480	-134.34	-134.22	69.55	69.65
CP50719t12	78482	78845	-134.22	-134.66	69.65	69.51
CP50719h06	78891	80828	-134.66	-134.52	69.49	68.40
CP50719t13	80828	81170	-134.52	-134.14	68.40	68.31
CP50719t14	81172	81574	-134.13	-133.53	68.31	68.30
CP50720t01	65602	65941	-133.41	-133.37	68.31	68.48
CP50720t02	66011	66474	-133.33	-133.35	68.52	68.63
CP50720h01	66711	68422	-133.49	-134.38	68.74	69.56
CP50720t03	68424	68707	-134.38	-134.49	69.56	69.53
CP50720t04	68710	69005	-134.49	-134.38	69.53	69.56
CP50720h02	69111	70865	-134.32	-133.38	69.51	68.63
CP50720t05	70867	71236	-133.38	-133.70	68.63	68.49
CP50720t06	71238	71640	-133.71	-134.04	68.49	68.40
CP50720h03	71627	73713	-134.03	-135.52	68.39	69.33
CP50720t07	73715	73959	-135.52	-135.29	69.33	69.36
CP50720t08	73961	74283	-135.29	-135.51	69.36	69.32
CP50720h04	74307	76243	-135.49	-134.03	69.31	68.39
CP50720t09	76245	76471	-134.03	-134.25	68.39	68.34
CP50720t10	76473	76699	-134.25	-134.51	68.34	68.40
CP50720h05	76684	77875	-134.50	-135.50	68.39	68.90
CP50720t11	77877	78099	-135.50	-135.78	68.90	68.94
CP50720t12	78101	78338	-135.78	-135.52	68.94	68.91
CP50720h06	78356	79474	-135.50	-134.52	68.90	68.40
CP50720t13	79476	79693	-134.52	-134.49	68.40	68.30
CP50720t14	79695	80001	-134.48	-134.52	68.30	68.40
CP50720h07	80046	81447	-134.58	-136.38	68.41	68.81
CP50720t15	81449	81660	-136.39	-136.66	68.81	68.83
CP50720t16	81662	81877	-136.66	-136.35	68.83	68.80
CP50720h08	81941	83322	-136.27	-134.52	68.79	68.39
CP50720t17	83324	83673	-134.51	-134.28	68.39	68.27
CP50720t18	83675	84287	-134.28	-133.56	68.27	68.30
CP50721t01	66046	66366	-133.37	-133.79	68.32	68.35
CP50721L01	66471	66669	-133.82	-133.82	68.40	68.51
CP50721L02	66801	67019	-133.85	-133.84	68.53	68.40
CP50721L03	67151	67349	-133.86	-133.86	68.39	68.51
CP50721L04	67471	67664	-133.89	-133.89	68.51	68.39
CP50721L05	67821	68005	-133.91	-133.91	68.39	68.50
CP50721t02	68007	68460	-133.91	-134.52	68.51	68.43
CP50721h01	68571	70124	-134.52	-134.51	68.37	67.50
CP50721t03	70126	70507	-134.51	-134.43	67.50	67.29

Run	Start time	End time	Start lon	End lon	Start lat	End lat
CP50721t04	70509	71045	-134.43	-134.52	67.29	67.52
CP50721h02	71531	72618	-134.51	-134.52	67.79	68.40
CP50721t05	72620	72906	-134.52	-134.72	68.40	68.52
CP50721t06	72908	73248	-134.72	-134.89	68.52	68.42
CP50721h03	73341	74755	-134.88	-134.89	68.37	67.50
CP50721t07	74757	75024	-134.89	-135.02	67.50	67.38
CP50721t08	75026	75324	-135.02	-134.88	67.38	67.48
CP50721h04	75351	76994	-134.88	-134.89	67.49	68.40
CP50721t09	76996	77453	-134.89	-134.77	68.40	68.56
CP50721R01	77455	77564	-134.77	-134.80	68.55	68.49
CP50721R02	77611	77699	-134.85	-134.99	68.47	68.47
CP50721R03	77751	77839	-135.04	-135.04	68.49	68.54
CP50721t10	77841	78814	-135.04	-133.53	68.54	68.30
CP50722t01	65843	66151	-133.58	-133.99	68.30	68.35
CP50722t02	66153	66521	-133.99	-134.51	68.35	68.40
CP50722h01	66557	67989	-134.56	-136.38	68.41	68.81
CP50722t03	67981	68274	-136.37	-136.25	68.81	68.81
CP50722L01	68571	73639	-136.14	-140.97	68.87	69.64
CP50722t04	73907	74481	-140.69	-139.68	69.63	69.48
CP50722h02	74526	76532	-139.62	-137.09	69.47	68.79
CP50722t05	76656	76864	-136.91	-136.70	68.75	68.73
CP50722t06	76866	77280	-136.70	-136.54	68.73	68.82
CP50722h03	77321	78824	-136.48	-134.51	68.83	68.40
CP50722t07	78826	79156	-134.51	-134.41	68.40	68.29
CP50722t08	79158	79559	-134.41	-134.50	68.29	68.39
CP50722h04	79556	80600	-134.49	-135.50	68.39	68.90
CP50722t09	80597	80805	-135.50	-135.75	68.90	68.93
CP50722t10	80807	81103	-135.75	-135.51	68.93	68.91
CP50722h05	81125	82340	-135.49	-134.53	68.90	68.40
CP50722t11	82342	82685	-134.53	-134.58	68.40	68.40
CP50722r01	83211	83349	-133.64	-133.41	68.30	68.30
CP50722r02	83486	83594	-133.44	-133.50	68.33	68.28
CP50722r03	83761	83855	-133.41	-133.50	68.27	68.32
CP50722t12	83857	84222	-133.50	-133.34	68.32	68.30
CP50723t01	65050	65352	-133.61	-133.45	68.31	68.44
CP50723L01	65701	65999	-133.40	-133.56	68.65	68.81
CP50723t02	66001	66269	-133.56	-133.71	68.81	68.95
CP50723h01	66346	67365	-133.75	-134.29	68.99	69.49
CP50723t03	67367	67625	-134.29	-134.35	69.50	69.62
CP50723t04	67627	67911	-134.35	-134.33	69.62	69.56
CP50723h02	67926	69361	-134.35	-135.50	69.56	68.90
CP50723t05	69367	69635	-135.50	-135.75	68.89	68.84
CP50723t06	69637	69972	-135.75	-135.53	68.85	68.88
CP50723h03	69981	71436	-135.52	-134.35	68.88	69.55
CP50723t07	71438	71684	-134.34	-133.96	69.55	69.56
CP50723t08	71686	71979	-133.96	-134.14	69.56	69.46

Run	Start time	End time	Start lon	End lon	Start lat	End lat
CP50723h04	71981	73874	-134.14	-135.60	69.46	68.55
CP50723t09	73876	74152	-135.60	-135.92	68.55	68.50
CP50723t10	74154	74468	-135.92	-135.59	68.50	68.56
CP50723h05	74501	76269	-135.57	-134.22	68.57	69.41
CP50723t11	76301	76539	-134.20	-134.19	69.43	69.53
CP50723t12	76541	76798	-134.19	-134.20	69.53	69.40
CP50723h06	76800	78059	-134.20	-133.48	69.40	68.72
CP50723t13	78229	78561	-133.39	-133.26	68.63	68.59
CP50723t14	78563	79150	-133.26	-133.45	68.59	68.30
CP50725t01	66102	66201	-133.58	-133.71	68.30	68.31
CP50725t02	66327	66514	-133.89	-134.16	68.35	68.37
CP50725h01	66691	68539	-134.31	-134.63	68.42	69.38
CP50725t03	68541	68649	-134.63	-134.65	69.38	69.44
CP50725t04	68876	69015	-134.66	-134.63	69.47	69.39
CP50725h02	69017	70812	-134.63	-134.30	69.39	68.40
CP50725t05	70814	70951	-134.30	-134.23	68.40	68.42
CP50725t06	70953	71084	-134.23	-134.31	68.42	68.41
CP50725h03	71107	72643	-134.30	-134.06	68.40	67.59
CP50725t07	72645	73023	-134.06	-133.90	67.59	67.53
CP50725t08	73025	73495	-133.90	-134.06	67.53	67.59
CP50725h04	73497	74935	-134.06	-134.30	67.59	68.40
CP50725t09	74937	75236	-134.30	-134.70	68.40	68.37
CP50725t10	75238	75641	-134.70	-135.26	68.37	68.38
CP50725h05	75656	77397	-135.26	-134.89	68.37	67.50
CP50725t11	77399	77693	-134.89	-134.63	67.50	67.42
CP50725t12	77695	78115	-134.63	-134.88	67.42	67.48
CP50725h06	78151	79609	-134.89	-135.26	67.51	68.39
CP50725t13	79611	79921	-135.26	-135.36	68.39	68.32
CP50725t14	79923	80291	-135.36	-135.26	68.32	68.38
CP50725h07	80293	81138	-135.26	-135.49	68.38	68.90
CP50725t15	81140	81377	-135.49	-135.63	68.90	68.97
CP50725t16	81379	81714	-135.63	-135.50	68.97	68.90
CP50725h08	81751	82776	-135.49	-135.27	68.88	68.38
CP50725t17	82778	83089	-135.27	-134.84	68.38	68.35
CP50725t18	83091	83986	-134.84	-133.42	68.35	68.31
CP50726t01	64860	64909	-133.39	-133.40	68.31	68.33
CP50726L01	64951	65214	-133.46	-133.94	68.34	68.41
CP50726t02	65461	66000	-134.26	-134.03	68.38	68.39
CP50726h01	66101	68030	-134.10	-135.51	68.44	69.33
CP50726t03	68032	68392	-135.51	-135.60	69.33	69.46
CP50726t04	68394	68774	-135.59	-135.49	69.46	69.33
CP50726h02	68801	69834	-135.51	-136.32	69.32	68.84
CP50726t05	69906	70271	-136.38	-136.41	68.81	68.75
CP50726t06	70273	70663	-136.41	-136.38	68.75	68.80
CP50726h03	70701	71774	-136.35	-135.50	68.82	69.32
CP50726t07	71776	72115	-135.50	-135.26	69.32	69.47

Run	Start time	End time	Start lon	End lon	Start lat	End lat
CP50726t08	72117	72582	-135.26	-135.51	69.47	69.33
CP50726h04	72629	74335	-135.51	-135.26	69.30	68.39
CP50726t09	74344	74590	-135.26	-135.28	68.38	68.25
CP50726t10	74592	74874	-135.28	-135.26	68.25	68.38
CP50726h05	74880	76889	-135.26	-134.42	68.39	69.46
CP50726t11	76893	77189	-134.42	-134.39	69.47	69.59
CP50726t12	77192	77828	-134.39	-134.47	69.60	69.40
CP50726h06	78031	79749	-134.56	-135.27	69.29	68.39
CP50726t13	79754	79932	-135.27	-135.46	68.38	68.41
CP50726t14	79934	80213	-135.46	-135.62	68.41	68.55
CP50726h07	80237	81312	-135.59	-134.02	68.55	68.38
CP50726t15	81314	81633	-134.02	-133.72	68.38	68.25
CP50726t16	81635	81971	-133.72	-133.34	68.25	68.31

Die "**Berichte zur Polar- und Meeresforschung**" (ISSN 1866-3192) werden beginnend mit dem Heft Nr. 569 (2008) als Open-Access-Publikation herausgegeben. Ein Verzeichnis aller Hefte einschließlich der Druckausgaben (Heft 377-568) sowie der früheren "**Berichte zur Polarforschung**" (Heft 1-376, von 1981 bis 2000) befindet sich im open access institutional repository for publications and presentations (**ePIC**) des AWI unter der URL <http://epic.awi.de>. Durch Auswahl "Reports on Polar- and Marine Research" (via "browse"/"type") wird eine Liste der Publikationen sortiert nach Heftnummer innerhalb der absteigenden chronologischen Reihenfolge der Jahrgänge erzeugt.

To generate a list of all Reports past issues, use the following URL: <http://epic.awi.de> and select "browse"/"type" to browse "Reports on Polar and Marine Research". A chronological list in declining order, issues chronological, will be produced, and pdf-icons shown for open access download.

Verzeichnis der zuletzt erschienenen Hefte:

Heft-Nr. 661/2013 — "The Expedition of the Research Vessel 'Polarstern' to the Antarctic in 2012 (ANT-XXVIII/3)", edited by Dieter Wolf-Gladrow

Heft-Nr. 662/2013 — "Climate Change in the Marine Realm: An international summer school in the framework of the European Campus of Excellence", edited by Angelika Dummermuth and Klaus Grosfeld

Heft-Nr. 663/2013 — "The Expedition of the Research Vessel 'Polarstern' to the Arctic in 2012 (ARK-XXVII/3)", edited by Antje Boetius

Heft-Nr. 664/2013 — "Russian-German Cooperation SYSTEM LAPTEV SEA: The Expeditions Laptev Sea - Mamontov Klyk 2011 & Buor Khaya 2012", edited by Frank Günther, Pier Paul Overduin, Aleksandr S. Makarov, and Mikhail N. Grigoriev

Heft-Nr. 665/2013 — "The Expedition of the Research Vessel 'Polarstern' to the Antarctic in 2013 (ANT-XXIX/3)", edited by Julian Gutt

Heft-Nr. 666/2013 — "The Expedition of the Research Vessel 'Polarstern' to the Antarctic in 2013 (ANT-XXIX/5)", edited by Wilfried Jokat

Heft-Nr. 667/2013 — "The Sea Ice Thickness in the Atlantic Sector of the Southern Ocean", by Axel Behrendt

Heft-Nr. 668/2013 — "The Expedition of the Research Vessel 'Polarstern' to the Antarctic in 2013 (ANT-XXIX/4)", edited by Gerhard Bohrmann

Heft-Nr. 669/2013 — "Processes in the Southern Ocean carbon cycle: Dissolution of carbonate sediments and inter-annual variability of carbon fluxes", by Judith Hauck

Heft-Nr. 670/2013 — "The Expedition of the Research Vessel 'Polarstern' to the Antarctic in 2012 (ANT-XXIX/1)", edited by Holger Auel

Heft-Nr. 671/2013 — "The Expedition of the Research Vessel 'Polarstern' to the Antarctic in 2012/2013 (ANT-XXIX/2)", edited by Olaf Boebel

Heft-Nr. 672/2014 — "The Expedition of the Research Vessel 'Polarstern' to the Antarctic in 2013 (ANT-XXIX/8)", edited by Vera Schlindwein

Heft-Nr. 673/2014 — "Airborne Measurements of Methane Fluxes in Alaskan and Canadian Tundra with the Research Aircraft 'Polar 5'", by Katrin Kohnert, Andrei Serafimovich, Jörg Hartmann, and Torsten Sachs